AD-A051 866 ARMY MISSILE RESEARCH AND DEVELOPMENT COMMAND REDSTO--ETC F/G 20/11
FRACTURE MECHANICS DESIGN HANDBOOK FOR COMPOSITE MATERIALS.(U)
SEP 77 D G SMITH, B R MULLINIX

UNCLASSIFIED DRDMI-T-78-6 NL

1 OF 2
AD
A051866

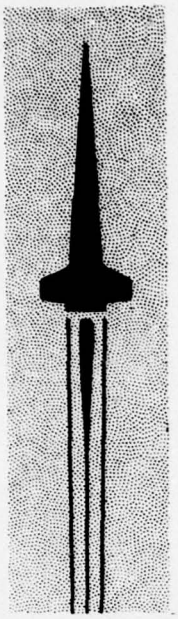

U.S. ARMY MISSILE RESEARCH AND DEVELOPMENT COMMAND

Redstone Arsenal, Alabama 35809

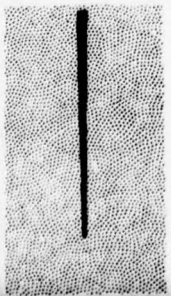

TECHNICAL REPORT T-78-6

FRACTURE MECHANICS DESIGN HANDBOOK FOR COMPOSITE MATERIALS

Dallas G. Smith and Bobby R. Mullinix
Ground Equipment and Missile Structures Directorate
Technology Laboratory

26 September 1977

Approved for public release; distribution unlimited.

DISPOSITION INSTRUCTIONS

DESTROY THIS REPORT WHEN IT IS NO LONGER NEEDED. DO NOT RETURN IT TO THE ORIGINATOR.

DISCLAIMER

THE FINDINGS IN THIS REPORT ARE NOT TO BE CONSTRUED AS AN OFFICIAL DEPARTMENT OF THE ARMY POSITION UNLESS SO DESIGNATED BY OTHER AUTHORIZED DOCUMENTS.

TRADE NAMES

USE OF TRADE NAMES OR MANUFACTURERS IN THIS REPORT DOES NOT CONSTITUTE AN OFFICIAL INDORSEMENT OR APPROVAL OF THE USE OF SUCH COMMERCIAL HARDWARE OR SOFTWARE.

UNCLASSIFIED

SECURITY CLASSIFICATION OF THIS PAGE (When Data Entered)

REPORT DOCUMENTATION PAGE

READ INSTRUCTIONS BEFORE COMPLETING FORM

1. REPORT NUMBER: T-78-6

2. GOVT ACCESSION NO.

3. RECIPIENT'S CATALOG NUMBER

4. TITLE (and Subtitle): (6) FRACTURE MECHANICS DESIGN HANDBOOK FOR COMPOSITE MATERIALS.

5. TYPE OF REPORT & PERIOD COVERED: (9) Technical Report,

6. PERFORMING ORG. REPORT NUMBER: T-78-6

7. AUTHOR(s): (10) Dallas G. Smith [redacted] Bobby R. Mullinix

8. CONTRACT OR GRANT NUMBER(s): (14) DRDMI-T-78-6

9. PERFORMING ORGANIZATION NAME AND ADDRESS
Commander
US Army Missile Research and Development Command
DRDMI-TLA
Redstone Arsenal, Alabama 35809

10. PROGRAM ELEMENT, PROJECT, TASK AREA & WORK UNIT NUMBERS: (16) 1L162303A214
AMCMS 612303.2140911

11. CONTROLLING OFFICE NAME AND ADDRESS
Commander
US Army Missile Research and Development Command
DRDMI-TI
Redstone Arsenal, Alabama 35809

12. REPORT DATE: (11) 26 Sep[redacted]977

13. NUMBER OF PAGES: 127 (12) 127p.

14. MONITORING AGENCY NAME & ADDRESS (if different from Controlling Office)

15. SECURITY CLASS. (of this report): UNCLASSIFIED

15a. DECLASSIFICATION/DOWNGRADING SCHEDULE

16. DISTRIBUTION STATEMENT (of this Report)

Approved for public release; distribution unlimited.

17. DISTRIBUTION STATEMENT (of the abstract entered in Block 20, if different from Report)

18. SUPPLEMENTARY NOTES

19. KEY WORDS (Continue on reverse side if necessary and identify by block number)

Fracture mechanics
Design manual
Composite materials
Applications
Crack tip stresses
Damage zone effects
Fracture toughness testing

20. ABSTRACT (Continue on reverse side if necessary and identify by block number)

This design manual is directed toward the needs of practicing engineers and stress analysts. Basic information on the philosophy and theory of the fracture mechanics of composite materials including such topics as common definitions, elastic solutions, damage zone effects, and fracture toughness testing are included. However, the major emphasis is placed on applications.

ABSTRACT (Continued)

DD FORM 1 JAN 73 1473 EDITION OF 1 NOV 65 IS OBSOLETE

UNCLASSIFIED

SECURITY CLASSIFICATION OF THIS PAGE (When Data Entered)

393 427 JOB

ABSTRACT (Continued)

Several techniques and the most applicable solutions presently available for use in the fracture mechanics of composite materials are documented with details covering their application and accuracy.

CONTENTS

PREFACE

This work represents the continuation of an effort begun earlier with the preparation of the Army report Fracture Mechanics Design Handbook. The objectives are to provide an introduction to fracture mechanics fundamentals and to provide a convenient source of fracture mechanics information for designers, stress analysts, and engineers. The first volume was limited to isotropic, homogeneous materials; this volume is limited to filamentary composite materials.

The subject of fracture mechanics of filamentary composites is not yet settled. While its validity for making strength predictions has been confirmed for a number of composite systems, its need is still not clear. The need is not clear for two reasons. While it is true that composites are subject to a certain amount of crack-like damage, they are not generally subject to fatigue cracks as metals are. Also, composites are inherently tough; the toughness increases with the unnotched strength. The question of need will perhaps become clearer in a few years as more structures are built of composites. The experience gained will indicate whether brittle fracture and the need to control it are major concerns.

This volume contains a summary of fracture mechanics techniques for filamentary composites. An elementary introduction to the notation and constitutive equations of composite laminates is included in Chapter 1. The basic stress fields on which fracture mechanics theory is based are given in Chapter 2 along with several numerical solutions which illustrate certain anisotropy and size effects. Chapter 3 is concerned with some fundamental ideas of fracture behavior, fracture mechanisms, and fracture criteria. Fracture toughness using various specimen geometries for epoxy and aluminum matrix composites is discussed in Chapter 4. Chapter 5 contains two theories which attempt to explain the fracture behavior of composites with stress concentrations.

For a variety of reasons a number of topics related to the present one were omitted from this volume. Chopped fiber composites and fatigue of composites were not included. Because work-of-fracture measurements are not normally specimen-independent, work-of-fracture ideas were not included. They are primarily used to obtain the relative fracture resistance of different materials. Mode III type crack loading, because it it is believed to be of infrequent importance, was not mentioned.

This report reflects only the state-of-the-art at the time of publication and it is expected that a stress analyst or engineer will supplement the data presented with other solutions commonly needed in his specific work as they become available.

No pretense of originality is made here. Information included was gathered from many sources and appreciation is extended to all those authors whose work is cited.

For administrative and contractual support of the part or this project performed in the summer of 1977, the authors gratefully acknowledge the scientific services program of the Army Research Office.

Chapter 1. INTRODUCTION

Fracture mechanics of composites is a new and complex subject. Reference 1 discussed the fundamentals of fracture mechanics of isotropic materials; the following chapters discuss the fracture mechanics of composites; its analytical foundation, its experimental basis, and the fundamentals of its application.

1.1 Fracture Mechanics of Composites

The concepts of linear elastic fracture mechanics were developed primarily for applications to metals. For a number of reasons, these concepts are currently being applied to composite materials. A strong advantage of filamentary composites is that they can be tailor-made with the strength and stiffness oriented as needed for a specific application, so that high strength-to-weight ratios result. Because of this, these composites are successfully competing with metals in many industries, especially the aerospace industry. In material comparisons, fracture mechanics provides a consistent way of ranking the fracture resistance of the candidate materials. Furthermore, the fail-safe design philosophy of damage tolerance or damage containment requires the estimation of residual strength of damage members. This has encouraged the investigation of fracture mechanics as a tool for making such estimations. Fracture mechanics is based upon the occurrence of crack-like flaws in the structure, and while fatigue cracks normally do not form in composites, flaw damage does occur in a number of ways. Ballistic damage to military aircraft is an outstanding example. Other flaws such as tool scratches and the like occur. Some flaws are inherent to the production process: internal flaws due to poor wetting of the fibers, improper adhesion of the matrix and fibers, air bubbles, and dirt are a few. The application of fracture mechanics has been further prompted by the behavior of composite laminates containing notches and holes. For such laminates, the strength does not conform to the conventional concept of a stress concentration factor; therefore, fracture mechanics together with the idea of an inherent flaw have been developed for making strength predictions in such cases.

The history of the application of fracture mechanics of composites is quite recent. The method involves determining stresses around a flaw which is modeled as a crack. Although heterogeneous as well as anisotropic, filamentary composites are commonly assumed for analysis purposes to be representable as homogeneous media. Within that context Sih, et al. [2,3] provided the fundamental solution in 1965 for the stresses near a flaw tip in an anisotropic plate. The stresses, although somewhat different from the isotropic case, retained the same type of stress singularity that forms the basis of conventional fracture mechanics. Sih defined the anisotropic stress intensity factors and showed for certain fundamental cases that these were the same as their isotropic

counterparts. Sih further showed that these stress intensity factors could be related to the strain energy release rate of Griffith [4]. Wu's experiments [5,6] then showed that fracture mechanics concepts could be applied to composites. His experiments were limited to unidirectional composites, with the initial crack parallel to the fibers.

In a typical composite laminate the mode of fracture is far more complex than it was for Wu's case. For angle plies, crack extension is frequently accompanied by a general area of crack tip damage: delamination between plies and splitting between fibers within plies. Fracture surface appearances range from what could perhaps be described as smooth to those of a "shaving brush." The application of fracture mechanics to a wide variety of laminate configurations been demonstrated by Konish and his associates [7, 8, and 9] through fracture toughness testing programs.

1.2 Introduction to Filamentary Composites

The materials under discussion here are limited to those known as filamentary composites, that is, materials made up of long continuous fibers embedded in a matrix material as shown in Figure 1. Common reinforcing

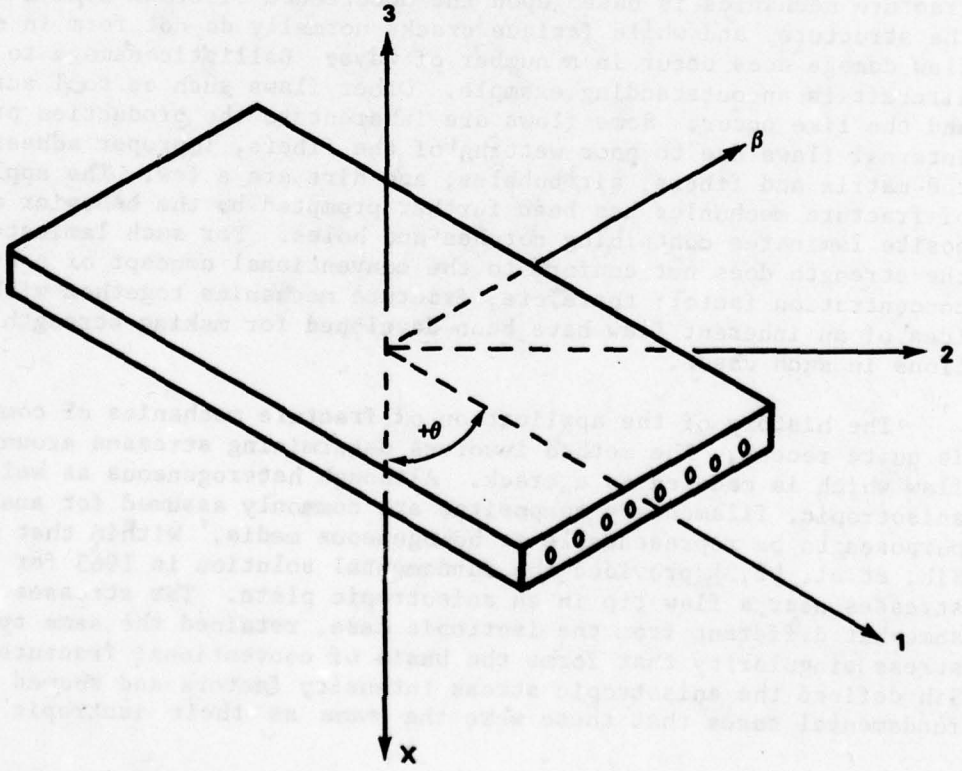

Figure 1. Fiber reinforced lamina.

fibers are glass, graphite, and boron; common matrix materials are epoxy and aluminum. The fibers have extremely small diameters: 5.6 and 8 mils are two common sizes for boron; graphite and glass are an order of magnitude smaller, having diameters of 0.3 to 0.4 mils. The amount of fiber material is normally specified by giving the fiber volume ratio, V/O, which is the ratio of the fiber volume to the total volume.

The laminates are built up from the matrix and fiber raw materials by a number of processes. Shell structures are typically fabricated by a filament winding process, a method whereby a machine winds a continuous bundle of the fibers wetted with the epoxy matrix material onto a mandrel of the proper shape. Other structural laminates are fabricated by the lay-up of a tape containing both the fibers and epoxy matrix materials. The 3-in. wide tape contains the untwisted fibers oriented in the longitudinal direction. The successive layers of tape are applied at whatever angle is required to give the resulting laminate its desired properties of strength, stiffness, and directionality. A built-up laminate is shown in Figure 2. After the laminate is built up from the tape it is subjected to a curing process of heat and pressure.

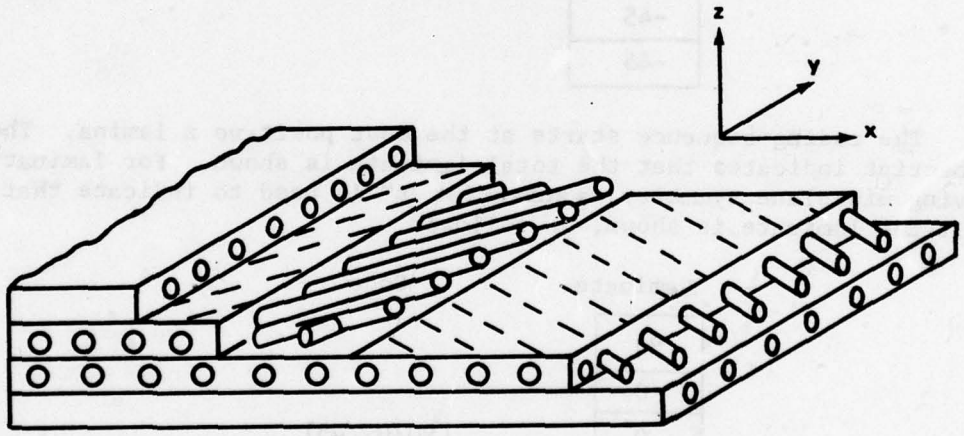

Figure 2. Filamentary composite laminate.

In the literature of composites a code notation is used to designate the stacking sequence and the angular direction of the ply fibers with the laminate axis (x-axis, Figure 2). A few examples [10] will illustrate the method.

Laminate	Code
45	
0	$[45/0/\overline{-60_2}/30]_T$
-60	
-60	
30	

+45	
-45	
-30	$[\pm 45/\pm 30/0/\pm(45_2)]_T$
+30	
0	
+45	
+45	
-45	
-45	

The coding sequence starts at the most positive z lamina. The "T" subscript indicates that the total laminate is shown. For laminates having mid-plane symmetry, a subscript "s" is used to indicate that only half the laminate is shown, as follows:

Laminate	Code
90	
0	
0	$[90/0_2/45]_s$
45	
45	
0	
0	
90	

If the symmetric laminate has an odd number of laminae, the code denoting the center lamina is overlined, indicating that half of the laminate lies on either side of that lamina:

Laminate	Code
0	$[0/45/\overline{90/}]_s$
45	
90	
45	
0	

A repeating sequence of laminae is termed a set; it is coded as follows:

Laminate		Code
45		
0	set	
90		
45		
0	set	
90		$[(45/0/90)_4]_T$ or $[45/0/90]_{4T}$
45		
0	set	
90		
45		
0	set	
90		
45		
0	set	
90		
45		
0	set	
90		$[(45/0/90)_2]_s$ or $[45/0/90]_{2s}$
90		
0	set	
45		
90		
0	set	
45		

In informal applications of the code, a laminate may be referred to by giving the laminate's set but not the number of sets. For example the preceding laminate might be referred to as simply a $(45/0/90)_s$ laminate.

1.3 Constitutive Equations

The constitutive equations are thoroughly discussed [11]; the following is only a brief review. First an anisotropic sheet in a state of plane stress is considered. The in-plane directions are denoted as 1 and 2. Then the stress-strain relationship is

$$\begin{bmatrix}\sigma_1\\ \sigma_2\\ \tau_{12}\end{bmatrix} = \begin{bmatrix}Q_{11} & Q_{12} & Q_{16}\\ Q_{12} & Q_{22} & Q_{26}\\ Q_{16} & Q_{26} & Q_{66}\end{bmatrix} \begin{bmatrix}\epsilon_1\\ \epsilon_2\\ \gamma_{12}\end{bmatrix} \tag{1}$$

where the stresses, σ_1, σ_2, and τ_{12}, and the strains ϵ_1, ϵ_2, and γ_{12}, are referred to the 1 and 2 axes. The quantities Q_{ij} are the elastic constants comprising the stiffness matrix. The stiffness matrix is symmetric so that six independent elastic constants completely specify the stress-strain behavior.

Consider now an orthotropic (three mutually perpendicular planes of symmetry) sheet as represented by a lamina of filamentary material, Figure 1. It is assumed that the lamina is homogeneous; then the stress-strain relation, in Equation (1) simplifies to

$$\begin{bmatrix}\sigma_1\\ \sigma_2\\ \tau_{12}\end{bmatrix} = \begin{bmatrix}Q_{11} & Q_{12} & 0\\ Q_{12} & Q_{22} & 0\\ 0 & 0 & Q_{66}\end{bmatrix} \begin{bmatrix}\epsilon_1\\ \epsilon_2\\ \gamma_{12}\end{bmatrix} \tag{2}$$

where the elements of the shiftness matrix are:

$$\begin{aligned} Q_{11} &= E_{11}/(1 - \nu_{12}\,\nu_{21})\\ Q_{22} &= E_{22}/(1 - \nu_{12}\,\nu_{21})\\ Q_{12} &= \nu_{21}E_{11}/(1 - \nu_{12}\,\nu_{21}) = \nu_{12}E_{22}/(1 - \nu_{12}\,\nu_{21})\\ Q_{66} &= G_{12}\\ Q_{16} &= Q_{26} = 0 \quad . \end{aligned} \tag{3}$$

There are four independent elastic constants: E_{11} and E_{22}, the Young's moduli in the 1 and 2 directions, respectively; G_{12}, the shear modulus; and ν_{12}, the major Poisson's ratio. Note also that from Equation (3):

$$\nu_{21}E_{11} = \nu_{12}E_{22} \quad .$$

The compliance matrix S_i can be found by inverting the stiffness matrix. Results are:

$$\begin{bmatrix} \epsilon_1 \\ \epsilon_2 \\ \gamma_{12} \end{bmatrix} = \begin{bmatrix} s_{11} & s_{12} & 0 \\ s_{12} & s_{22} & 0 \\ 0 & 0 & s_{66} \end{bmatrix} \begin{bmatrix} \sigma_1 \\ \sigma_2 \\ \tau_{12} \end{bmatrix} \tag{4}$$

where the elements of the compliance matrix are:

$$\begin{aligned} s_{11} &= 1/E_{11} \\ s_{22} &= 1/E_{22} \\ s_{12} &= -\nu_{12}/E_{11} = -\nu_{21}/E_{22} \\ s_{66} &= 1/G_{12} \\ s_{16} &= s_{26} = 0 \quad . \end{aligned} \tag{5}$$

It is important to note that the stress-strain relations in Equations (2) and (4) are for a specially orthotropic lamina, where the constitutive relations are referred to the principal axes (1,2) of the orthotropic lamina.

Normally the principal axes of the lamina do not coincide with the reference x and y axes for the laminate. In that case the constitutive relationship must be transformed through an angle θ to the laminate axis x and y as shown in Figure 1. For brevity, the details which are included in Reference 11 will be skipped. The resulting stress strain relation is:

$$\begin{bmatrix} \sigma_{xx} \\ \sigma_{yy} \\ \tau_{xy} \end{bmatrix} = \begin{bmatrix} \bar{Q}_{11} & \bar{Q}_{12} & \bar{Q}_{16} \\ \bar{Q}_{12} & \bar{Q}_{22} & \bar{Q}_{26} \\ \bar{Q}_{16} & \bar{Q}_{26} & \bar{Q}_{66} \end{bmatrix} \begin{bmatrix} \epsilon_{xx} \\ \epsilon_{yy} \\ \gamma_{xy} \end{bmatrix} \tag{6}$$

where $\bar{Q}_{ij}$, the components of the stiffness matrix referred to the arbitrary x-y axis, are [11]:

$$\begin{aligned}
\bar{Q}_{11} &= Q_{11} \cos^4\theta + 2(Q_{12} + 2\,Q_{66}) \sin^2\theta \cos^2\theta + Q_{22} \sin^4\theta \\
\bar{Q}_{22} &= Q_{11} \sin^4\theta + 2(Q_{12} + 2\,Q_{66}) \sin^2\theta \cos^2\theta + Q_{22} \cos^4\theta \\
\bar{Q}_{12} &= (Q_{11} + Q_{22} - 4\,Q_{66}) \sin^2\theta \cos^2\theta + Q_{12} (\sin^4\theta + \cos^4\theta) \\
\bar{Q}_{66} &= (Q_{11} + Q_{22} - 2\,Q_{12} - 2\,Q_{66}) \sin^2\theta \cos^2\theta \\
&\quad + Q_{66} (\sin^4\theta + \cos^4\theta) \\
\bar{Q}_{16} &= (Q_{11} - Q_{12} - 2\,Q_{66}) \sin\theta \cos^3\theta + (Q_{12} - Q_{22} \\
&\quad + 2\,Q_{66}) \sin^3\theta \cos\theta \\
\bar{Q}_{26} &= (Q_{11} - Q_{12} - 2\,Q_{66}) \sin^3\theta \cos\theta + (Q_{12} - Q_{22} \\
&\quad + 2\,Q_{66}) \sin\theta \cos^3\theta \quad .
\end{aligned} \tag{7}$$

None of the terms in the stiffness matrix are zero now. In fact, the stiffness matrix has the same form as for a fully anisotropic plate, Equation (1). However, there are still only four independent elastic constants. The terms $\bar{Q}_{16}$ and $\bar{Q}_{26}$ are merely linear combinations of the first four Q's. Of course, this stiffness matrix can be inverted to find the corresponding compliance matrix $\bar{S}_{ij}$ for an orthotropic plate. Thus,

$$\begin{bmatrix} \epsilon_{xx} \\ \epsilon_{yy} \\ \gamma_{xy} \end{bmatrix} = \begin{bmatrix} \bar{S}_{11} & \bar{S}_{12} & \bar{S}_{16} \\ \bar{S}_{12} & \bar{S}_{22} & \bar{S}_{26} \\ \bar{S}_{16} & \bar{S}_{26} & \bar{S}_{66} \end{bmatrix} \begin{bmatrix} \sigma_{xx} \\ \sigma_{yy} \\ \tau_{xy} \end{bmatrix} \tag{8}$$

where $[\bar{S}]$ is the inverse of $[\bar{Q}]$, or $[\bar{S}] = [\bar{Q}]^{-1}$.

1.4 Laminate Constitutive Equations

Given the location and orientation of all the plies, it is possible to compute the macroscopic elastic properties of a laminate from the elastic properties of its constituent plies. To do so, the constitutive equations for each k ply shown in Figure 3, are first referred to the laminate axes x and y, then the stress resultants are computed across the laminate thickness, B, by integrating the stresses across each lamina thickness.

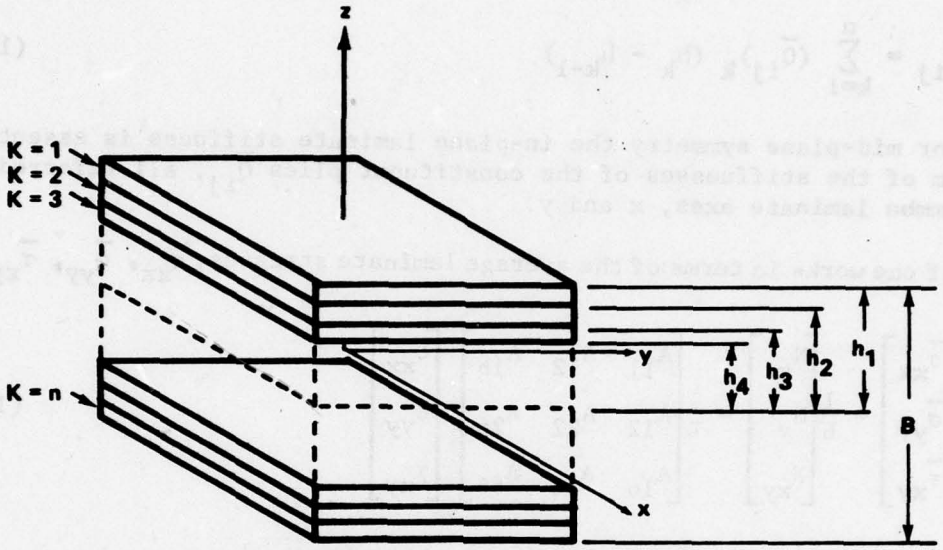

Figure 3. Notation for lamina coordinate within a laminate.

In general, the results are rather lengthy: the in-plane stress resultants not only depend upon the mid-plane strains but upon the bending curvature as well; the laminate exhibits coupling of extension and bending. This means that applied extension causes bending or warping or, conversely, an applied moment causes in-plane forces. This is normally an undesirable situation in that panels subjected to tension would warp out of plane even if the tension were due to thermal stresses resulting from a change in temperature.

It can be shown that the bending-moment coupling disappears if the laminates possess mid-plane symmetry [11]. Mid-plane symmetry means that for every ply above the laminate mid-plane there is one of equal properties and orientation an equal distance below the mid-plane. Most laminates have mid-plane symmetry to prevent the undesirable warping mentioned previously. Consequently, all of the following will be restricted to mid-plane symmetric laminates. Moreover, applied moments are not considered; therefore, the moment-curvature constitutive relations will not be required. With these limitations then, the stress resultants (N_x, N_y, N_{xy}) on the laminate element in Figure 3 are related to the strains (ϵ_{xx}, ϵ_{yy}, γ_{xy}) by

$$\begin{bmatrix} N_x \\ N_y \\ N_{xy} \end{bmatrix} = \begin{bmatrix} A_{11} & A_{12} & A_{16} \\ A_{12} & A_{22} & A_{26} \\ A_{16} & A_{26} & A_{66} \end{bmatrix} \begin{bmatrix} \epsilon_{xx} \\ \epsilon_{yy} \\ \gamma_{xy} \end{bmatrix} \tag{9}$$

where

$$A_{ij} = \sum_{k=1}^{n} (\bar{Q}_{ij})_k \, (h_k - h_{k-1}) \tag{10}$$

Thus for mid-plane symmetry the in-plane laminate stiffness is essentially the sum of the stiffnesses of the constituent plies $\bar{Q}_{ij}$, all referred to the common laminate axes, x and y.

If one works in terms of the average laminate stresses, $\bar{\sigma}_{xx}$, $\bar{\sigma}_{yy}$, $\bar{\tau}_{xy}$, where

$$\begin{bmatrix} \bar{\sigma}_{xx} \\ \bar{\sigma}_{yy} \\ \bar{\tau}_{xy} \end{bmatrix} = \frac{1}{B} \begin{bmatrix} N_x \\ N_y \\ N_{xy} \end{bmatrix} = \frac{1}{B} \begin{bmatrix} A_{11} & A_{12} & A_{16} \\ A_{12} & A_{22} & A_{26} \\ A_{16} & A_{26} & A_{66} \end{bmatrix} \begin{bmatrix} \epsilon_{xx} \\ \epsilon_{yy} \\ \gamma_{xy} \end{bmatrix} \tag{11}$$

then the laminate stress-strain relationship becomes

$$\begin{bmatrix} \bar{\sigma}_{xx} \\ \bar{\sigma}_{yy} \\ \bar{\tau}_{xy} \end{bmatrix} = \begin{bmatrix} C_{11} & C_{12} & C_{16} \\ C_{12} & C_{22} & C_{26} \\ C_{16} & C_{26} & C_{66} \end{bmatrix} \begin{bmatrix} \epsilon_{xx} \\ \epsilon_{yy} \\ \gamma_{xy} \end{bmatrix} \tag{12}$$

where

$$[C] = \frac{1}{B} [A] \tag{13}$$

The compliance matrix [a] can be found by taking the inverse of the stiffness matrix, [C]. That is,

$$[a] = [C]^{-1} \tag{14}$$

so that

$$\begin{bmatrix} \epsilon_{xx} \\ \epsilon_{yy} \\ \gamma_{xy} \end{bmatrix} = \begin{bmatrix} a_{11} & a_{12} & a_{16} \\ a_{12} & a_{22} & a_{26} \\ a_{16} & a_{26} & a_{66} \end{bmatrix} \begin{bmatrix} \bar{\sigma}_{xx} \\ \bar{\sigma}_{yy} \\ \bar{\tau}_{xy} \end{bmatrix} \tag{15}$$

Equations (12) and (15) are the laminate constitutive equations. The elements C_{ij}, of the stiffness matrix are computed from Equations (10)

and (13); and the elements a_{ij}, of the compliance matrix are given by Equation (14).

If for every ply having a $+\theta$ orientation there is a ply of equal properties with a $-\theta$ orientation, then $a_{16} = a_{26} = 0$ and the laminate is specially orthotropic, having only four independent elastic constants. In that case, the elements a_{ij} of the compliance matrix are defined in terms of the laminate's engineering constants in a manner identical to Equation (5), which were derived for a single orthotropic lamina. A laminate which contains an equal number of laminae of $+\theta$ and $-\theta$ fiber orientation is referred to as a "balanced" laminate.

The term quasi-isotropic, sometimes used in the literature, refers to a particular type of laminate which is nearly isotropic in stiffness. Examples are: a three-ply laminate with a $[0°/\pm60]_s$ orientation, and a four-ply laminate with a $[0°/\pm45°/90°]_s$ orientation.

Chapter 2. CRACK TIP STRESSES FOR ANISTROPIC MATERIALS

The application of fracture mechanics is based upon the mathematical form of the stresses around the tip of a sharp flaw. Results leading to basic definitions have been obtained for fundamental geometries in anisotropic materials. Some of these results will be discussed. Additionally, some numerical solutions which demonstrate certain geometric and material effects for selected filamentary laminates will be considered.

2.1 Crack-Tip Stress Fields in Anisotropic Plates

In Chapter 1, the form of the stress-strain relationship for an anisotropic plate (or laminate) was noted to take the form

$$\begin{bmatrix} \epsilon_{xx} \\ \epsilon_{yy} \\ \gamma_{xy} \end{bmatrix} = \begin{bmatrix} a_{11} & a_{12} & a_{16} \\ a_{12} & a_{22} & a_{26} \\ a_{16} & a_{26} & a_{66} \end{bmatrix} \begin{bmatrix} \sigma_{xx} \\ \sigma_{yy} \\ \tau_{xy} \end{bmatrix} \tag{16}$$

where the a_{ij} are the compliance coefficients for the plate. If the anisotropic plate is also a laminated plate then the stresses σ_{xx}, σ_{yy}, and τ_{xy} must be considered to be stresses averaged over the laminate thickness. Here the bar denoting average has been dropped and the stresses, when applied to a laminate, will be understood to represent average stresses.

The form of the crack-tip stresses for an anisotropic plate shown in Figure 4, has been presented by Sih et al. [2] and others [3,12] using either those methods discussed by Lekhnitskii [13] or the Westergaard stress function approach [12]. Use of the equilibrium equations together with the compatibility equations results in a fourth-order governing equation. Solving this equation involves finding the roots μ_k of the characteristic equation,

$$a_{11}\mu^4 - 2a_{16}\mu^3 + (2a_{12} + a_{66})\mu^2 - 2a_{26}\mu + a_{22} = 0 \quad . \tag{17}$$

These roots are complex or purely imaginary and occur in conjugate pairs, i.e., $\mu_3 = \bar{\mu}_1$ and $\mu_4 = \bar{\mu}_2$, where the bar denotes conjugate. Omitting the details, the stresses and displacements [2] are given in the following equations for two cases: (1) the loads symmetric about the crack plane and (2) the loads skew symmetric about it.

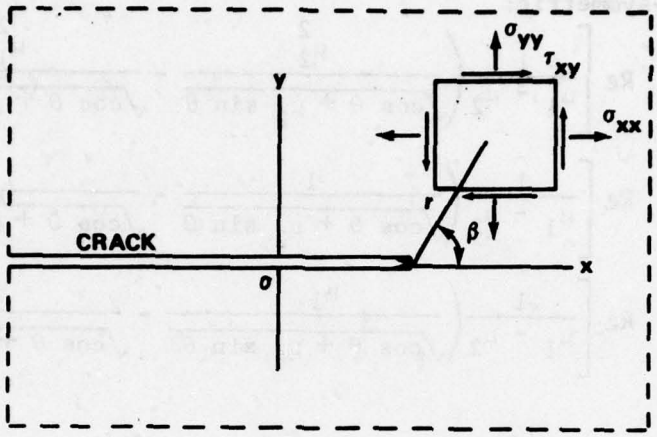

Figure 4. Stress components in the neighborhood of the crack tip.

Loads symmetric:

$$\sigma_{xx} = \frac{K_I}{\sqrt{2\pi r}} \, Re\left[\frac{\mu_1\mu_2}{\mu_1 - \mu_2}\left(\frac{\mu_2}{\sqrt{\cos\theta + \mu_2 \sin\theta}} - \frac{\mu_1}{\sqrt{\cos\theta + \mu_1 \sin\theta}}\right)\right]$$

$$\sigma_{yy} = \frac{K_I}{\sqrt{2\pi r}} \, Re\left[\frac{1}{\mu_1 - \mu_2}\left(\frac{\mu_1}{\sqrt{\cos\theta + \mu_2 \sin\theta}} - \frac{\mu_2}{\sqrt{\cos\theta + \mu_1 \sin\theta}}\right)\right]$$

$$\tau_{xy} = \frac{K_I}{\sqrt{2\pi r}} \, Re\left[\frac{\mu_1\mu_2}{\mu_1 - \mu_2}\left(\frac{1}{\sqrt{\cos\theta + \mu_1 \sin\theta}} - \frac{1}{\sqrt{\cos\theta + \mu_2 \sin\theta}}\right)\right] \tag{18}$$

and

$$u = K_I\sqrt{\frac{2r}{\pi}} \, Re\left[\frac{1}{\mu_1 - \mu_2}\left(\mu_1 p_2\sqrt{\cos\theta + \mu_2 \sin\theta} - \mu_2 p_1\sqrt{\cos\theta + \mu_1 \sin\theta}\right)\right]$$

$$v = K_I\sqrt{\frac{2r}{\pi}} \, Re\left[\frac{1}{\mu_1 - \mu_2}\left(\mu_1 q_2\sqrt{\cos\theta + \mu_2 \sin\theta} - \mu_2 q_2\sqrt{\cos\theta + \mu_1 \sin\theta}\right)\right]$$

Loads skew-symmetric:

$$\sigma_{xx} = \frac{K_{II}}{\sqrt{2\pi r}} \; Re\left[\frac{1}{\mu_1 - \mu_2}\left(\frac{\mu_2^2}{\sqrt{\cos\theta + \mu_2 \sin\theta}} - \frac{\mu_1^2}{\sqrt{\cos\theta + \mu_1 \sin\theta}}\right)\right]$$

$$\sigma_{yy} = \frac{K_{II}}{\sqrt{2\pi r}} \; Re\left[\frac{1}{\mu_1 - \mu_2}\left(\frac{1}{\sqrt{\cos\theta + \mu_2 \sin\theta}} - \frac{1}{\sqrt{\cos\theta + \mu_1 \sin\theta}}\right)\right]$$

$$\tau_{xy} = \frac{K_{II}}{\sqrt{2\pi r}} \; Re\left[\frac{1}{\mu_1 - \mu_2}\left(\frac{\mu_1}{\sqrt{\cos\theta + \mu_1 \sin\theta}} - \frac{\mu_2}{\sqrt{\cos\theta + \mu_2 \sin\theta}}\right)\right] \qquad (19)$$

and

$$u = K_{II}\sqrt{\frac{2r}{\pi}} \; Re\left[\frac{1}{\mu_1 - \mu_2}\left(p_2\sqrt{\cos\theta + \mu_2 \sin\theta} - p_1\sqrt{\cos\theta + \mu_1 \sin\theta}\right)\right]$$

$$v = K_{II}\sqrt{\frac{2r}{\pi}} \; Re\left[\frac{1}{\mu_1 - \mu_2}\left(q_2\sqrt{\cos\theta + \mu_2 \sin\theta} - q_1\sqrt{\cos\theta + \mu_1 \sin\theta}\right)\right]$$

The polar coordinates, r and θ, shown in Figure 4; μ_1 and μ_2 are roots of the characteristic equation, K_I and K_{II} are stress intensity factors, u and v are displacements in the x and y direction, respectively, and the quantities p_j and q_j are convenient combinations of certain elastic properties given by:

$$p_j = a_{11}\,\mu_j^2 + a_{12} - a_{16}\,\mu_j \quad ,$$

$$q_j = a_{12}\,\mu_j + \frac{a_{22}}{\mu_j} - a_{26} \qquad (j = 1,2) \qquad (20)$$

From Equations (18) and (19), it can be noted that the stresses exhibit a crack-tip stress singularity of $r^{-1/2}$ as in the isotropic case. The angular distribution of the stresses, that is, the variation of the stresses with θ, depends upon the material properties through the roots μ_j. The displacements also exhibit an anisotropic effect: for symmetric loading, displacements are not necessarily symmetric; for skew-symmetric loading, displacements are not necessarily skew-symmetric as in the isotropic case. This means that skew-symmetric loading causes crack opening in addition to forward sliding; symmetric loading causes crack forward sliding in addition to crack opening. This displacement effect disappears if the crack is oriented along one of the material's principal directions.

The stress intensity factors, K_I and K_{II}, represent the strength of the stress singularities. They have been defined in a way which is analogous to the isotropic case. Formulas for finding K_I and K_{II} from the appropriate stress functions are given in Reference 2. Omitting those details, consider the results for some fundamental cases. For example, the results for the geometry shown in Figure 5, a crack of length 2a in an infinite plate, are:

$$K_I = \sigma (\pi a)^{1/2}$$
$$K_{II} = 0 \quad . \tag{21}$$

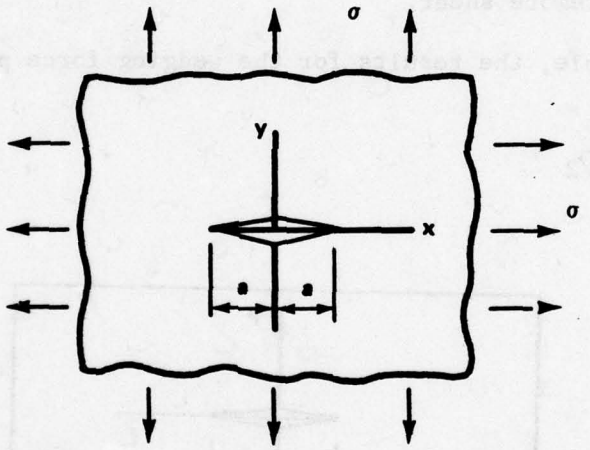

Figure 5. Tunnel or line crack in an anisotropic plate loaded with biaxial tension.

Results for the probelm in Figure 6 are:

$$K_I = 0.$$
$$K_{II} = \tau (\pi a)^{1/2} \quad . \tag{22}$$

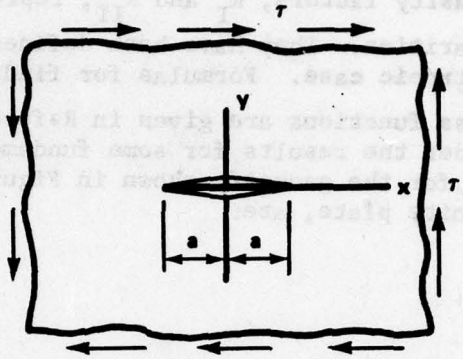

Figure 6. Tunnel or line crack in an anisotropic plate under remote shear.

As a final example, the results for the wedging force problem in Figure 7 are:

$$K_I = \frac{P}{(\pi a)^{1/2}} \qquad (23)$$

$$K_{II} = 0 \quad .$$

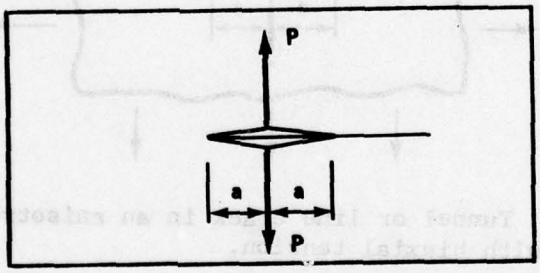

Figure 7. Tunnel or line crack with a crack surface wedging force.

It will be noted that the expressions for K_I and K_{II}, Equations (21), (22), and (23) are identical with their isotropic counterparts. They depend upon the loading and crack length the same way as for the isotropic case. For cracks in infinite anisotropic bodies where the stress resultant on the crack is zero, these results are true in general: the anisotropic stress intensity factor is the same as for the isotropic case with the same geometry and loading. In other words, the stress intensity factors are not material dependent for cracks in infinite plates. If the stress resultant on the crack surface is not zero or if stress free boundaries occur near the crack, then the anisotropic stress intensity factor will differ from the isotropic one. This latter case will be discussed in more detail later.

One must be careful in using formulas for stress intensity factors. Two similar definitions of both K_I and K_{II}, differing by the factor $\sqrt{\pi}$, are in common usage. The two definitions are normally distinguished by the use of lower-case or upper-case K; this is the notation adopted here. That is, $K_I = \sqrt{\pi}\, k_I$ and $K_{II} = \sqrt{\pi}\, k_{II}$.

The basis of the equivalence of the Griffith concept of fracture and the stress intensity approach is the relationshup between the stress intensity factor and g, the strain energy release rate. As in the isotropic case, the strain energy release rate can be determined by calculating the work done by the crack-tip stresses in closing the crack over a vanishingly small distance at the crack tip. To avoid almost insurmountable mathematical complications in performing this calculation, it is assumed that the crack extends in a collinear manner although in an anisotropic material this frequently will not be the case. If symmetric loading (Mode I) and skew-symmetric loading (Mode II) are considered separately, results are [2],

$$g_I = -\frac{K_I^2}{2}\, a_{22}\, \mathcal{I}m\left[\frac{\mu_1 + \mu_2}{\mu_1\mu_2}\right]$$
$$g_{II} = \frac{K_{II}^2}{2}\, a_{11}\, \mathcal{I}m\left[\mu_1 + \mu_2\right] \qquad (24)$$

where g_I and g_{II} are the strain energy release rates for symmetric and skew-symmetric loading, respectively. When both modes are present, then the cross-influences of the displacements cause cross-product terms of K_I and K_{II} in the expressions for g, namely,

$$g_I = -\frac{K_I}{2}\, a_{22}\, \mathcal{I}m\left[\frac{K_I\,(\mu_1 + \mu_2) + K_{II}}{\sqrt{\pi}\,\mu_1\mu_2}\right]$$
$$g_{II} = \frac{K_{II}}{2}\, a_{11}\, \mathcal{I}m\left[\frac{K_{II}}{\sqrt{\pi}}\,(\mu_1 + \mu_2) + \frac{K_I}{\sqrt{\pi}}\,\mu_1\mu_2\right] \qquad (25)$$

where

$$g_{total} = g_I + g_{II} \quad .$$

For the special case of an orthotropic material with the crack on one of the material's planes of symmetry, the two modes are independent, so that

$$g_I = K_I^2 \sqrt{\frac{a_{11}a_{22}}{2}} \left[\sqrt{\frac{a_{22}}{a_{11}}} + \frac{2\,a_{12} + a_{66}}{2\,a_{11}} \right]^{1/2}$$

$$g_{II} = K_{II}^2 \frac{a_{11}}{\sqrt{2}} \left[\sqrt{\frac{a_{22}}{a_{11}}} + \frac{2\,a_{12} + a_{66}}{2\,a_{11}} \right]^{1/2} \qquad (26)$$

$$g_{total} = g_I + g_{II} \quad .$$

In summary, it is well to note the numerous similarities between the isotropic and anisotropic cases. Equations (18) and (19) indicate that for a given material the crack-tip stress distribution for different specimen geometries will be identical, and the $r^{-1/2}$ stress singularity of isotropic materials is preserved. Furthermore, the stress intensity factor depends upon the load and specimen geometry in the same way as for isotropic problems, and is related to Griffith's strain energy release rate. In fact, as already noted, the stress intensity factor for a crack in an anisotropic plate, except for two conditions, is exactly the same as for a crack in an isotropic plate having the same loading and geometry. The two conditions are that the plate must be infinite in extent and the resultant of any loads on the crack surfaces must be zero. The finite plate effect is a detail which will be dealt with in the next article. It thus seems reasonable to assume that the stress intensity factor concept can be employed to predict fracture for anisotropic materials as is done for isotropic materials. Proof that this idea also applies to filamentary composites, which are heterogeneous as well as anisotropic, must be based upon experimental investigations of crack extension in various composites.

2.2 Effect of Finite Specimen Size

To apply conventional fracture mechanics to composite materials a knowledge of the stress intensity factor is required. This is needed both for cracked structural components under analysis for residual strength and for specimens proposed for fracture toughness testing. A considerable collection of stress intensity factor solutions already exists for isotropic materials of various geometries and loading conditions [1, 14]. Thus, it would be advantageous to understand to what extent isotropic stress intensity factors could be applied to anisotropic cases to recognize problems for which this practice would be expected to be accurate and to have a basis for judging the degree of accuracy. As mentioned before, for problems involving free boundaries near the crack tip, the stress intensity factor exhibits a dependency upon the anisotropic material properties. Solutions for such problems involve numerical techniques such as the boundary integral equation method [15, 16, 17] finite elements [18], and boundary collocation [19].

The double-edge-cracked (DEC) and the center-cracked tension (CCT) specimens are familiar fracture toughness specimens for isotropic materials. Thus it is not suprising to find that numerical work for composite laminates has been largely devoted to these specimens.

Snyder and Cruse [16] determined the finite correction factor for the CCT specimen for a number of practical laminate configurations. The lamina properties were chosen as

$$E_{11} = 21 \times 10^6 \text{ psi}$$

$$E_{22} = 1.7 \times 10^6 \text{ psi}$$

$$G_{12} = 1.4 \times 10^6 \text{ psi} \qquad (27)$$

$$\nu_{12} = 0.21$$

which are representative of graphite-epoxy. A sample of the results are shown in Table 1 and Figure 8. The lamina angles are relative to the crack direction. All results are for a plate length to width aspect ratio of 2L/W = 3. Results are given in the form,

$$Y = \frac{K_I}{\sigma\sqrt{a}} \qquad (28)$$

where Y is the finite plate width correction, K_I, is the Mode I stress intensity factor, σ is the applied stress, and a is the half crack length. The value of Y for a crack in a infinite isotropic plate is $\sqrt{\pi}$. In Table 1 the results for the isotropic case should first be compared with the quasi-isotropic laminate, $(0/\pm45/90)_s$. Except for 2a/W = 0.8, the results for the two are within a fraction of 1% of each other; therefore, the isotropic and quasi-istropic results agree well. This must be kept in mind in comparing the results on Figure 8. Note that the amount of departure of the angle-ply results from those for the quasi-isotropic case is a measure of anisotropy. All results are fairly close to isotropic (quasi-isotropic) results; with the greatest departure occurring for the $(\pm45)_s$ laminate. The results for the $(\pm45)_s$ laminate are approximately 11% higher than for the isotropic plate. The stress intensity for the $(90)_s$ laminate (fibers perpendicular to the crack) is nearly the same as for the isotropic case; the results for the $(0)_s$ laminate (fibers parallel to the crack) are slightly lower than for the isotropic case. The variation of the stress intensity with ply angle, α, for the $(\pm\alpha)_s$ laminates is shown in Figure 9 for 2a/W = 0.6.

TABLE 1. FINITE WIDTH CORRECTION FACTORS FOR CENTER-CRACKED PLATES (2L/W = 3) [16]

Material[1]	2a/W[3]	$Y = \frac{K_I}{\sigma\sqrt{a}}$
Isotropic	0.4	1.954
Isotropic	0.6	2.308
Isotropic	0.8	2.910
$(0/\pm45/90)_s$	0.4	1.962
$(0/\pm45/90)_s$	0.6	2.298
$(0/\pm45/90)_s$	0.8	3.157
$(90_2/\pm45)_s$	0.4	1.972
$(90_2/\pm45)_s$	0.6	2.323
$(90_2/\pm45)_s$	0.8	3.231
$(90_4/\pm45)_s$	0.4	1.962
$(90_4/\pm45)_s$	0.6	2.298
$(90_4/\pm45)_s$	0.8	3.177
$(90)_s$	0.4	1.977
$(90)_s$	0.6	2.296
$(90)_s$	0.8	3.111
$(\pm45)_s$	0.4	2.050
$(\pm45)_s$	0.6	2.493
$(\pm45)_s$	0.8	3.596
$(\pm30)_s$	0.4	2.011
$(\pm30)_s$	0.6	2.415
$(\pm30)_s$	0.8	3.277
$(\pm60)_s$	0.4	2.020
$(\pm60)_s$	0.6	2.430
$(\pm60)_s$	0.8	3.444
$(0)_s$	0.4	1.932
$(0)_s$	0.6	2.220
$(0)_s$	0.8	2.942
$(90)_s^2$	0.6	2.234

1. Lamina angles measured from crack axis.
2. Constant displacement applied to ends of specimen.
3. See Figure 8.

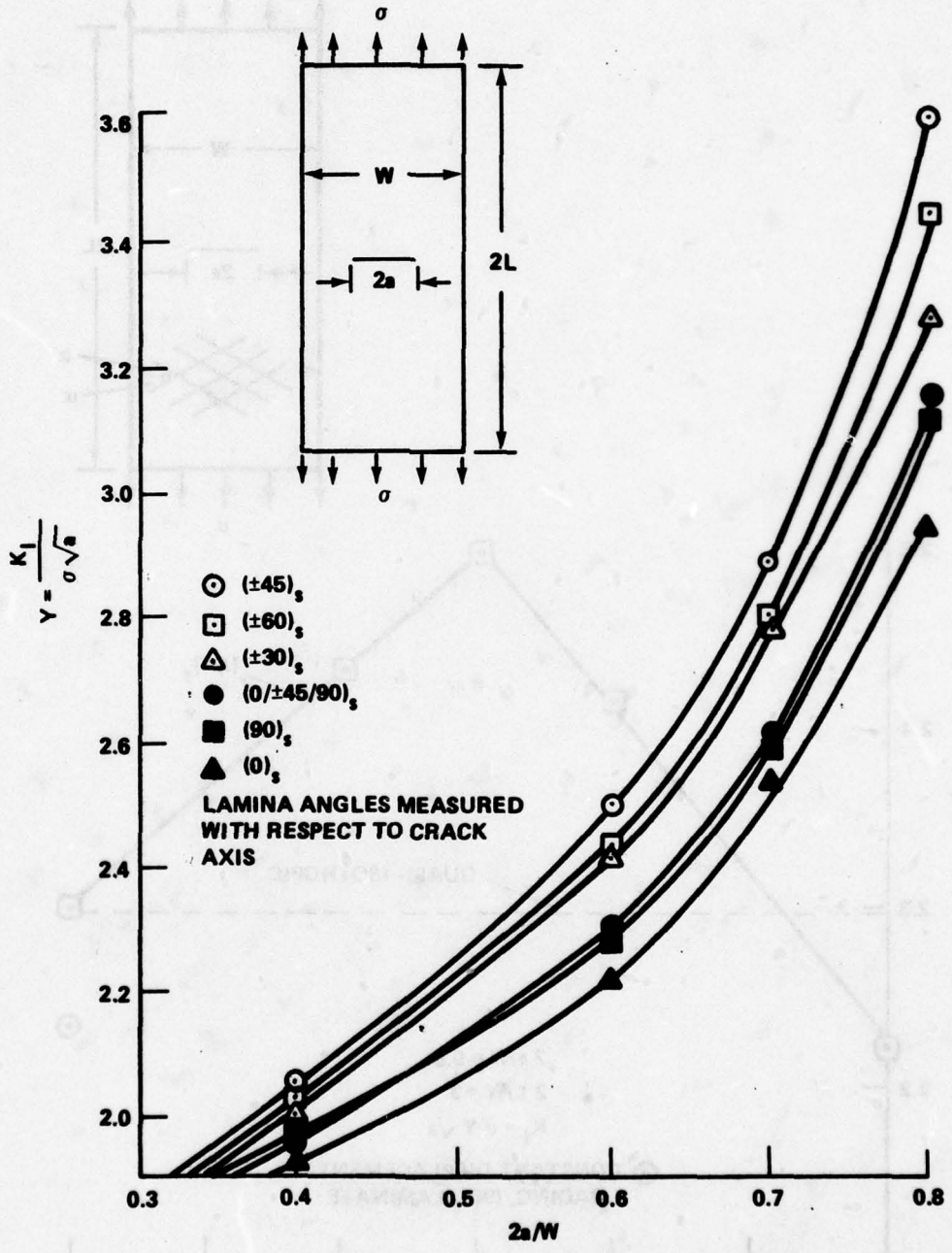

Figure 8. Finite width correction factor for graphite-epoxy center-cracked specimens (2L/W = 3) [16].

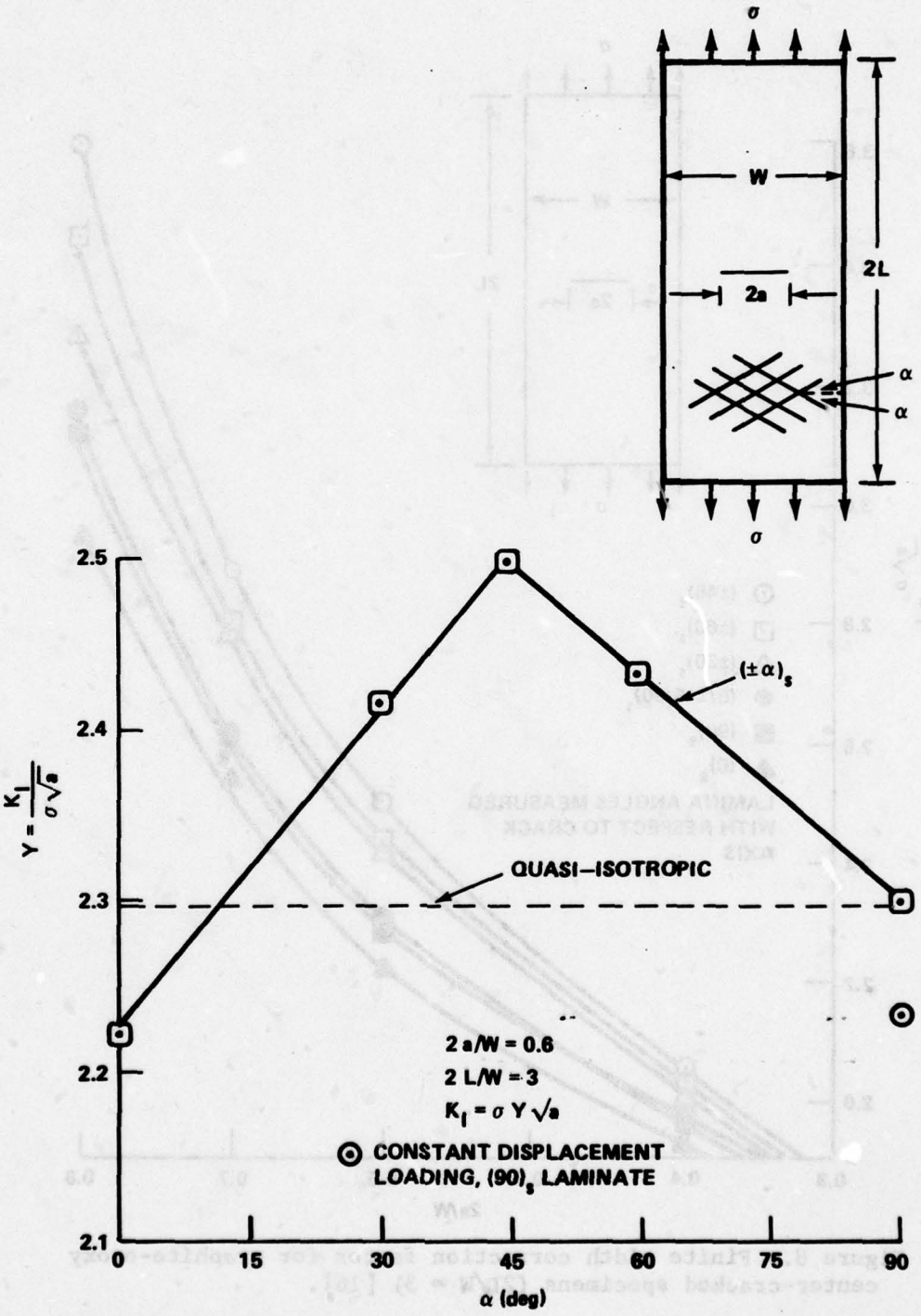

Figure 9. Finite width correction factor versus lamina angle α for angle-ply $(\pm \alpha)_s$ laminates (center-cracked specimen) [16].

Again, the greatest departure from the isotropic (quasi-isotropic) case is for $\alpha = 45°$. Snyder and Cruse [16] used both a constant displacement loading and a constant stress loading on the ends of the plate. The two cases were within 2% except for the $(90)_s$ laminate where the constant displacement loading was approximately 3% lower than the constant stress loading. For a shorter plate this difference would increase.

Konish [20] using the boundary integral technique, obtained results similar to those in Reference 16 for the CCT. His results are written in the form

$$K_I = HY^* \sigma\sqrt{a} \tag{29}$$

where Y^* is the isotropic geometry correction factor which is a function of the specimen geometry only and H is an anistrophy factor. The ratio of the anisotropic stress intensity factor and its isotropic counterpart, H, is defined by

$$H = \frac{K_I}{Y^* \sigma\sqrt{a}} = \frac{K_I:\ \text{anisotropic}}{K_I:\ \text{isotropic}} \quad . \tag{30}$$

Thus, the deviation of H from unity is a direct measure of the effect of material anisotropy on the stress intensity factor.

The variation of the anisotropy factor H with crack length and ply angle is tabulated in Table 2 and shown graphically in Figure 10 for the CCT specimen. Results are likewise given for the DEC specimen in Table 3 and Figure 11. For both specimens the properties of the graphite plies were

$$\begin{aligned} E_{11} &= 20.5 \times 10^6 \text{ psi} \\ E_{22} &= 1.37 \times 10^6 \text{ psi} \\ G_{12} &= 0.752 \times 10^6 \text{ psi} \\ \nu_{12} &= 0.31 \quad , \end{aligned} \tag{31}$$

which, except for G_{12}, are very nearly the same as those used by Snyder and Cruse [16], Equations (27). The ply angle α in Tables 2 and 3 and in Figures 10 and 11 is referred to a line perpendicular to the crack rather than parallel to the crack as in Reference 16.

The anisotropy factor H increases with crack length for the CCT specimen while it decreases with increasing crack length for the DEC

specimen. This suggests that the effect of anisotropy is strongest when the crack tip is near a free boundary. For both specimens, the severest stress intensity occurs when the plies are oriented at ±45°, which agrees with the behavior observed by Synder and Cruse [16] in Figure 9. The lowest stress intensity occurred when the fibers were either aligned with the crack ($\alpha = 90°$) or perpendicular to the crack ($\alpha = 0°$). The intensity was approximately the same for those two orientations,

TABLE 2. ANISOTROPY FACTOR IN CCT ANGLE-PLY SPECIMENS OF T300/5208 GRAPHITE/EPOXY [20]

2a/W* α*	0.1 H	0.2 H	0.3 H	0.4 H	0.5 H	0.6 H	0.7 H
$(0°)_s$	1.000	0.997	0.991	0.984	0.975	0.964	0.952
$(\pm10°)_s$	1.001	1.000	0.997	0.994	0.990	0.985	0.979
$(\pm15°)_s$	1.002	1.002	1.003	1.003	1.004	1.004	1.005
$(\pm20°)_s$	1.003	1.005	1.010	1.016	1.023	1.030	1.037
$(\pm25°)_s$	1.004	1.010	1.020	1.033	1.047	1.061	1.074
$(\pm30°)_s$	1.005	1.016	1.032	1.052	1.073	1.094	1.113
$(\pm35°)_s$	1.007	1.021	1.043	1.070	1.098	1.125	1.145
$(\pm45°)_s$	1.007	1.025	1.053	1.087	1.120	1.152	1.164
$(\pm55°)_s$	1.002	1.016	1.037	1.062	1.087	1.107	1.149
$(\pm60°)_s$	0.999	1.008	1.023	1.040	1.058	1.080	1.115
$(\pm65°)_s$	0.996	1.002	1.010	1.020	1.033	1.050	1.073
$(\pm70°)_s$	0.995	0.997	1.001	1.006	1.012	1.021	1.034
$(\pm75°)_s$	0.995	0.995	0.995	0.995	0.996	0.997	1.002
$(\pm80°)_s$	0.996	0.995	0.992	0.988	0.984	0.980	0.976
$(90°)_s$	0.998	0.995	0.990	0.983	0.974	0.964	0.952

*See Figure 10

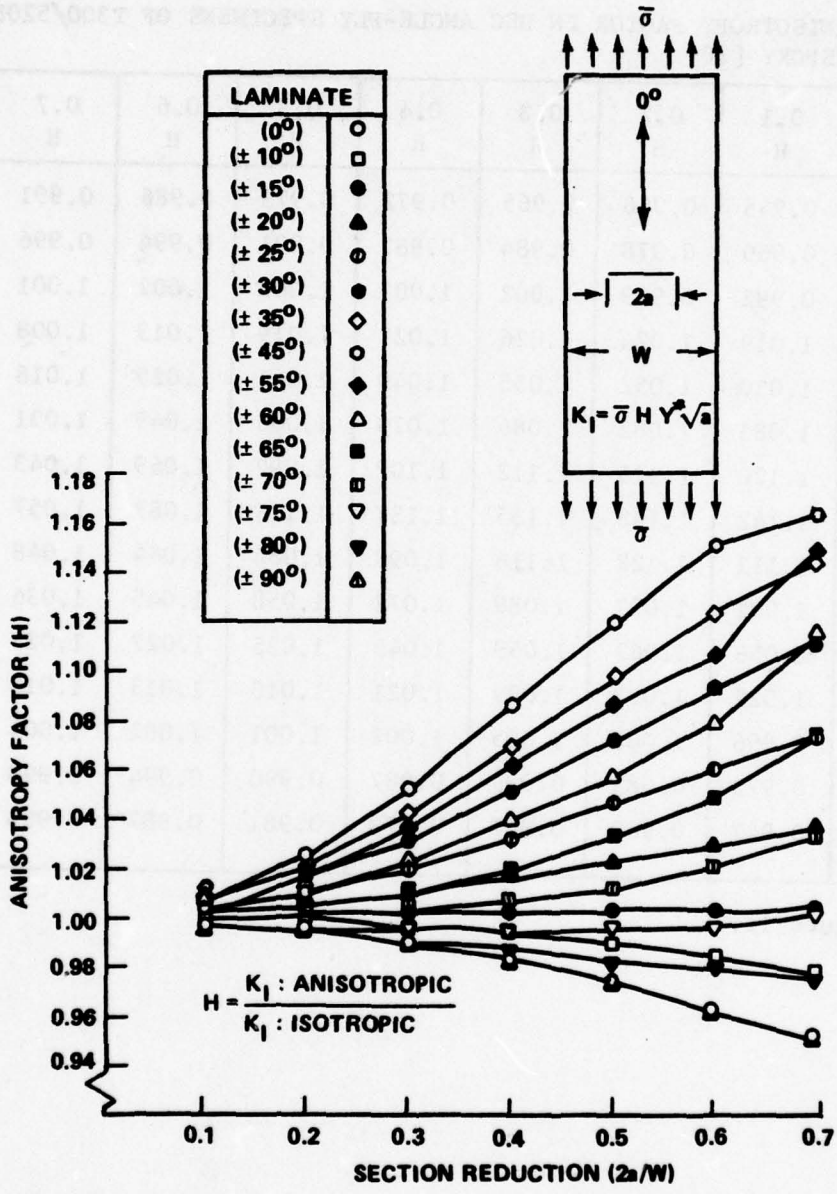

Figure 10. Anisotropy factor versus net section reduction for center-cracked specimens [20].

TABLE 3. ANISOTROPY FACTOR IN DEC ANGLE-PLY SPECIMENS OF T300/5208 GRAPHITE/EPOXY [20]

2a/W* α*	0.1 H	0.2 H	0.3 H	0.4 H	0.5 H	0.6 H	0.7 H
$(0°)_s$	0.945	0.956	0.965	0.972	0.979	0.986	0.991
$(\pm10°)_s$	0.969	0.978	0.984	0.987	0.991	0.994	0.996
$(\pm15°)_s$	0.992	0.999	1.002	1.003	1.003	1.002	1.001
$(\pm20°)_s$	1.019	1.024	1.026	1.023	1.019	1.013	1.008
$(\pm25°)_s$	1.050	1.052	1.055	1.049	1.041	1.029	1.018
$(\pm30°)_s$	1.083	1.082	1.086	1.079	1.066	1.049	1.031
$(\pm35°)_s$	1.120	1.115	1.112	1.107	1.092	1.069	1.043
$(\pm45°)_s$	1.142	1.148	1.135	1.131	1.116	1.087	1.057
$(\pm55°)_s$	1.112	1.122	1.116	1.098	1.084	1.064	1.048
$(\pm60°)_s$	1.092	1.097	1.089	1.072	1.058	1.045	1.036
$(\pm65°)_s$	1.056	1.067	1.059	1.045	1.035	1.027	1.023
$(\pm70°)_s$	1.022	1.037	1.029	1.021	1.016	1.013	1.012
$(\pm75°)_s$	0.996	1.008	1.005	1.002	1.001	1.002	1.004
$(\pm80°)_s$	0.973	0.985	0.986	0.987	0.990	0.994	0.998
$(90°)_s$	0.947	0.960	0.967	0.973	0.981	0.987	0.993

*See Figure 11.

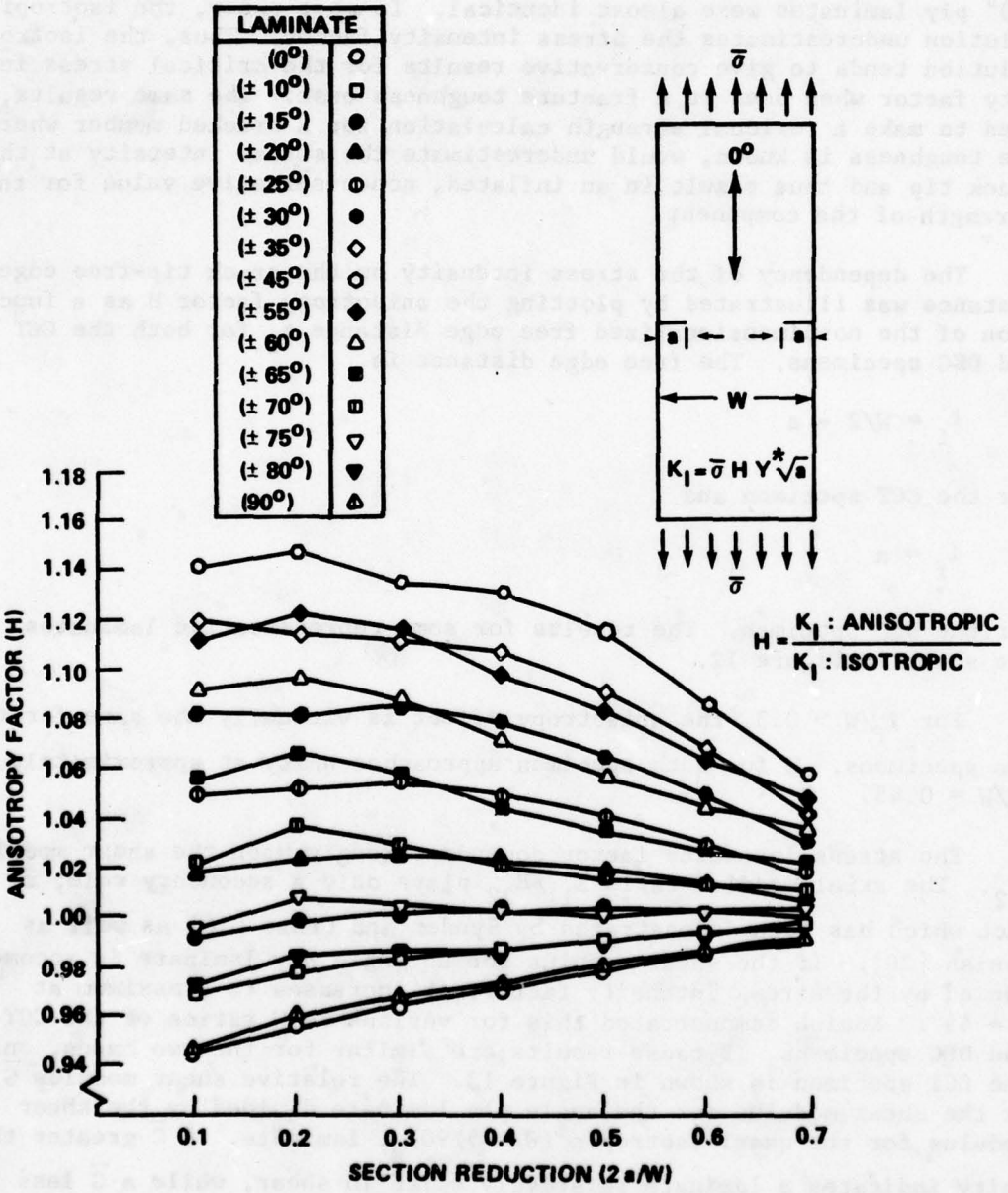

Figure 11. Anisotropy factor versus net section reduction for DEC specimens [20].

again in agreement with Reference 16, Figure 8. The stress intensity factor for a given ply orientation angle and that angle's complement were approximately the same. For example, the values for the ±10° and ±80° ply laminates were almost identical. In most cases, the isotropic solution underestimates the stress intensity factor. Thus, the isotropic solution tends to give conservative results for the critical stress intensity factor when used in a fracture toughness test. The same results, used to make a residual strength calculation for a cracked member where the toughness is known, would underestimate the stress intensity at the crack tip and thus result in an inflated, nonconservative value for the strength of the component.

The dependency of the stress intensity on the crack tip-free edge distance was illustrated by plotting the anisotropy factor H as a function of the nondimensionalized free edge distance ℓ_f for both the CCT and DEC specimens. The free edge distance is

$$\ell_f = W/2 - a$$

for the CCT specimen and

$$\ell_f = a$$

for the DEC specimen. The results for some representative laminates are shown in Figure 12.

For $\ell_f/W > 0.3$, the anisotropy effect is virtually the same for the two specimens. H for both specimen approaches unity at approximately $\ell_f/W = 0.45$.

The stress intensity factor depends strongly upon the shear modulus G_{12}. The axial modulus ratio E_{11}/E_{22} plays only a secondary role, a fact which has been demonstrated by Synder and Cruse [16] as well as Konish [20]. If the shear modulus for an angle ply laminate is accompanied by the stress intensity factor, it increases to a maximum at $\alpha = 45°$. Konish demonstrated this for various 2a/W ratios of the CCT and DEC specimens. Because results are similar for the two cases, only the CCT specimen is shown in Figure 13. The relative shear modulus $\bar{G}$ is the shear modulus for the angle ply laminate divided by the shear modulus for the quasi-isotropic $(0/\pm45/90)_s$, laminate. A $\bar{G}$ greater than unity indicates a laminate relatively stiff in shear, while a $\bar{G}$ less than unity indicates a laminate relatively soft in shear. It can be seen in Figure 13 that for laminates stiff in shear ($G > 1$), the stress intensity exceeds the isotropic value; for laminates soft in shear, the stress intensity is lower than the isotropic value.

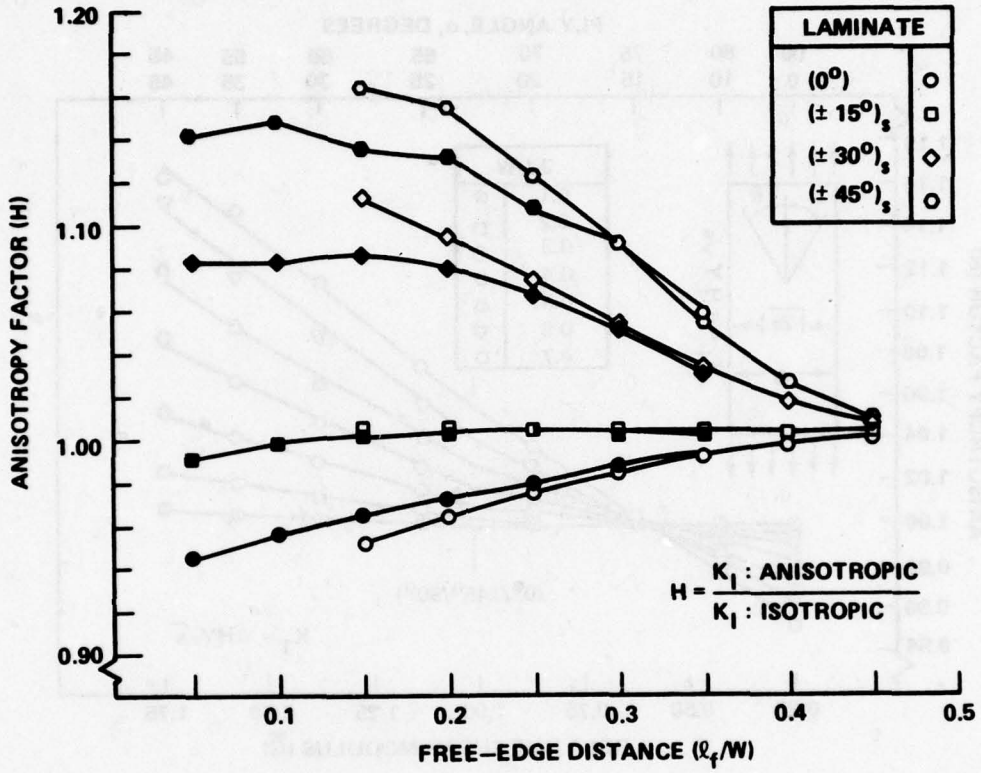

Figure 12. Anisotropy factor versus free-edge distance for representative laminates. Open points denote center-cracked specimens; filled points denote DEC specimens [20].

Figure 14 shows a comparison of results obtained by Osias and Cruse [15] and Konish [20] for the CCT specimen with fibers at ±45°. The material properties were slightly different. The properties of Equations (31) were used in Reference 20 while properties of Equations (15) were used in Reference 15. The G_{12} used by Osias and Cruse [15] was approximately twice that used by Konish [20]; hence, the Osias-Cruse results should be higher than those of Konish. However, that is not the case; the Konish results are slightly higher. There is little practical difference between the two: compare H = 1.10 to H = 1.16 for a/b = 0.7. It should be kept in mind that the greatest departure from the isotropic value occurs for the present case, i.e., when the fibers are at an angle of ±45°.

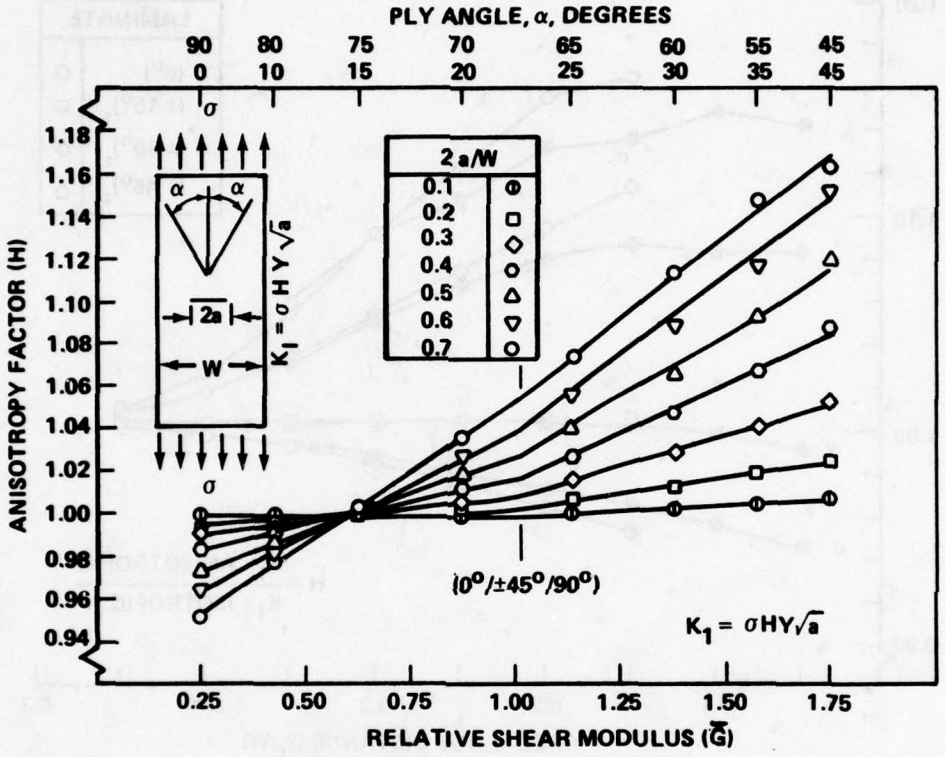

Figure 13. Anisotropy factor versus relative shear modulus for center-cracked specimens [20].

Thus far, the discussion has indicated that the anisotropy effect on the stress intensity is not extremely large. It must be pointed out though that the numerical results are not in universal agreement with this. For example, consider the boundary collocation results of Bowie and Freese [19] for the square orthotropic CCT specimen in Figure 15. For values of E_x/E_y greater than unity, results for different cracks lengths are only moderately lower than for an isotropic case, but for values of E_x/E_y less than unity, that is, with the stiff axis perpendicular to the crack, the stress intensity increases sharply to values considerably above the isotropic. Furthermore, for a/b = 0.4, the results have been verified by Atluri et al. [18] using the finite element technique. The reason for the behavior exhibited in Figure 15 can perhaps be explained by two effects. First, the plate is square, which, compared to a long plate, increases the finite correction. The second effect is related to the material properties. The problem was formulated in terms of two material

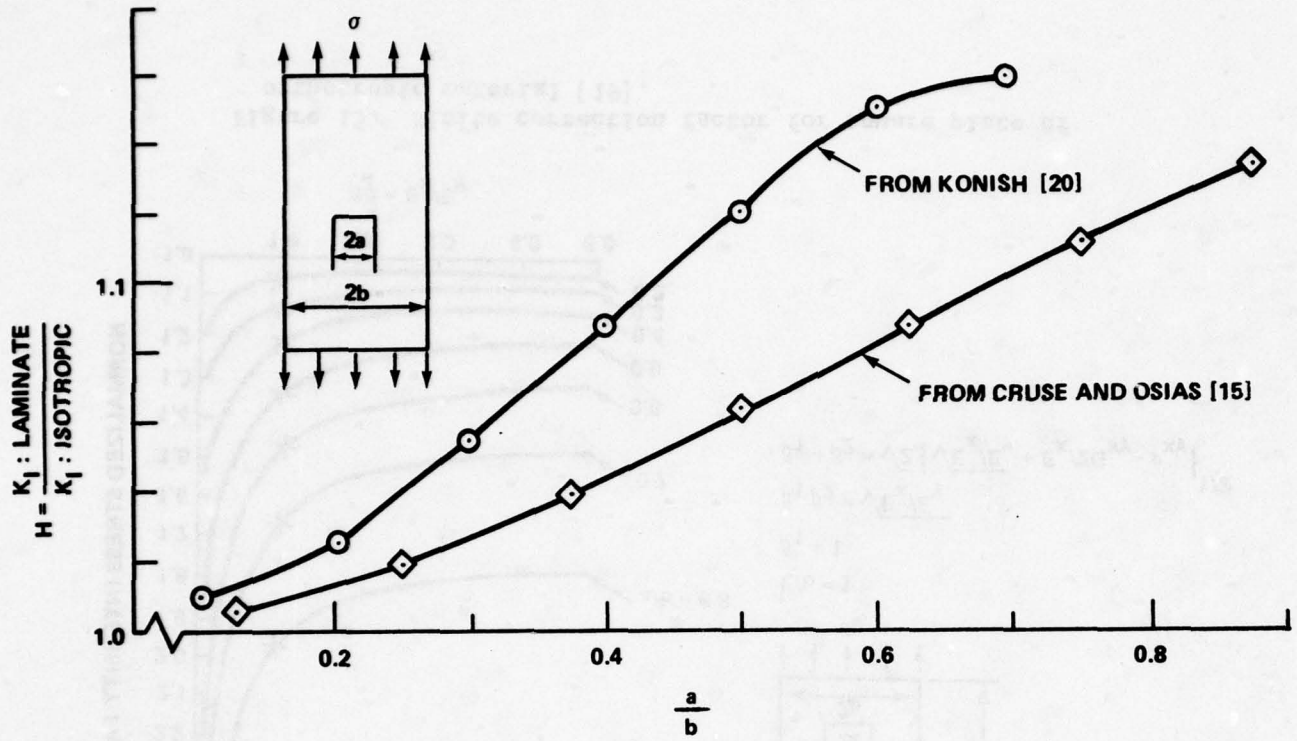

Figure 14. Anisotropic effects for a center-cracked $(\pm 45)_s$ laminate plate.

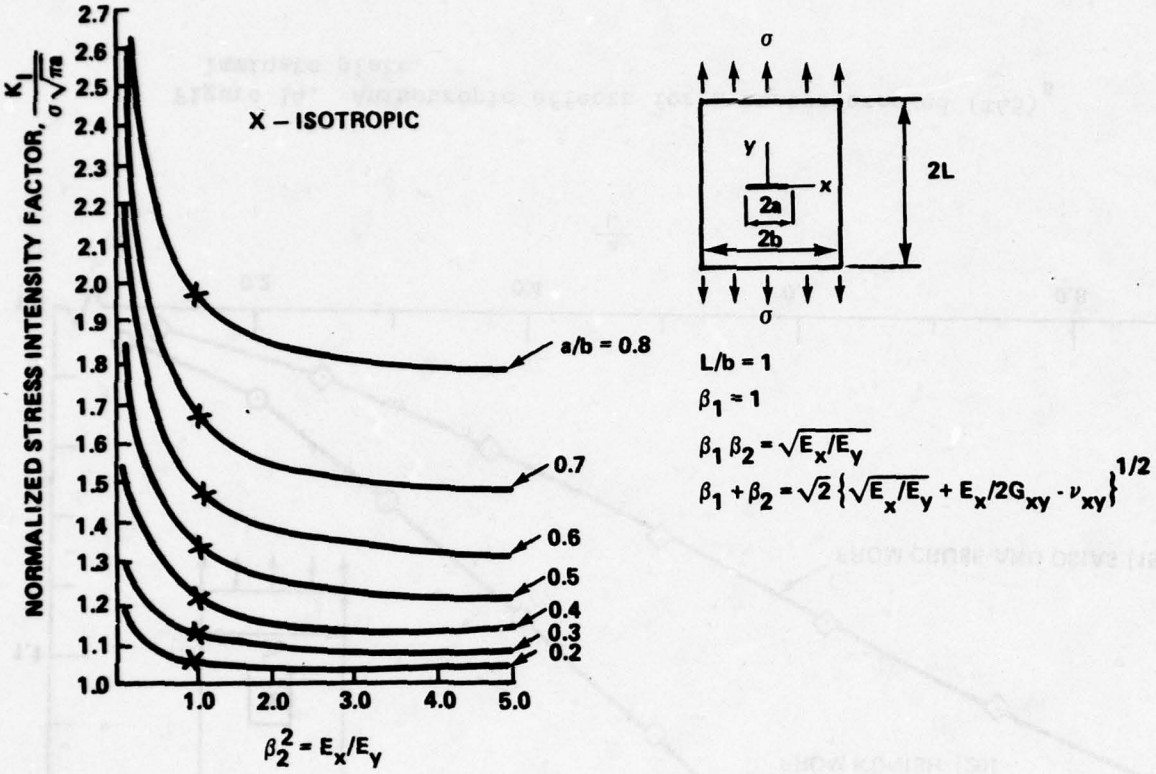

Figure 15. Finite correction factor for square plate of orthotropic material [19].

constants, β_1 and β_2, which are combinations of the four orthotropic material constants E_x, E_y, G_{xy} and ν_{xy}, i.e.,

$$\beta_1\beta_2 = \sqrt{E_x/E_y}$$

$$\beta_1 + \beta_2 = \sqrt{2}\left\{\sqrt{E_x/E_y} + E_x/2G_{xy} - \nu_{xy}\right\}^{1/2} \quad . \tag{32}$$

Elastic constants for real materials were not chosen. Instead, relative values of β_1 and β_2 were used, i.e., $\beta_1 = 1$ was chosen, which leads to $\beta_2^2 = E_x/E_y$. The solution was then completed by choosing values of $\beta_2(E_x/E_y)$. This left the shear modulus, G_{xy}, and Poisson's ratio, ν_{xy}, unspecified. Their values, however, are implied by the second of Equations (32). In fact, if a typical value for Poisson's ratio is assumed and G_{xy} is calculated in terms of either E_x or E_y for $E_x/E_t = 0.3$, G_{xy} turns out to be larger by a factor of four or five than a unidirectional graphite epoxy laminate. In other words, picking specific values of β_1 and β_2 in some cases implies a shear stiffness which is artifically high compared to real materials. It has already been noted, based on the work of Konish [20] as well as others [15, 16], that high values of shear stiffness lead to high anisotropy factors as shown in Figure 13.

The work of Konish [20], Snyder and Cruse [16], and Osias and Cruse [15], indicates that the anisotry factor for angle plies is greatest when $\alpha = \pm 45°$. A finite element solution obtained by Mandell [21] disagrees with this. Figure 16 shows a comparison of the stress intensity from the finite element technique [21] compared to the boundary integral equation method [20]. The two methods agree fairly well from 0° to approximately 30° and from 75° to 90°, but disagree sharply in the region from 30° to 75°. In fact, the finite element results show the stress intensity to decrease to a minimum value at approximately $\alpha = 50°$, near the place where the maximum occurs according to the boundary integral equation method [20]. The reason for the disagreement is not known; more numerical work will be needed to settle the issue completely. It is believed that because the boundary integral equation technique has been widely applied to anisotropic crack problems by several researchers, a great deal of confidence can be placed in it.

The effect of plate length to width aspect ratio for a DEC specimen was illustrated by Atluri, et al. [18]. The results for fibers either parallel or perpendicular to the crack are shown in Figure 17 for a length to width ratio, L/b, of 4. These results agree with the behavior found by Konish and noted already: for low a/b the isotropic solution would overestimate the stress intensity; for large a/b the isotropic and anisotropic cases converge. Figure 18 for L/b = 1 (square plate) tells a different story. With the material's stiff axis parallel to the crack

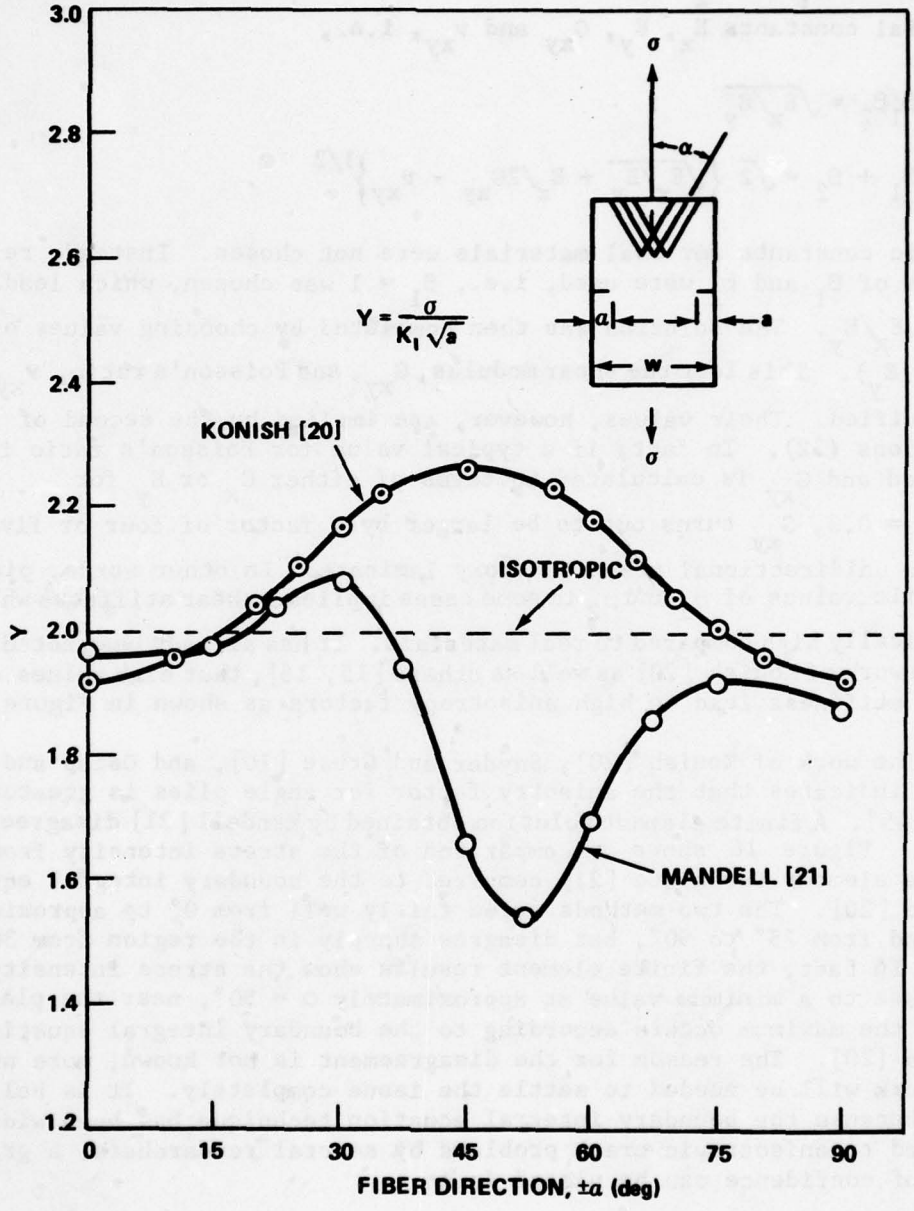

Figure 16. K-Calibration for various ply orientations (double-edge-notched specimens, graphite/epoxy, 2a/W = 0.3).

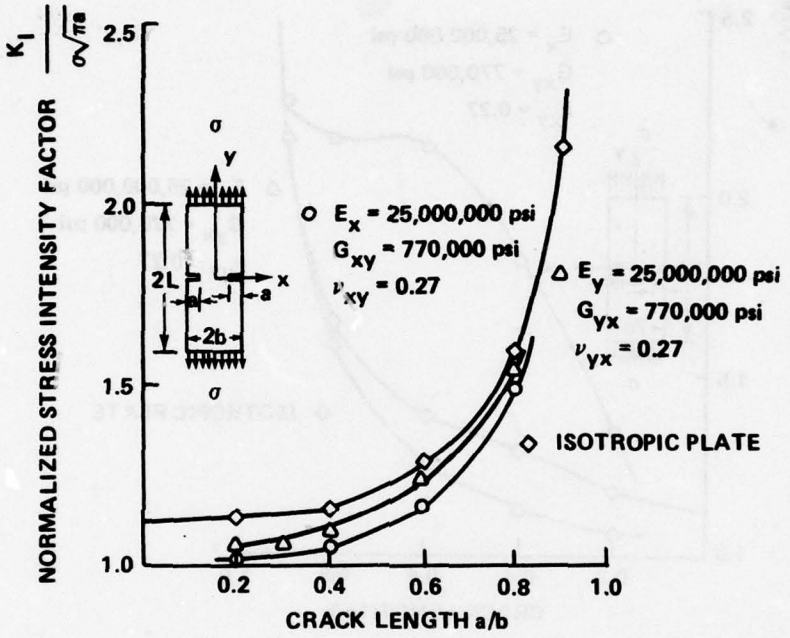

Figure 17. Stress intensity factor in an orthotropic tension plate with double external cracks. Material principal directions parallel to geometric axes of symmetry. (L/b = 4) [18].

the anisotropic stress intensity factor is as much as 50% greater than the isotropic value. Whereas the isotropic case is not very sensitive to the aspect ratio, a/b, (compare the isotropic solution in Figure 17 with that in Figure 18) the anisotropic solution is very sensitive. While this indicates that a great deal of caution must be exercised when using isotropic solutions for unidirectional laminates, it should be kept in mind that L/b = 1 is a rather severe aspect ratio—one that for testing purposes could easily be avoided. With the material's stiff axis perpendicular to the crack, the isotropic solution once again gives a conservative estimate of the anisotropic stress intensity factor.

For all examples considered thus far, the crack line has coincided with one of the laminate's principle axes. Atluri et al. [18] studied the stress intensity behavior in the DEC specimen with the principal axes at either +45° or -45° to the crack line as shown in Figure 19.

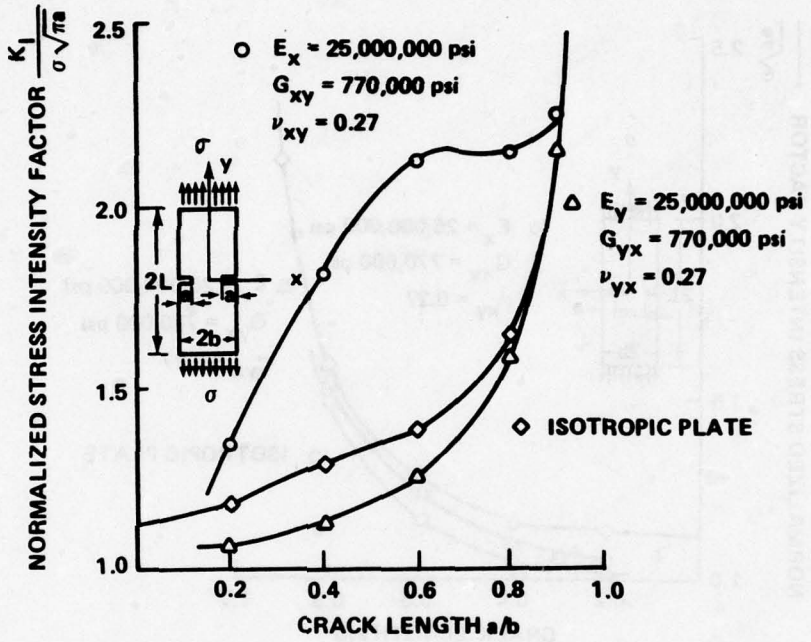

Figure 18. Stress intensity factor in an orthotropic tension plate with double external cracks. Material principal directions parallel to geometric axes of symmetry. (L/b = 1) [18].

The laminate corresponds to a graphite-epoxy material. For this problem, which lacks the symmetry of the previous examples, a value of K_{II} exists also. The greatest departure of K_I from the isotropic case and the largest value of K_{II} occur at approximately the same location, a/b = 0.4. It should be noted that even though this problem represents a severe example in terms of material directionality and fiber orientation to the crack, for a/b > 0.6, the isotropic and anistropic solutions for K_I agree quite closely.

2.3 Mixed Orthotropic Laminates

Results so far have been restricted to either unidirectional or angle ply laminates. In practice, a mixed type of orthotropic laminate is frequently encountered. It is reasonable to expect that the effect of anisotropy would be less for these materials because they are less directional. Figure 20 [15] confirms this, where a (±45) laminate for a CCT specimen is compared with three mixed laminates. The isotropic solution is within approximately 4% of the three mixed laminates. Data [20] for several mixed orthotropic laminates of various component materials

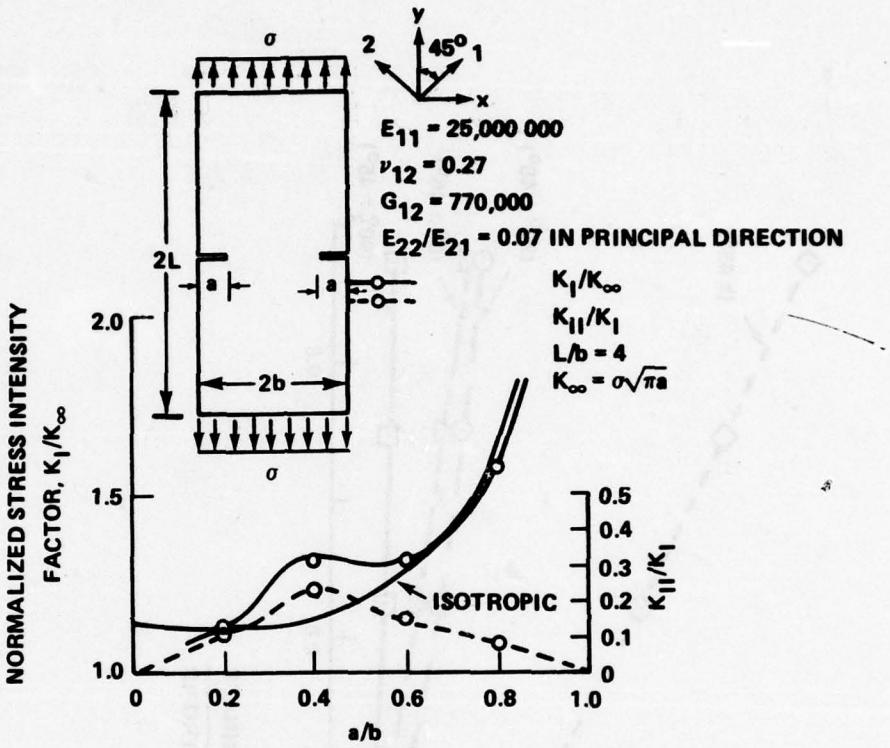

Figure 19. Stress intensity factor in an orthotropic tension plate with double external cracks. Material principal directions 45° to geometric axes of symmetry [18].

are shown in Tables 4 and 5. Again, the isotropic solution is seen to be within 4% of correct results and indeed for most cases within 1%.

A number of problems were solved by Cruse and Osias [15] for circular and elliptical holes with symmetric radial cracks contained in plates of mixed laminates. An example is shown in Figure 21. The anisotropy factor for a ±45° laminate is compared with three mixed laminates. Except for small crack length, a, the quantity H is near unity for the three mixed laminates. Again, it can be seen that the (±45) laminate deviates the most from isotropic behavior, being approximately 10% higher than the isotropic solution. It is important to note the behavior for the short cracks. As the crack first penetrates the hole's edge, the anisotropic solution either overshoots or undershoots the isotropic value on the order of 10%. As the crack grows in length, the solution (for the mixed laminates) approaches the isotropic solution. Thus, Figure 21 indicates that when making residual strength caluclations for short edge cracks, a great deal of caution is required. If most of the fibers are perpendicular to the crack, then the calculated isotropic stress intensity should perhaps be increased by approximately 10% for a conservative

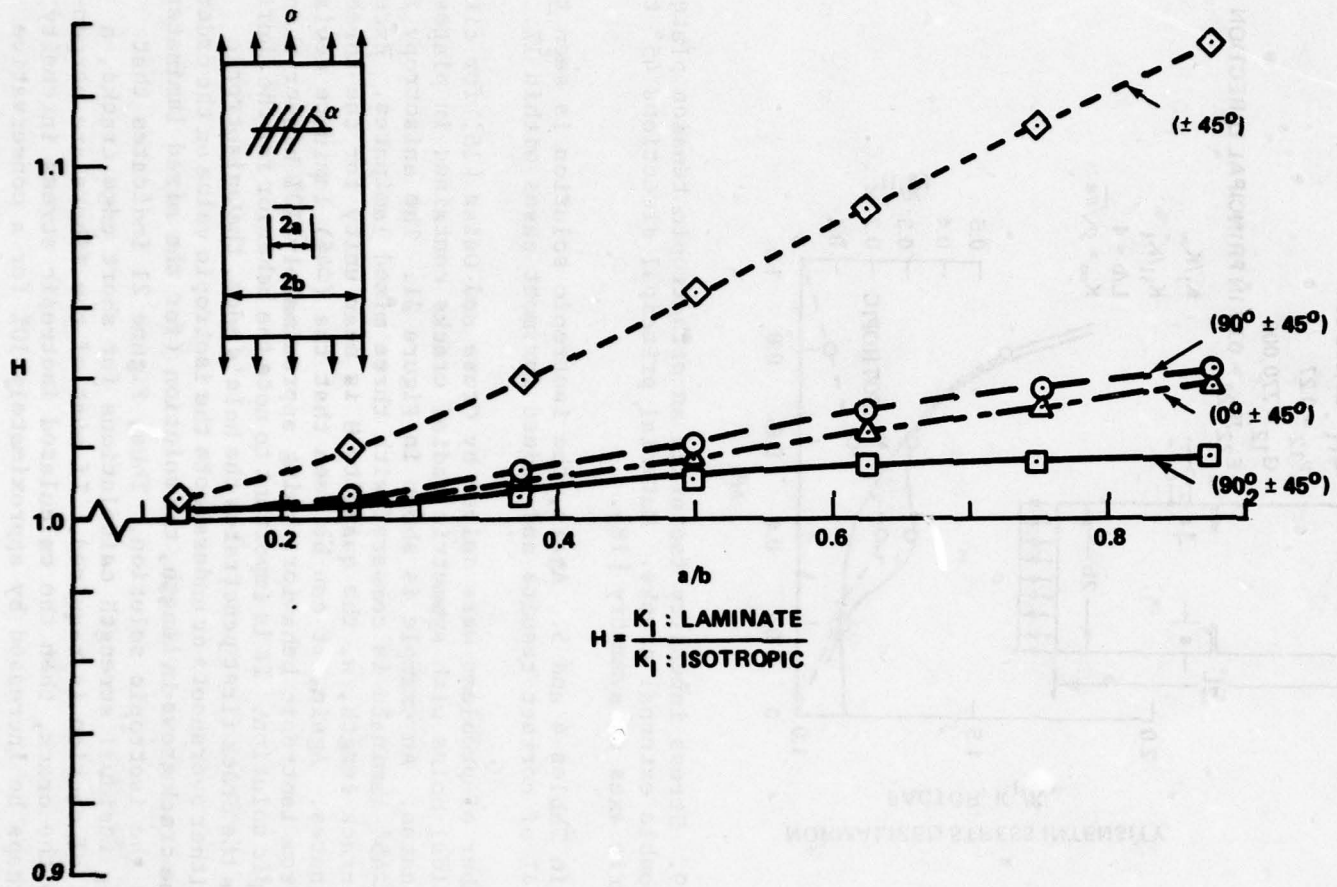

Figure 20. Anisotropic effects for center-cracked plate [15].

TABLE 4. ANISOTROPY FACTOR IN DEC SPECIMENS OF MIXED ORTHOTROPIC LAMINATES [20]

a Material 2a/W*	$(0°/\pm45°)_s$ HTS H	$(0°_2/\pm45°)_s$ Boron/Epoxy H	$(0°_2/\pm45°)_s$ HTS H	$(0°_2/\pm45°)_s$ Glass/Epoxy H	$(0°_4/\pm45°)_s$ HTS H
0.1	1.040	1.010	1.010	1.003	0.997
0.2	1.037	1.012	1.012	1.004	0.992
0.3	1.037	1.014	1.014	1.006	0.995
0.4	1.033	1.013	1.013	1.006	0.997
0.5	1.030	1.014	1.014	1.008	1.001
0.6	1.018	1.007	1.006	1.003	0.998
0.7	1.011	1.004	1.004	1.002	0.998

See Figure 11./

TABLE 5. ANISOTROPY FACTOR IN CCT SPECIMENS OF MIXED ORTHOTROPIC LAMINATES [20]

a Material 2a/W	$(0°/\pm45°)_s$ HTS H	$(0°_2/\pm45°)_s$ Boron/Epoxy H	$(0°_2/\pm45°)_s$ HTS H	$(0°_2/\pm45°)_s$ Glass/Epoxy H	$(0°_4/\pm45°)_s$ HTS H
0.1	1.002	1.002	1.002	1.001	1.001
0.2	1.006	1.003	1.003	1.001	1.001
0.3	1.012	1.005	1.005	1.002	1.000
0.4	1.019	1.008	1.008	1.003	0.999
0.5	1.028	1.011	1.011	1.004	0.998
0.6	1.037	1.014	1.014	1.005	0.996
0.7	1.045	1.017	1.017	1.006	0.994

*See Figure 10.

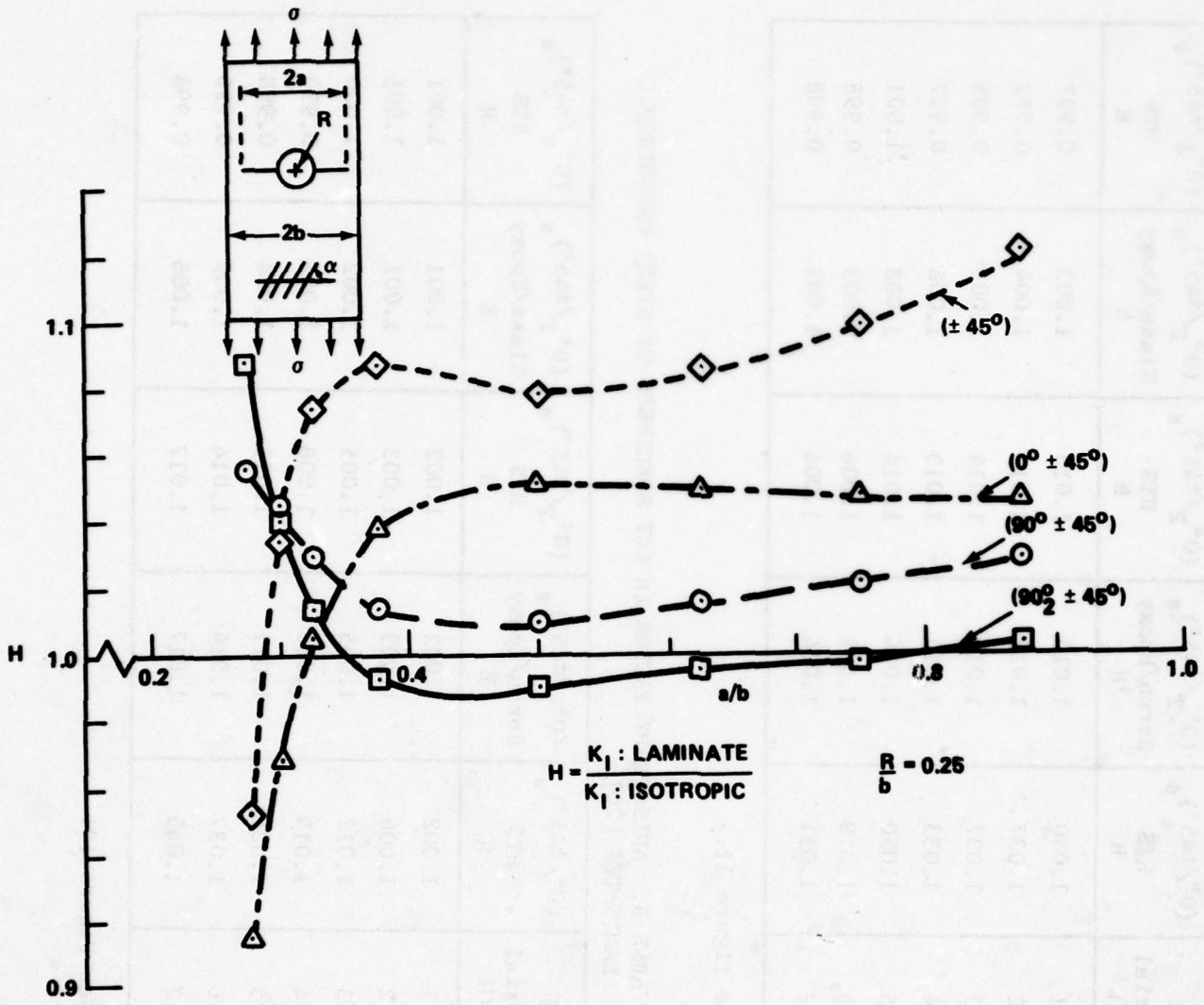

Figure 21. Anisotropic effects for small circular notched plate [15].

strength estimate. For engineering calculations a similar approximate correction could also be applied to the isotropic solution for (±45) laminates (except for extremely short edge cracks), but for most mixed laminates the isotropic solution appears to be sufficiently accurate for most practical applications.

The effect of short cracks at the edge of a hole is also illustrated in Figure 22 for a specific hole radius of 0.15 in. in several mixed laminates. The values were calculated by Bowie and Freese but were included via personal communication in a report by Olster and Woodbury [22]. The results [22] were used for making residual strength calculations of panels damaged by ballistic impact (Chapter 5). For all laminates, the material properties increase the stress intensity above the isotropic value; but as the crack grows, the laminate values approach the isotropic solution.

Chapter 3. FUNDAMENTAL FRACTURE CRITERIA

As seen in Chapter 2, within the framework of fiber-reinforced laminate theory where it is assumed that filamentary laminates behave in a homogeneous and anisotropic manner, the stress analysis for cracks presents no serious obstacle. The physical process of crack extension in a laminate, however, tends to be very complicated; many modes of failure are possible. In a unidirectional composite, the crack most frequently extends collinearly in the direction of the fibers; in a cross-ply laminate, the crack frequently extends in an irregular manner following the fibers of one ply for a distance and then turning to follow the fibers of a cross ply. Delamination of the lamina may occur in the crack-tip region. Resulting fracture surfaces range from smooth to the "shaving brush" type. Obviously, the heterogeneity of the laminate strongly influences the crack behavior. In light of this, the question is: Is it possible to characterize the fracture behavior of filamentary composites using the theory of linear elastic fracture mechanics (LEFM) along with its assumption of homogeneity? Considerable supporting evidence of this idea now exists—evidence shows that conventional fracture mechanics can indeed be used to predict the strength of cracked (notched) laminates.

3.1 Fracture of Unidirectional Composites

The discussion in this section is limited to the fracture behavior of a unidirectional laminate containing a crack oriented along the fiber direction. Admittedly a special case, the validity of LEFM applied to unidirectional laminates is fundamental to the more general question of the validity of LEFM for built-up laminates. A series of tests was conducted by Wu [5, 6] to determine under what conditions LEFM could be applied to the fracture of unidirectional composites. His specific experimental objectives were as follows:

a) To determine the mode of crack extension in the presense of both symmetric and skew symmetric loads.

b) To determine if the concept of critical k_I and k_{II} could be applied.

c) To determine a fracture criterion for the case of combined mode.

Two materials were used in the tests: balsa wood sheets and fiber glass reinforced epoxy sheets known as Scotch Ply 1002.

The balsa wood sheets, 0.0625 in. thick, and the Scotchply sheets, 0.05 in. thick, were both prepared with artificial flaws oriented along the grain or fiber direction. The balsa wood plates were loaded to failure using the four load paths shown in Figure 23; and the Scotchply was loaded to failure using load paths No. 1, 2, and 4. Thus, the flawed plates were tested with tension normal to the crack; a combination of

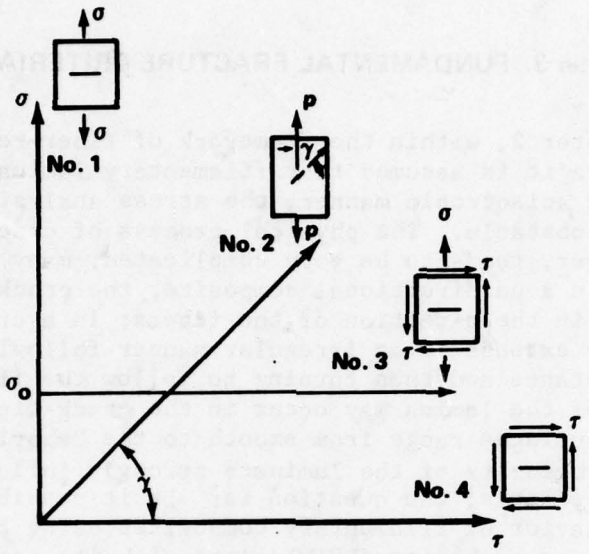

Figure 23. Load paths used by Wu [5, 6].

tension and shear, and pure shear. To prevent buckling in shear, the balsa wood sheets were clamped between glass plates; the Scotchply sheets were clamped between Teflon-lined plastic plates. There were several reasons for oreinting the flaw along the grain. The orientation of the flaw must be known to find k_I or k_{II} and the preferred orientation of a natural flaw is along the fibers. Also there was a consideration of displacements; the stress intensity factor for the anisotropic case is consistent with the isotropic case insofar as stress distribution is concerned, but not for displacements, i.e., a symmetric load can produce skew-symmetric displacements and a skew symmetric load can cause crack opening. This effect disappears if the crack is along one of the material's principal directions. Moreover, the extreme of the critical stress intensity factor should occur when the crack is oriented along one of the principal directions.

For all load paths including pure shear, the crack propagated collinearly along the direction of the fibers. To determine if critical values of k_I and k_{II} are indeed material constants, it is necessary to determine their form in terms of crack length and load. For example, for load path No. 1, $K_I = \sigma\sqrt{a}$, $K_{II} = 0$ (recall that $K_I = \sqrt{\pi}\, K_I$ and $K_{II} = \sqrt{\pi}\, k_{II}$). Thus, if critical k_I is a material constant, then the critical stress should be proportional to (critical crack length)$^{1/2}$. Thus, a plot of critical stress versus critical crack length on a log-log scale should result in a straight line with a slope m of -1/2.

Wu plotted the critical stress (either the critical normal stress or the critical shear stress component as appropriate to the load path) versus critical crack length and fitted the data with a straight line of slope m. Figure 24 shows the results for load path No. 1 (tension) for both balsa wood and Scotch Ply 1002. The values of m for all load paths ranged from -0.47 to -0.55 for balsa wood and from -0.46 to -0.50 for Scotch Ply, in both cases very near the value of -1/2. Thus, it was concluded that k_{IC} and k_{IIC} were indeed material constants.

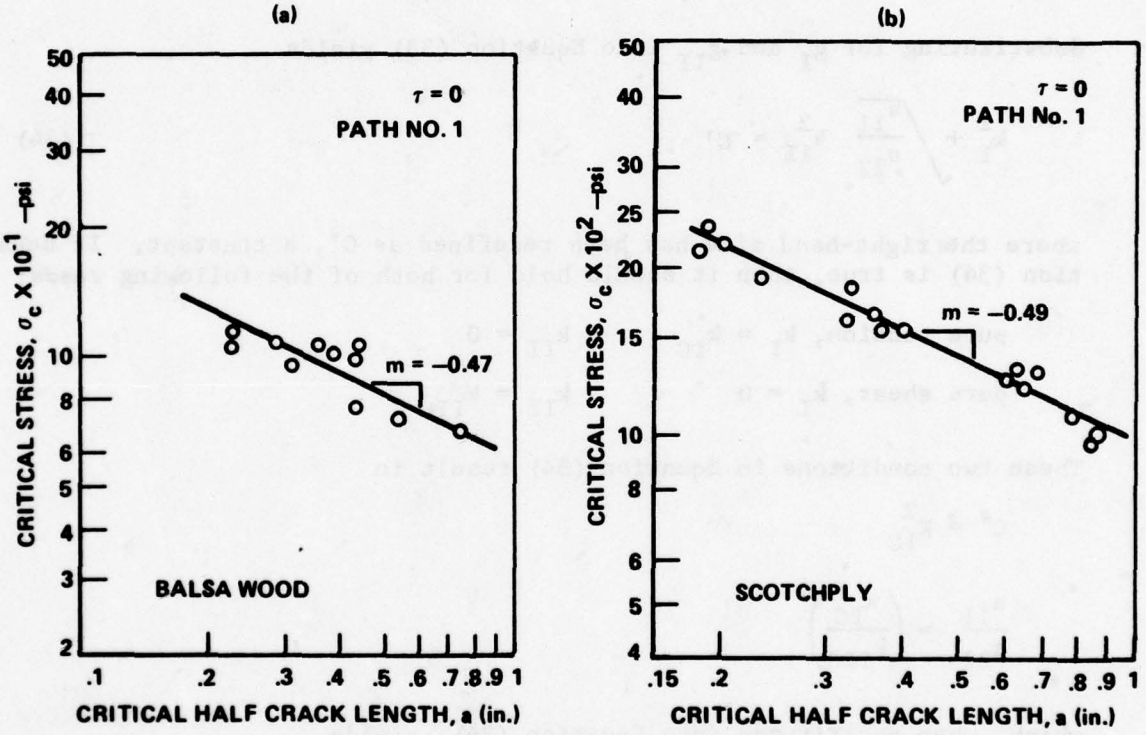

Figure 24. Result of tension tests for balsa wood and fiber reinforced epoxy (Scotchply 1002) [5].

An extending crack in an isotropic plate, typically turns to a direction normal to the greatest applied principal stress. But the crack in these experiments extended collinearly under a combination of Mode I and Mode II. Thus, unlike the isotropic case, it becomes important to determine a fracture criterion for combined mode extension. Wu [6] considered the maximum energy release rate criterion of Irwin [23].

$$g_I + g_{II} = g_C = \text{constant} \tag{33}$$

where from Equations (14)

$$g_I = \pi k_I^2 \sqrt{\frac{a_{22}a_{11}}{2}}\left[\sqrt{\frac{a_{22}}{a_{11}}} + \frac{2\,a_{12} + a_{66}}{2\,a_{11}}\right]^{1/2}$$

$$g_{II} = \pi k_{II}^2 \frac{a_{11}}{\sqrt{2}}\left[\sqrt{\frac{a_{22}}{a_{11}}} + \frac{2\,a_{12} + a_{66}}{2\,a_{11}}\right]^{1/2}$$

Substituting for g_I and g_{II} into Equation (33) yields

$$k_I^2 + \sqrt{\frac{a_{11}}{a_{22}}}\; k_{II}^2 = C' \qquad (34)$$

where the right-hand side has been redefined as C', a constant. If Equation (34) is true, then it should hold for both of the following cases:

pure tension, $k_I = k_{IC}$ $\qquad$ $k_{II} = 0$

pure shear, $k_I = 0$ $\qquad$ $k_{II} = k_{IIC}$

These two conditions in Equation (34) result in

$$C' = K_{IC}^2$$

$$\frac{a_{11}}{a_{22}} = \left(\frac{k_{IC}}{k_{IIC}}\right)^4$$

which, when substituted into Equation (34), yields

$$\left(\frac{k_I}{k_{IC}}\right)^2 + \left(\frac{k_{II}}{k_{IIC}}\right)^2 = 1 \qquad (35)$$

This is the energy release rate criterion in terms of stress intensity factors. Figure 25 shows the values of failure of k_I and k_{II} for the Scotchply material tested by Wu. It is instructive to compare the data with the strain energy release rate criterion, Equation (33) or equivalently, Equation (34). Let the right-hand side be given by k_{IC}^2 and use the value reported by Wu for k_{IC} of 930 psi-(in.)$^{1/2}$. Further, Wu reported $a_{11}/a_{22} = 0.33$. These values, inserted into Equation (34), result in

the dashed line on Figure 25. It is apparent that $g_I + g_{II}$ = constant does not adequately describe the fracture behavior in the presence of combined mode.

For purposes of fitting the data, the results were plotted in nondimensional form as shown in Figure 26. The equation

$$\frac{k_I}{k_{IC}} + \left(\frac{k_{II}}{k_{IIC}}\right)^2 = 1 \qquad (36)$$

fits the data very well and is shown as the solid dark line. Equation (25) is represented by the dotted line. While Equation (36) provided a good fit to the data for both balsa wood and Scotchply, it should be kept in mind that Equation (36) is basically only an empirical equation which explains nothing fundamental about the fracture mechanism. On the other hand, the g approach represented by Equation (35) is fundamental. Its failure to represent the data must be considered.

During the fracture tests, the crack extension process observed. It was noticed that, though the crack basically followed the fiber direction, it did not extend in a completely planar fashion, that it intermittently skipped back and forth across bundles of fibers as shown in Figure 27. This resulted in the upper and lower fracture surfaces being connected by fibers. Corten [12] discussed the idea that these fibers acted as shear connectors for Mode II displacements but that because the fibers were parallel to the fracture surface, they carried almost no load normal to the crack surface. The effect of the shear connectors was to cause an apparent value of k_{IIC} larger than the actual k_{IIC}.

One other point about the g approach, Equation (35), must be discussed. Lauratis [24] conducted some off-axis tension tests on Scotchply which contained only natural flaws in the form of bubbles, voids fiber-matrix delamination from lack of wetting, etc. She obtained good correlation of Equation (35) with her test results. The question is, if Equation (35) would not correlate for Wu's experiments, did it correlate for Lauraitis? Unfortunately, Lauraitis failed to discuss this point even though she used Wu's data for k_{IC} and a_{11}/a_{22}. One can speculate as to why she found good correlation. The answer may lie in the model she chose. She modeled the microflaws as tunnel cracks and inferred the microflaw crack length from her tension tests. A penny-shaped flaw, (as she mentions) or an elliptical flaw may well have been more representative of the actual flaw geometry. A different flaw model would have changed not only the magnitude of k_I but would also have changed the relative amounts of k_I and k_{II}. Thus, the tunnel shaped model may very well have been fortuitious and a more realistic crack shape might have actually given poorer correlation. In any case, the answer is not clear at this time and more work will be needed to settle the question. In the course of her work

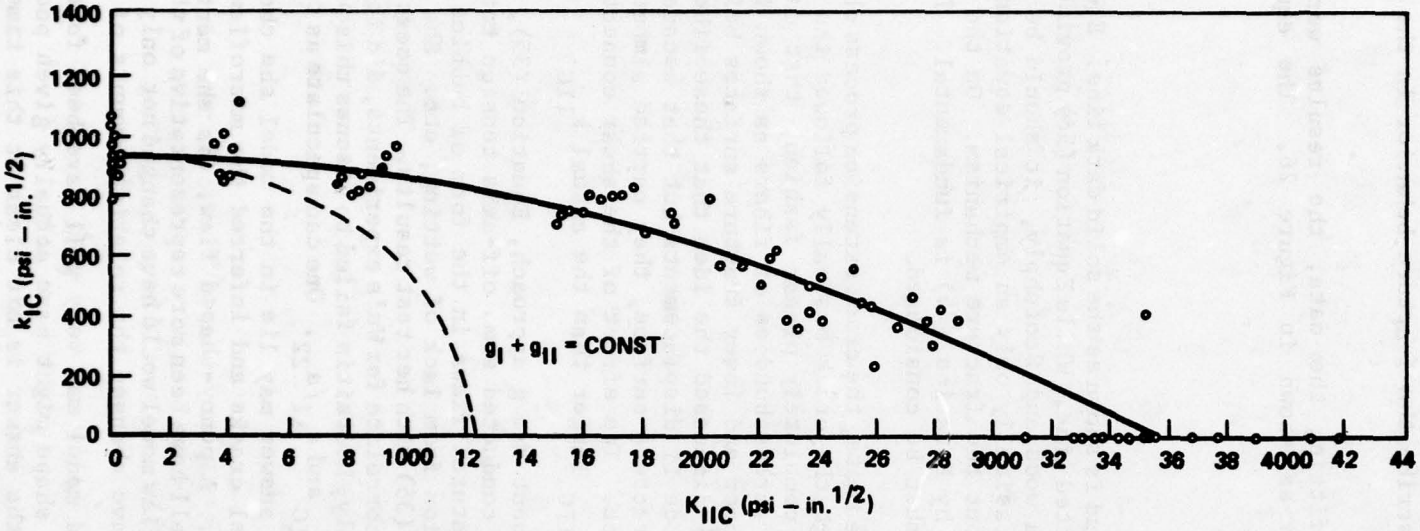

Figure 25. Interaction between k_I and k_{II} for rapid crack extension in fiber glass epoxy (Scotchply 1002)[6]. (The dashed line has been changed slightly from that in [6].)

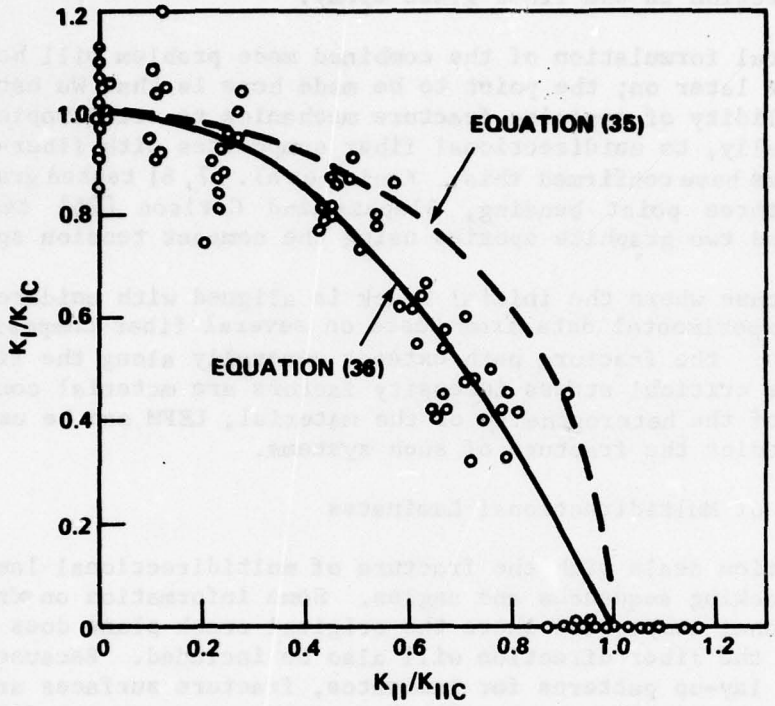

Figure 26. Dimensionless representation of interaction between stress intensity factors k_{IC} and k_{IIC} for Scotch Ply [6].

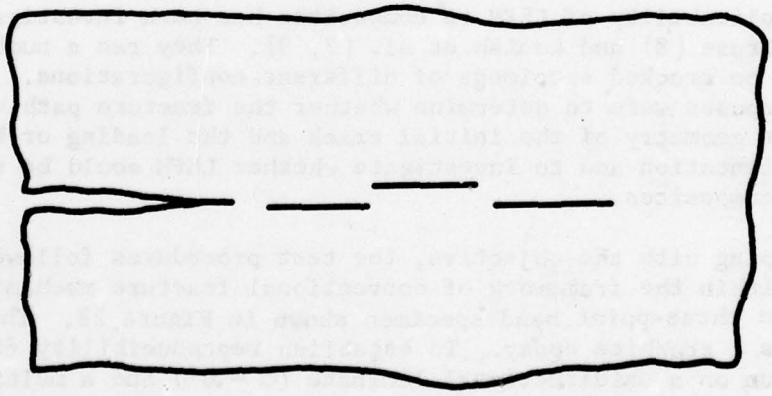

Figure 27. Crack extension by skipping across fiber bundles.

Lauraitis [24] established the existence of microflaws oriented along the fiber direction in the fiber glass epoxy.

The general formulation of the combined mode problem will be discussed further later on; the point to be made here is that Wu established the validity of applying fracture mechanics to orthotropic plates, more specifically, to unidirectional fiber composites with fiber-aligned cracks. Others have confirmed this. Konish et al. [7, 8] tested graphite-epoxy using three point bending, Slepetz and Carlson [25] tested glass epoxy and two graphite epoxies using the compact tension specimen.

For the case where the initial crack is aligned with unidirectional fibers, the experimental data from tests on several fiber composite systems agree: the fracture path extends generally along the fiber direction, the critical stress intensity factors are material constants, and in spite of the heterogeneity of the material, LEFM can be usefully applied to predict the fracture of such systems.

3.2 Fracture of Multidirectional Laminates

This section deals with the fracture of multidirectional laminates of varying stacking sequences and angles. Some information on fracture of unidirectional composites where the original crack plane does not coincide with the fiber direction will also be included. Because of the many possible lay-up patterns for laminates, fracture surfaces are varied and frequently complex in shape. General statements are more difficult to make than in the last section; results for several laminates of different stacking sequences and angles must be considered. In doing this, there will be less emphasis on fracture toughness values (Chapter 4) than on the degree of applicability of LEFM to such systems.

The applicability of LEFM to composites has been investigated by Konish and Cruse [8] and Konish et al. [7, 9]. They ran a number of experiments on cracked specimens of different configurations. The specific purposes were to determine whether the fracture path was determined by the geometry of the initial crack and the loading or by the material orientation and to investigate whether LEFM could be usefully applied to composites.

In keeping with the objective, the test procedures followed those developed within the framework of conventional fracture mechanics. They employed the three-point bend specimen shown in Figure 28. The material was a graphite epoxy. To establish reproducibility five tests each were run on a unidirectional laminate ($\alpha = 0°$) and a multidirectional laminate [$\alpha = (0°/\pm45°/90°)_s$]. The crack length, a, for both materials was 0.4 in. Single tests were then run for $\alpha = 0°$, 45°, 90° $(\pm45)_s$ and $(0°/\pm45°/90°)_s$, all with starter cracks of 0.2, 0.4, and 0.6 in. The short crack lengths were included to permit evidence of material dominance

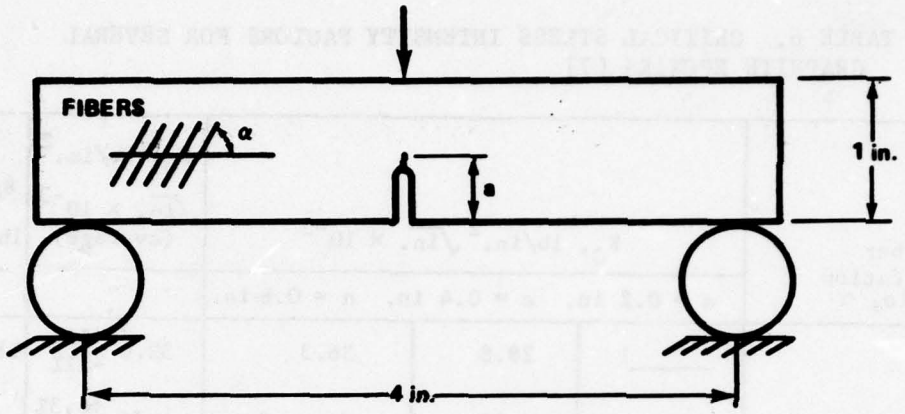

Figure 28. Three-point bend specimen showing fiber direction.

to develop. The beams were loaded to failure and the critical stress intensity factors, called K_Q here, were computed for all three crack lengths. The K_Q values were determined from the isotropic formulas. Results for K_Q along with g_Q, the critical strain energy release rate, are shown in Table 6. To be a material constant, K_Q should be independent of the crack length. While perhaps not conclusive, results indicate that within experimental error K_Q is essentially constant for each laminate. It should be noted that for the 45° laminate, the presence of tension-shear coupling would induce both Mode I and Mode II behavior at the crack-tip. K_Q will reflect the presence of both modes although the relative amount of K_I and K_{II} was not known. The grouping of the toughness values; the toughness of the 80° and 45° laminates, is an order of magnitude less than the other three because the 90° and 45° laminates fractured through the matrix whereas the others fractured across fibers.

Figure 29 shows the load-displacement curves for the reproducibility tests for the $\alpha = (0°/\pm45°/90°)_s$ laminate. As a matter of convenience, the cross-head displacement was monitered rather than the crack-opening displacement as specified by ASTM for the testing of metals [26]. The shape of the curves in Figure 29 is important. The curves exhibit linear behavior over most of their range with only a very slight amount of nonlinearity preceding the maximum load or instability. In the testing of composites, there is a crack-tip damage zone which is somewhat analogous to the crack-tip plastic zone for metals. This damage zone is due to such things as splitting parallel to the fibers and delamination between plies. A great amount of such crack-tip damage causes increasing compliance with increasing load, leading to a highly nonlinear load-displacement curve. In the extreme case, the fracture would be a slow tearing type and the application of brittle fracture mechanics becomes

TABLE 6. CRITICAL STRESS INTENSITY FACTORS FOR SEVERAL GRAPHITE EPOXIES [7]

Fiber Orientation Angle, α	K_Q, lb/in.^{2} $\sqrt{\text{in.}} \times 10^{-3}$			K_Q, lb/in.^{2} $\sqrt{\text{in.}} \times 10^{-3}$ (average)	g_Q, in. lb/in.^{2}
	a = 0.2 in.	a = 0.4 in.	a = 0.6 in.		
0°	____[1]	28.8	36.3	32.6 +11% -11%	117.
90°	1.66	1.46	____[2]	1.56 +6.3% -6.3%	0.943
45°	0.690[3]	2.22	2.39	2.30 +3.9% -3.8%	____[4]
$(\pm 45°)_s$	18.5	18.5	16.3	17.7 +4.8% -9.4%	45.0
$(0°/\pm 45°/90°)_s$	23.5	21.7	20.5	21.9 +7.3% -8.6%	55.1

Notes:

1. Specimen was crushed before crack propagation occurred.
2. Instrumentation failure.
3. This value omitted when calculating ave. K_Q
4. No g_Q available because the crack propagated in a mixed mode, which could not be directly uncoupled.

suspect. The curves in Figure 29, however, exhibit only a slight amount of nonlinearity, indicating that the failures are essentially brittle, i.e., catastropic with little prior warning, and that the usual ideas of brittle fracture mechanics apply.

The tests [7] were run for several laminate types and the fracture surfaces varied. In the absense of photographs, a brief description is given of each type as follows:

a) $\alpha = 0°$ —The path of crack growth, though somewhat irregular, was roughly coplanar.

b) $\alpha = 45°$ —The crack grew along a plane containing no fibers, i.e., at 45°, to the starter crack, and the resulting fracture surface was very nearly planar. Crack propagation took place here under a combination of K_I and K_{II}.

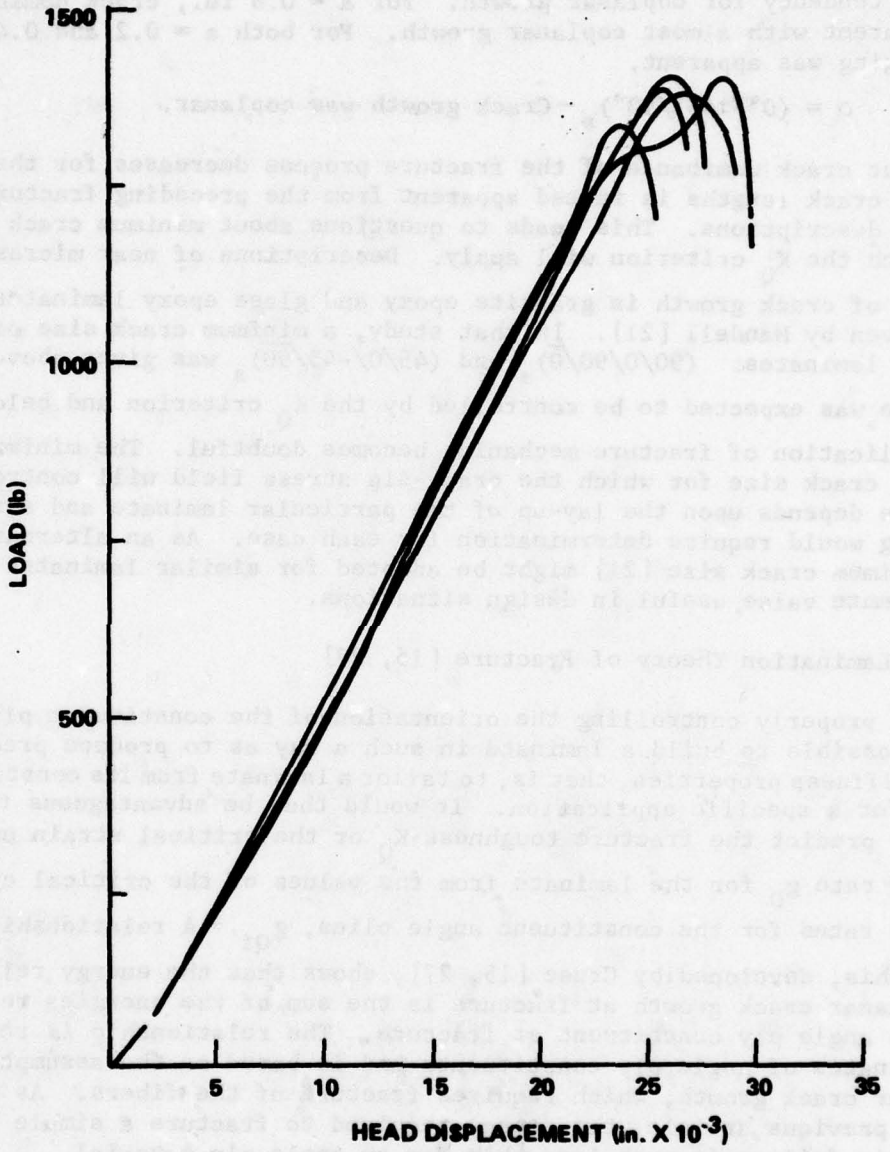

Figure 29. Load versus cross-head displacement for five three-point bend specimens (reproducibility tests) of a $(0°/\pm45°/90°)_s$ graphite epoxy laminate (a = 0.4 in.) [7].

c) $\alpha = 90°$ — The crack grew along a plane containing no fibers, coplanar with the starter crack.

d) $\alpha = (\pm45°)_s$ — For a = 0.2 in., the crack almost immediately turned 45° from the started direction. For a = 0.4 in., there was a

greater tendency for coplanar growth. For a = 0.6 in., crack dominance was apparent with almost coplanar growth. For both a = 0.2 and 0.4, zig-zagging was apparent.

e) $\alpha = (0°/\pm 45°/90°)_s$ – Crack growth was coplanar.

That crack dominance of the fracture process decreases for the shorter crack lengths is indeed apparent from the preceding fracture surface descriptions. This leads to questions about minimum crack size for which the K_Q criterion will apply. Descriptions of near microscopic details of crack growth in graphite epoxy and glass epoxy laminates have been given by Mandell [21]. In that study, a minimum crack size of 0.1 in. for two laminates: $(90/0/90/\overline{0})_s$ and $(45/0/-45/\overline{90})_s$ was given above which fracture was expected to be controlled by the K_Q criterion and below which the application of fracture mechanics becomes doubtful. The minimum initial crack size for which the crack-tip stress field will control the fracture depends upon the lay-up of the particular laminate and strickly speaking would require determination for each case. As an alternative, the minimum crack size [21] might be adopted for similar laminates as an approximate value useful in design situations.

3.3 A Lamination Theory of Fracture [15, 27]

By properly controlling the orientation of the constituent plies, it is possible to build a laminate in such a way as to produce predictable stiffness properties, that is, to tailor a laminate from its constituent plies for a specific application. It would thus be advantageous to be able to predict the fracture toughness K_Q or the critical strain energy release rate g_Q for the laminate from the values of the critical energy release rates for the constituent angle plies, g_{Qi}. A relationship for doing this, developed by Cruse [15, 27], shows that the energy released by coplanar crack growth at fracture is the sum of the energies released by each angle ply constituent at fracture. The relationship is restricted to laminates of angle ply constituents and is based on the assumption of coplanar crack growth, which requires fracture of the fibers. As noted in the previous article, the energy required to fracture a simple ply by matrix failure is much less than for an angle ply material.

The crack is modeled as a narrow ellipse (Figure 30) with $a/b \ll 1$. The stress σ_2 at the ends of the ellipse ($x_1 = \pm a$) is given by

$$\frac{\sigma_2}{\sigma} = 1 - \frac{a}{b}\, \vartheta m \left[\frac{\mu_1 + \mu_2}{\mu_1 \mu_2}\right] \tag{37}$$

where μ_1 and μ_2 are the roots of the characteristic Equation (17). This equation is rewritten as

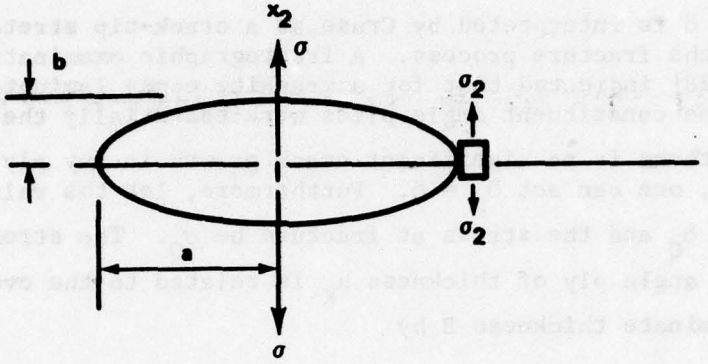

Figure 30. Elliptical crack model [27].

$$-\vartheta m \frac{\mu_1 + \mu_2}{\mu_1 \mu_2} = \frac{b}{a}\left(\frac{\sigma_2}{\sigma} - 1\right) \tag{38}$$

and the last term is neglected in comparison with σ_2/σ. Equation (24) is now recalled for g_I, the strain energy rate. Substituting Equation (38) into Equation (24) results in

$$g = \frac{K_I^2}{2} a_{22} \left(\frac{b}{a}\right) \frac{\sigma_2}{\sigma} \tag{39}$$

where the subscript I has been dropped from g. Assuming that the stress intensity for an anisotropic specimen is the same as for an isotropic specimen of identical geometry, the following is written:

$$K_I = \sigma Y \sqrt{a} \tag{40}$$

where Y is the finite correction factor. Substituting Equation (40) into Equation (39), the following is obtained:

$$g = \frac{1}{2} Y^2 \sigma b (a_{22} \sigma_2) \quad . \tag{41}$$

At the tip of the ellipse, the state of stress is uniaxial, i.e., $\sigma_1 = \tau_{12} = 0$. Since $a_{22} = 1/E_{22}$, then $a_{22} \sigma_2$ is the local hoop strain ϵ_2. In the limit for vanishing b, ϵ_2 is unbounded but the product $b\epsilon_2$ is bounded [27]. Defining $b\epsilon_2$ to be δ; Equation (41) becomes

$$g = Y^2 \sigma \delta/2 \quad . \tag{42}$$

The quanity δ is interpreted by Cruse as a crack-tip stretching, physically related to the fracture process. A fractographic examination by Cruse and Stout [28] indicated that for a graphite epoxy laminate, the values of δ_K for the constituent angle plies were essentially the same. This means that there is no significant crack growth in any ply prior to fracture. Thus, one can set $\delta_K = \delta$. Furthermore, let the value of δ at fracture be δ_Q and the stress at fracture be σ_Q. The stress σ_K on the constituent angle ply of thickness h_K is related to the overall stress σ on the laminate thickness B by

$$\sigma B = \sum_{k=1}^{N} \sigma_K h_K \tag{43}$$

where N is the number of constituent angle plies. Substituting for σ from Equation (43) into Equation (42) and letting fracture conditions apply results in

$$g_Q = \left[\sum_{k=1}^{N} \sigma_{QK} h_k / B\right] \delta_Q \, Y^2/2 \quad . \tag{44}$$

Similarly, the fracture criterion for a constituent angle ply can be written:

$$g_Q = Y^2 \sigma_{QK} \, \delta_{QK}/2 \quad . \tag{45}$$

Using the preceding observation that $\delta_{QK} = \delta_Q$, Equation (45) can be combined with Equation (44) to yield

$$g_Q = \sum_{k=1}^{N} g_{QK} h_K / B \quad . \tag{46}$$

This shows that the energy released by coplanar crack growth is the sum of the energies released by the angle ply constituents, a result which perhaps is intuitively apparent. It must, however, be kept in mind that Equation (46) applies only to Mode I, i.e., the crack propagates in its plane, and the damage area at the crack tip due to splitting between fibers and delamination between plies is small. Cruse [27] applied his results, Equation (46) to the data from Reference 7, which are shown in Table 6. The value of g_Q for the (0/±45/90) laminate is computed from Equation (46) to be:

$$g_Q = 117 \left(\tfrac{1}{4}\right) + 45 \left(\tfrac{1}{2}\right) + 0.9 \left(\tfrac{1}{4}\right) + 52 \text{ in.-lb/in.}^2 \quad .$$

Compared with 55.1 in.-lb/in.^{2}, the value is low by only 6%. Considering that in a laminate failure, there are probably other energy consuming damage processes not included in Equation (46), the results are remarkably close. Cruse and Osias [15] have checked the model against the g_Q results from three-point bending for a number of other laminates, including (90/±45), (90_2/±45), (0/±45), and (0_2/±45). The g_Q predicted from Equation (46) was for most cases within 5% of the measured g_Q. Equal accuracy for many other laminates would not be expected. As Cruse [27] points out, if the crack grows by delamination followed by independent ply failure, then Equation (46) would not apply.

3.4 The Energy Density Theory [29, 30]

As already noted, the Griffith-Irwin equation which relates g_I and k_I is based upon collinear crack propagation. Further, the idea of total strain energy release, $g_I + g_{II} = g_C$, for combined mode problems depends upon collinear crack propagation, which as already shown, is often contrary to experimental evidence. In an effort to circumvent this difficulty, Sih and Chen [30, 31, 32] have devised a fracture criterion that constitutes a fundamental departure from the classical theory of fracture mechanics. The method, which employs the familiar quantities k_I and k_{II}, is based upon the strain energy density outside a small core region surrounding the crack tip. With this method, it is possible to calculate the initial crack propagation direction as well as the critical load. For composites, the method applies to unidirectional laminates; it assumes that fracture occurs by crack propagation in the matrix.

The energy density theory must first be explained before its application to composites. A basic idea of the theory is that the continuum mechanics solution, on which k_I and k_{II} are based, stops short of the crack tip by a distance r_o, Figure 31.

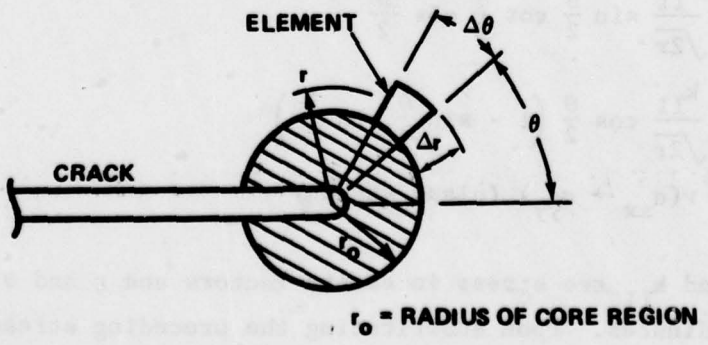

Figure 31. Core region surrounding the crack tip.

The radius r_o is approximately the same order of magnitude as the crack-tip radius. Let the crack tip be embedded in an isotropic (matrix) material having Young's modulus, E, Poisson's ratio, ν, and shear modulus, $G = E/[2(1 + \nu)]$. Now the strain energy dw/dA stored by the element $\Delta A = r\,\Delta\theta\,\Delta r$ is considered:

$$\frac{dw}{dA} = \frac{1}{2E}\left(\sigma_{xx}^2 + \sigma_{yy}^2 + \sigma_{zz}^2\right) - \frac{\nu}{E}\left(\sigma_{xx}\sigma_{yy} + \sigma_{yy}\sigma_{zz} + \sigma_{zz}\sigma_{xx}\right) + \frac{1}{2G}\left(\tau_{xy}^2 + \tau_{yz}^2 + \tau_{xz}^2\right) \tag{47}$$

where the stress components τ_{xz} and τ_{yz} are zero for plane strain. The isotropic crack-tip stresses for Mode I loading are [1, 3],

$$\begin{aligned}
\sigma_{xx} &= \frac{k_I}{\sqrt{2r}}\cos\frac{\theta}{2}\left(1 - \sin\frac{\theta}{2}\sin\frac{3\theta}{2}\right)\\
\sigma_{yy} &= \frac{k_I}{\sqrt{2r}}\cos\frac{\theta}{2}\left(1 + \sin\frac{\theta}{2}\sin\frac{3\theta}{2}\right)\\
\tau_{xy} &= \frac{k_I}{\sqrt{2r}}\cos\frac{\theta}{2}\sin\frac{\theta}{2}\cos\frac{3\theta}{2}\\
\sigma_{zz} &= \nu(\sigma_{xx} + \sigma_{yy}) \text{ (plane strain)}
\end{aligned} \tag{48}$$

and for Mode II,

$$\begin{aligned}
\sigma_{xx} &= \frac{-k_{II}}{\sqrt{2r}}\sin\frac{\theta}{2}\left(2 + \cos\frac{\theta}{2}\cos\frac{3\theta}{2}\right)\\
\sigma_{yy} &= \frac{k_{II}}{\sqrt{2r}}\sin\frac{\theta}{2}\cos\frac{\theta}{2}\cos\frac{3\theta}{2}\\
\tau_{xy} &= \frac{k_{II}}{\sqrt{2r}}\cos\frac{\theta}{2}\left(1 - \sin\frac{\theta}{2}\sin\frac{3\theta}{2}\right)\\
\sigma_{zz} &= \nu(\sigma_{xx} + \sigma_{yy}) \text{ (plane strain)}
\end{aligned} \tag{49}$$

where k_I and k_{II} are stress intensity factors and r and θ are crack tip polar coordinates. Upon substituting the preceding stresses into Equation (47), the energy density can be written as

$$\frac{dW}{dA} = \frac{1}{r}\left(\alpha_{11}k_I^2 + 2\,\alpha_{12}k_Ik_{II} + \alpha_{22}k_{II}^2\right) \quad . \tag{50}$$

The coefficients α_{11}, α_{12} and α_{22} for plane strain are given by

$$\alpha_{11} = \frac{1}{16G}[(3 - 4\nu - \cos\theta)(1 + \cos\theta)]$$

$$\alpha_{12} = \frac{1}{16G}(2\sin\theta)\,[\cos\theta - (1 - 2\nu)] \tag{51}$$

$$\alpha_{22} = \frac{1}{16G}[4(1 - \nu)(1 - \cos\theta) + (1 + \cos\theta)(3\cos\theta - 1)] \quad .$$

The local strain energy density function dW/dA is proportional to $\frac{1}{r}$; as r becomes smaller and smaller dW/dA becomes larger and larger. The intensity of the strain energy is referred to as the strain energy density factor, denoted by S, where

$$S = \alpha_{11}k_I^2 = 2\,\alpha_{12}k_Ik_{II} = \alpha_{22}k_{II}^2 \quad . \tag{52}$$

This is the key quantity in the application of the theory. It depends upon θ; thus, it is direction sensitive and its role in characterizing the strain energy is somewhat analogous to the role of k_I or k_{II} in characterizing the stress field. In the energy-density theory, the two hypotheses of unstable crack propagation are as follows:

a) Crack initiation takes place in the direction of the stationary value of the strain-energy density factor, that is,

$$\frac{\partial S}{\partial\theta} = 0, \text{ at } \theta = \theta_o \tag{53}$$

and the crack extends in the direction θ_o.

b) Crack extension occurs when the strain-energy density factor reaches a critical value, i.e., when

$$S(k_I, k_{II}) = S_c \quad , \quad \text{for } \theta = \theta_o \quad . \tag{54}$$

The difference between S and S_c must be clearly understood. For a given value of θ, S can be calculated in terms of crack length and applied load

through k_I and k_{II}. On the other hand, S_c is a characteristic of the material, a measure of the material's resistance to fracture. The advantages of the S-theory are that it is applicable in the presence of both Mode I and Mode II loading and it will predict the initial direction of crack propagation.

Sih and Chen [30] applied the theory to Wu's data [5, 6] for glass epoxy. They adopted the model shown in Figure 32. A crack length of 2a is embedded in the matrix material parallel to the fibers, where the clear distance between the fibers is 2h. For finding the stress intensity factors, they assumed that the material at a distance greater than h from the crack is homogeneous and orthotropic, with properties E_1, E_2, ν_{12}, ν_{21} and G_{12}, parallel and perpendicular to the crack, Figure 32. The crack is contained in an isotropic layer of thickness 2h between these two orthotropic materials as shown in Figure 33.

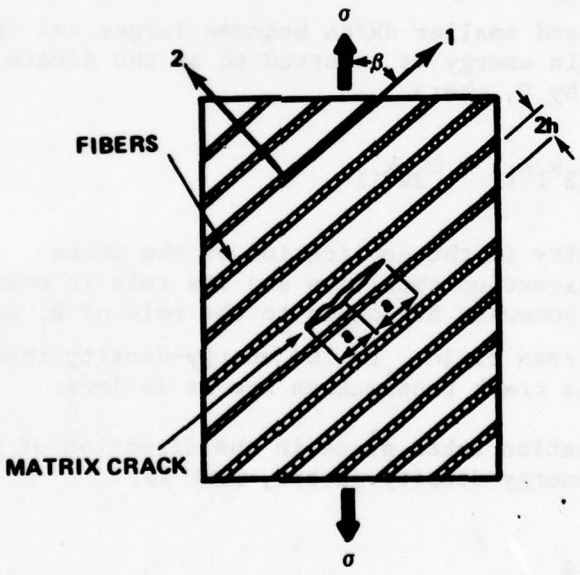

Figure 32. Fiber composite in tension with crack parallel to the fibers.

The average clear spacing 2h between the fibers can be calculated in terms of the fiber volume fraction v_f by assuming that the fibers are distributed uniformly throughout the matrix. Consider the fiber of radius R shown in Figure 34 surrounded by its portion of the matrix material. The dotted lines represent the centerlines between fibers. For a unit thickness perpendicular to the paper, the total volume V_T is

$$V_T = (h + 2R)^2 \tag{55}$$

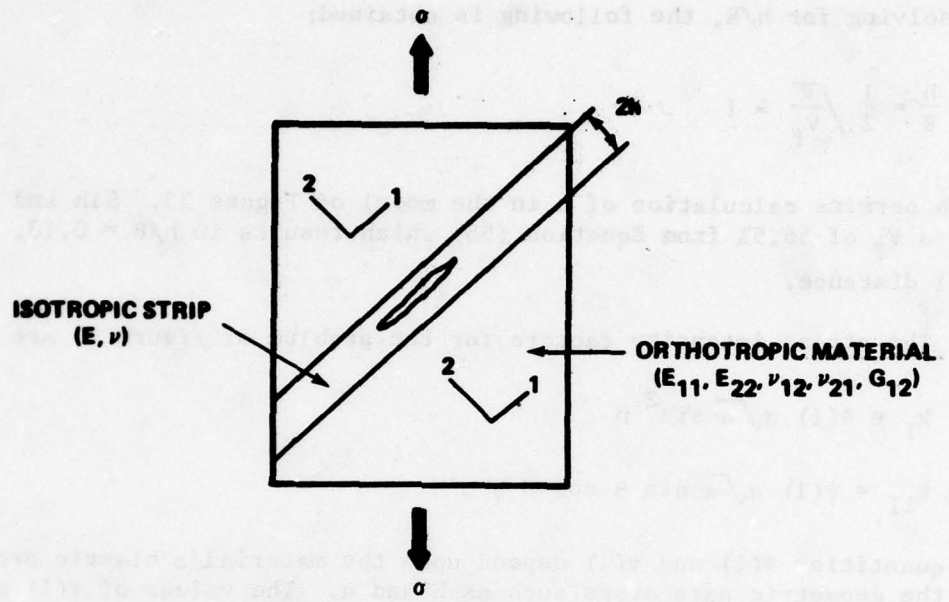

Figure 33. Sih and Chen [30] model of crack in fiber composite.

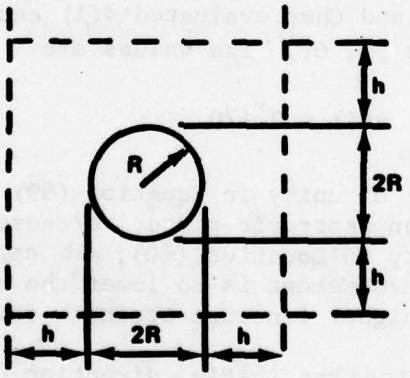

Figure 34. Cross section of fiber and matrix.

and the volume of the fiber V_R is

$$V_R = \pi R^2 \quad . \tag{56}$$

Using the definition of the fiber volume fraction, v_f is

$$v_f = \frac{V_R}{V_T} = \frac{\pi R^2}{(h + 2R)^2} \tag{57}$$

and solving for h/R, the following is obtained:

$$\frac{h}{R} = \frac{1}{2}\sqrt{\frac{\pi}{V_f}} - 1 \tag{58}$$

which permits calculation of h in the model of Figure 33. Sih and Chen used a V_f of 56.5% from Equation (58) which results in h/R = 0.18, a small distance.

The stress intensity factors for the problem of Figure 33 are [30]

$$k_I = \phi(1)\ \sigma\sqrt{a}\ \sin^2\beta$$
$$k_{II} = \psi(1)\ \sigma\sqrt{a}\ \sin\beta\ \cos\beta \quad . \tag{59}$$

The quantities $\phi(1)$ and $\psi(1)$ depend upon the material's elastic properties and the geometric parameters such as h and a. The values of $\psi(1)$ and $\phi(1)$ must be found from Fredholm integral equations which have very complicated kernels. For h/a small, i.e., $h/a \ll 1$, the expressions for $\psi(1)$ and $\phi(1)$ become greatly simplified, no longer requiring integration of a complicated function. The case of $h/a \ll 1$ includes a wide range of fiber composites and flaws. Sih and Chen evaluated $\phi(1)$ and $\psi(1)$ for the Scotchply 1002 material used by Wu [5, 6]. The values are

$$\phi(1) = 0.290 \quad , \quad \psi(1) = 0.170 \tag{60}$$

Values for $\phi(1)$ and $\psi(1)$ of unity in Equation (59) would correspond to the case of a crack in an isotropic plate. Because the values are considerably less than unity in Equation (60), it can be seen that the effect of the fiber reinforcement is to lower the crack-tip stress intensities, resulting in a higher fracture strength for the fiber composite.

The S_c – theory predicts the initial direction θ_o of crack growth from Equation (53). Except for the special case of tension normal to the crack plane, θ_o will not be zero. As noted in Section 3.1, the crack in a unidirectional laminate normally grows parallel to the fibers, seemingly at variance with the S_c – theory. However, it must be kept in mind that θ_o is only the initial crack direction; the crack can turn after its initial increment of extension. For Scotchply 1002, Sih and Chen argue that the fracture process is brittle, that there is a distinct point of instability on the load-deflection curve, and that most of the stored energy is dissipated at the point of incipient fracture where the crack extends by a small amount Δa. In other words, it is the initial increment of crack extension Δa which causes fracture and the remaining

energy required for the actual separation of the plate into two pieces is small. Of course, it is only the initial crack direction which makes an angle of θ_o with the main crack surface.

This argument, if valid, is only valid for brittle behavior. The crack is contained in a layer of matrix material whose half thickness h is only 0.18R. With no more room than this, the discussed amount of initial crack growth Δa at an angle of θ_o would indeed have to be small. Would this small amount of extension consume most of the fracture energy? Whether the argument is strictly correct or not is perhaps academic if the theory gives good correlation with experimental data, which it did for Scotchply 1002 [5, 6].

To apply the theory, expressions for k_I and k_{II} from Equation (59) are substituted into Equation (52) so that the energy density factor S is known in terms of θ. Equation (53) is then used to find the initial crack direction θ_o. For the present case, several different values of β, the load direction, are being considered so that for each value of β there is a corresponding value of θ_o. Figure 35 shows how the angle θ_o varies with β. For $\beta = 90°$, $\theta_o = 0$, the crack direction is along the original crack plane, as expected. For each value of β the value of θ_o can be inserted into Equation (52). Furthermore, let critical conditions apply, i.e., $S \rightarrow S_c$ and $\sigma \rightarrow \sigma_c$. Then the following fracture criterion results:

$$S_c = \sigma_c^2 \, a \left[0.084\alpha_{11} \sin^4 \beta + 0.049\alpha_{12} \sin^3 \beta \cos \beta + 0.029\alpha_{22} \cos^4 \beta\right] . \tag{61}$$

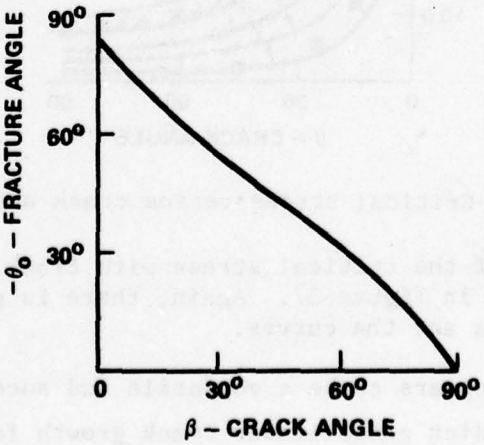

Figure 35. Fracture angle as a function of crack angle [30].

Sih and Chen determined a value of S_c from the data [5, 6]. With the material constant S_c known, from Equation (61) the way in which critical stress σ_c varies with β can be determined for several chosen crack lengths. Figure 36 shows the results for five selected half crack lengths: a = 0.01, 0.02, 0.05, 0.1, and 0.51 in. The results from the experiments [5, 6] for a = 0.51 in. are shown as dark squares. Except for small values of β, the curve for a = 0.51 in. agrees well with the data. The curve for a = 0.02 in. agrees well with σ_c for uncracked specimens [24], represented by dark triangles. This indicates that microflaws on the order of 0.04 in. in length must have existed in the uncracked specimens. Lauraitis' microscopic examination [24] had previously revealed flaws in the form of bubbles and gaps along the fibers. She had already inferred the flaw length to be approximately 0.035 in. which agrees well with the 2a = 0.04 in. value indicated in Figure 36.

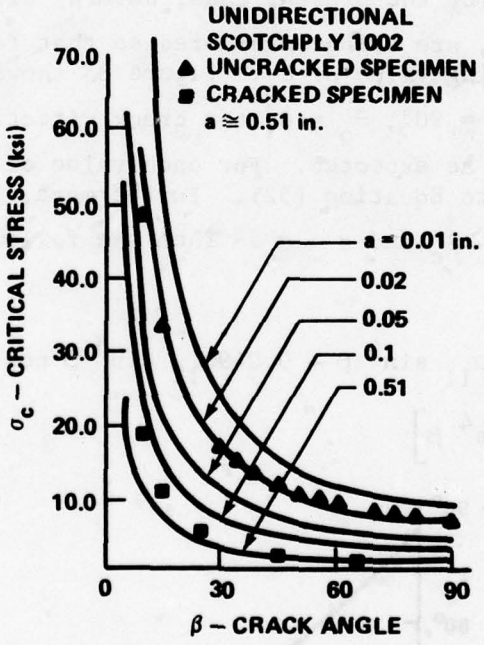

Figure 36. Critical stress versus crack angle [30].

The variation of the critical stress with crack length for several values of β is shown in Figure 37. Again, there is good agreement between the experimental data and the curves.

The S_c theory appears to be a versatile and successful fracture criterion. It will predict noncollinear crack growth for situations where a mixture of k_I and k_{II} exist. The method deserves further consideration.

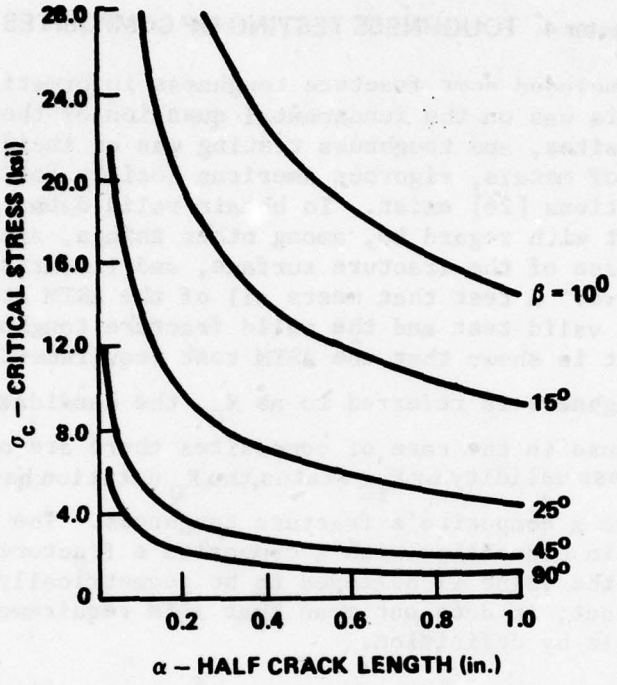

Figure 37. Variations of critical stress with half crack length [30].

To verify its usefulness, it should be applied to a variety of unidirectional composites. Attempts should be made to adapt the theory to cross-ply laminates. From an engineering viewpoint, the main disadvantage in applying the model discussed here is the difficulty of finding a stress analysis for a particular geometry, or loading, keeping in mind that the model requires the crack to be contained in a strip of isotropic material surrounded by orthotropic material. Certain approximations may be possible to alleviate the problem. Certainly, considerable simplification resulted [30] for finding $\phi(1)$ and $\psi(1)$ when h is small; h would be small for most composites of interest. The form of k_I and k_{II} in Equation (59) suggests a possible approximation. For a finite plate it might be possible to determine k_I and k_{II} assuming the crack to be embedded in a homogeneous orthotropic plate and then apply $\phi(1)$ and $\psi(1)$ determined from an infinite plate solution as correction factors to account for the crack lying in an isotropic strip surrounded by orthotropic material. This idea is speculation and has not been tested.

Chapter 4. TOUGHNESS TESTING OF COMPOSITES

Chapter 3 included some fracture toughness information; however, there the emphasis was on the fundamental question of the applicability of LEFM to composites, and toughness testing was an incidental issue. For the testing of metals, rigorous American Society for Testing Materials (ASTM) specifications [26] exist. To obtain valid data, certain requirements must be met with regard to, among other things, specimen thickness, crack length, shape of the fracture surface, and linearity of the load-displacement curve. A test that meets all of the ASTM standards is then referred to as a valid test and the valid fracture toughness is denoted by K_{IC}. Until it is shown that the ASTM test requirements are satisfied, the fracture toughness is referred to as K_Q, the candidate fracture toughness. Because in the case of composites there are no standards for verifying toughness validity or K_{IC} status, the K_Q notation has been generally adopted to denote a composite's fracture toughness. The word valid, when it is used in connection with a composite's fracture toughness, means only that the value is believed to be geometrically independent, a material constant; it does not mean that ASTM requirements were met; this is impossible by definition.

In this chapter, a sample of results which address some of the unique problems of toughness testing of composites is included. Emphasis will be on general material behavior, techniques, and methods rather than on individual values of fracture toughness for any given material.

4.1 Characteristics of Fracture Toughness

Fracture toughness testing technology was developed for use on metals. It is well to consider the various ways in which the toughness behavior of composites differs from that of metals. One very strong contrast between the toughness behavior of composites and metals is the difference in the relationships between the ultimate strength and the fracture toughness for the two. The ultimate tensile strength and toughness of a composite are directly related to the tensile behavior of the filaments. This is indicated in the curves of Figure 38 for a number of laminate configurations. The ultimate strength increases as the percentage of plies in the load direction increases. Because boron is significantly stronger than graphite, the boron curve is steeper. Figure 38 (b) shows that in addition to the ultimate strength the fracture toughness also increases as the percentage of load-oriented plies increases. The fracture toughness and ultimate strength are directly related. As the ultimate strength increases, the fracture toughness increases. This is in marked contrast to the behavior of metals which usually exhibit an inverse relationship between the ultimate strength and fracture toughness. Metals of high tensile strength are normally brittle.

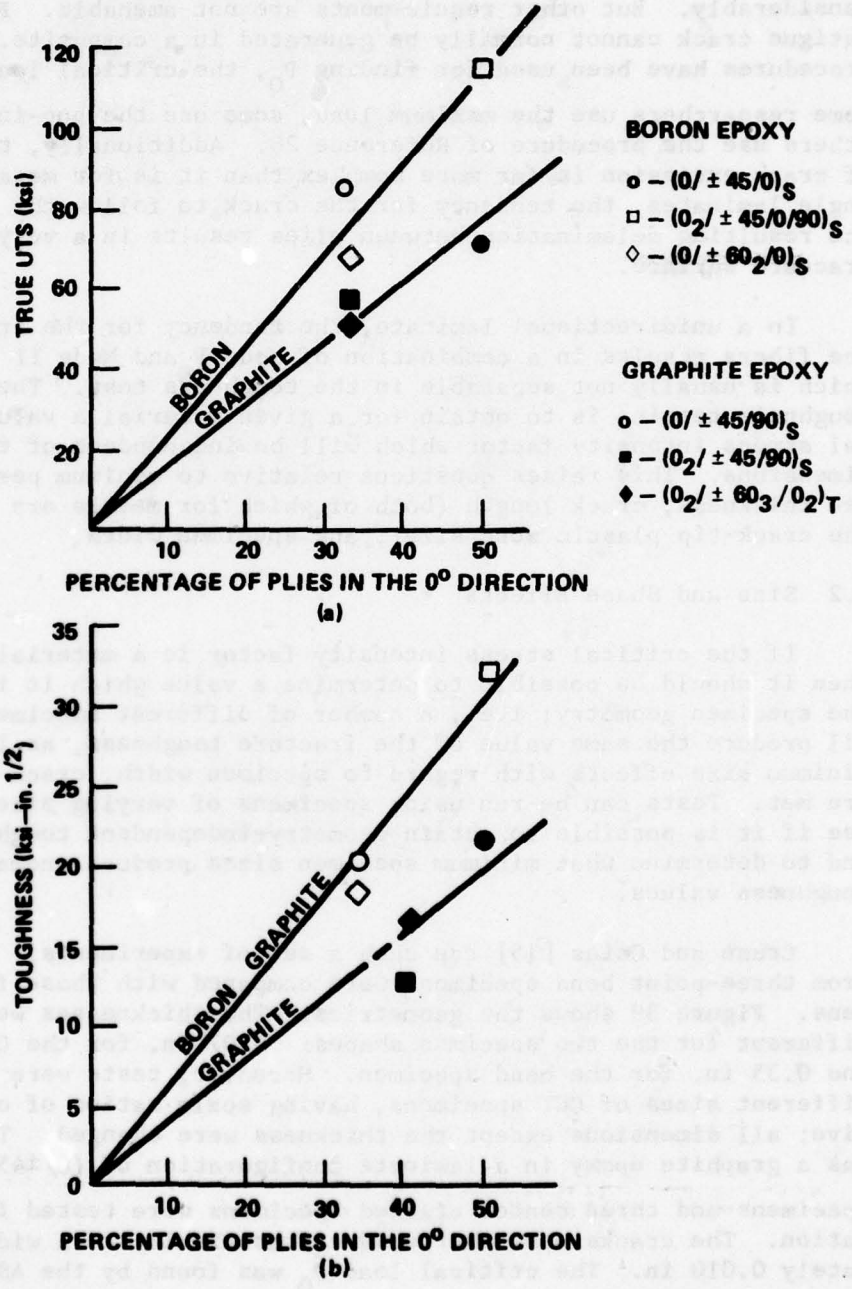

Figure 38. Behavior of strength and toughness with increasing load-oriented plies [22].

In the design of a composite fracture test, the procedures, methods, and requirements [26] for the testing of metals are frequently used as guidelines. For example, the compact tension specimen and the three-point bend specimen, the two standard specimens for metals have been used considerably. But other requirements are not amenable. For example, fatigue crack cannot normally be generated in a composite. Various procedures have been used for finding P_Q, the critical load in a test. Some researchers use the maximum load, some use the pop-in value, and others use the procedure of Reference 26. Additionally, the mechanism of crack extension is far more complex than it is for metals. In multi-angle laminates, the tendency for the crack to follow the fibers and the resulting delamination between plies results in a very irregular fracture surface.

In a unidirectional laminate, the tendency for the crack to follow the fibers results in a combination of Mode I and Mode II extension which is usually not separable in the toughness test. The object of toughness testing is to obtain for a given material a value of the critical stress intensity factor which will be independent of the specimen dimensions. This raises questions relative to minimum permissible specimen thickness, crack length (both of which for metals are controlled by the crack-tip plastic zone size), and specimen width.

4.2 Size and Shape Effects

If the critical stress intensity factor is a material constant, then it should be possible to determine a value which is independent of the specimen geometry; i.e., a number of different specimen shapes should all produce the same value of the fracture toughness, as long as certain minimum size effects with regard to specimen width, crack length, etc. are met. Tests can be run using specimens of varying size and shape to see if it is possible to obtain geometry-independent toughness values and to determine what minimum specimen sizes produce anomalies in measured toughness values.

Cruse and Osias [15] ran such a set of experiments. The results from three-point bend specimens were compared with those from CCT specimens. Figure 39 shows the geometries. The thicknesses were considerably different for the two specimen shapes: 0.07 in. for the CCT specimen and 0.35 in. for the bend specimen. Moreover, tests were run for three different sizes of CCT specimens, having scale ratios of one, two, and five; all dimensions except the thickness were changed. The material was a graphite epoxy in a laminate configuration of $(0/\pm45)_s$. Five beam specimens and three center cracked specimens were tested for each configuration. The cracks were sharpened ultrasonically to a width of approximately 0.010 in. The critical load P_Q was found by the ASTM method [26]; the critical stress intensity factor, K_Q, was calculated using the

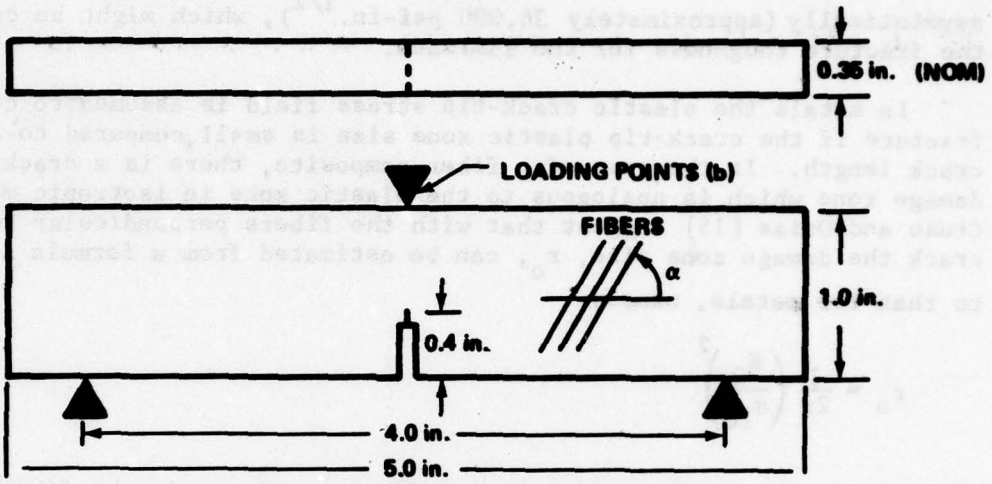

(a) THREE-POINT BEND SPECIMEN GEOMETRY.

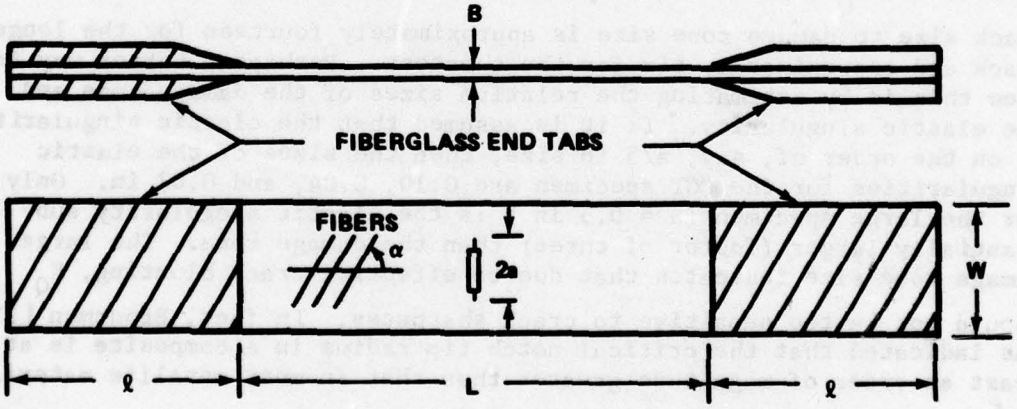

L (in.)	2a (in.)	W (in.)	B (in.)	ℓ (in.)
4.8	0.2	0.5	0.070	2.1
4.8	0.4	1.0	0.074	2.1
9.9	1.0	2.5	0.074	8.1

(b) CCT SPECIMEN GEOMETRY

Figure 39. The three-point bend and center-cracked tension specimens used by Cruse and Osias [15].

isotropic formulas [1]. The results are shown graphically in Figure 40. As the crack length is increased, K_Q appears to approach a constant value asymtotically (approximately 36,000 psi-in.$^{1/2}$), which might be called the fracture toughness for the laminate.

In metals the elastic crack-tip stress field is assumed to control fracture if the crack-tip plastic zone size is small compared to the crack length. In the case of a fiber composite, there is a crack-tip damage zone which is analogous to the plastic zone in isotropic metals. Cruse and Osias [15] suggest that with the fibers perpendicular to the crack the damage zone size, r_o, can be estimated from a formula similar to that for metals, namely

$$r_o = \frac{1}{2\pi}\left(\frac{K_Q}{\sigma_{1U}}\right)^2 \tag{62}$$

where K_Q is the candidate fracture toughness and σ_{1U} is the fiber direction ultimate stress. If r_o is small compared to the crack length, then the crack-tip elastic stress field would be expected to control the fracture behavior. If r_o becomes too large, then the usual elastic stress field characterized by the stress intensity factor is no longer an accurate representation of the crack-tip stresses and geometrically independent results for K_Q would not be expected. In Figure 40, the ratio of half crack size to damage zone size is approximately fourteen for the longest crack and approximately six for the shortest. Perhaps a better way to view this is by estimating the relative sizes of the damage zone and the elastic singularity. If it is assumed that the elastic singularity is on the order of, say, a/5 in size, then the sizes of the elastic singularities for the CCT specimen are 0.10, 0.04, and 0.02 in. Only for the large specimen (a = 0.5 in.) is the elastic singularity substantially larger (factor of three) than the damage zone. The large damage zone size indicates that due to effective crack blunting, K_Q should not be too sensitive to crack sharpness. In fact, Broutman [33] has indicated that the critical notch tip radius in a composite is at least an order of magnitude greater than that in most metallic materials.

Another size effect which Cruse and Osias [15] considered is that due to the fiber ply thickness. In metals it is assumed that inhomogeneities are small compared to the size of the stress singularities; otherwise, the crack tip may experience a mixture of modes. In composites, this implies that the ply thickness should be small compared to the singularities. The ratio of singularity size to ply thickness (approximately 0.0064 in.) varied from more than 15 for the large CCT specimen to more than 3 for the smallest.

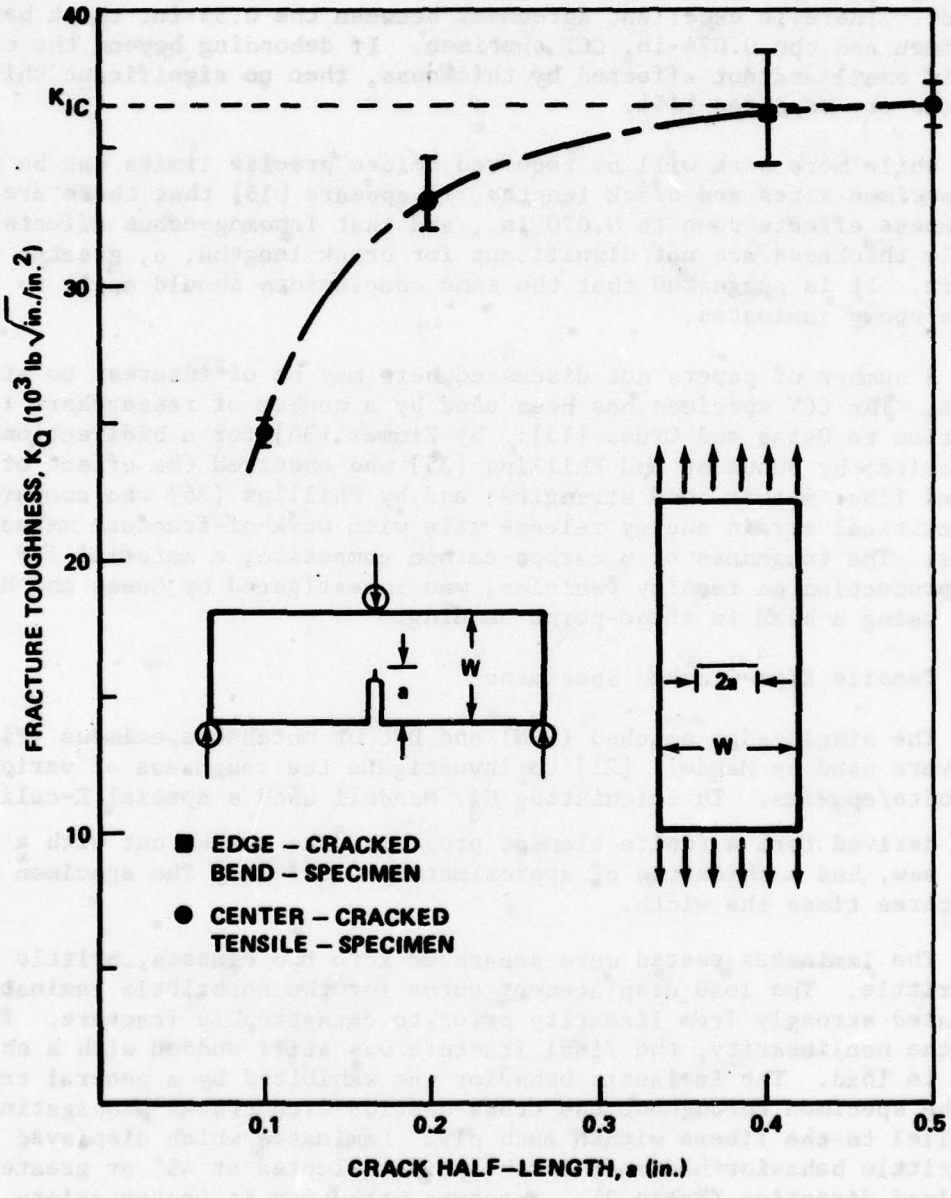

Figure 40. Fracture toughness versus crack length for the three-point bend and CCT specimens [15].

Results in Figure 40 indicate that there was no strong thickness effect. There is excellent agreement between the 0.35-in. thick bending specimen and the 0.074-in. CCT specimen. If debonding beyond the crack tip is small and not affected by thickness, then no significant thickness effects are expected [15].

While more work will be required before precise limits can be placed on specimen sizes and crack lengths, it appears [15] that there are no thickness effects down to 0.070 in., and that inhomogeneous effects due to ply thickness are not significant for crack lengths, a, greater than 0.5 in. It is suggested that the same conclusions should apply to boron/epoxy laminates.

A number of papers not discussed here may be of interest to students. The CCT specimen has been used by a number of researchers in addition to Osias and Cruse [15]: by Zimmer [34] for a bidirectional composite; by Beaumont and Phillips [35] who observed the effect of varied fiber matrix bond strengths; and by Phillips [36] who compared the critical strain energy release rate with work-of-fracture measurements. The toughness of a carbon-carbon composite, a material for thermal protection on reentry vehicles, was investigated by Guess and Hoover [37] using a beam in three-point bending.

4.3 Tensile Edge-Cracked Specimens

The single-edge-notched (SEN) and DEC or notched specimens (Figure 41) were used by Mandell [21] to investigate the toughness of various graphite/epoxies. In calculating K_Q, Mandell used a special K-calibration derived form a finite element program. The crack, cut with a diamond saw, had a thickness of approximately 0.011 in. The specimen length was three times the width.

The laminates tested were separated into two classes, brittle and nonbrittle. The load displacement curve for the nonbrittle laminates deviated strongly from linearity prior to catastrophic fracture. Following the nonlinearity, the final fracture was still sudden with a sharp drop in load. The inelastic behavior was exhibited by a general cracking of the specimen throughout the cross section with cracks propagating parallel to the fibers within each ply. Laminates which displayed the nonbrittle behavior had most of the plies oriented at 45° or greater to the load direction (Table 7). Fracture mechanics is inappropriate for the nonbrittle laminates.

For the first two laminates in Table 7, fracture tests were run using the SEN specimen for varying crack lengths: a = 0.30, 0.60 and 0.88 in. Figure 42 shows the results. Data scatter prevents firm conclusions but no significant variation of K_Q with crack length is apparent for the three crack lengths investigated.

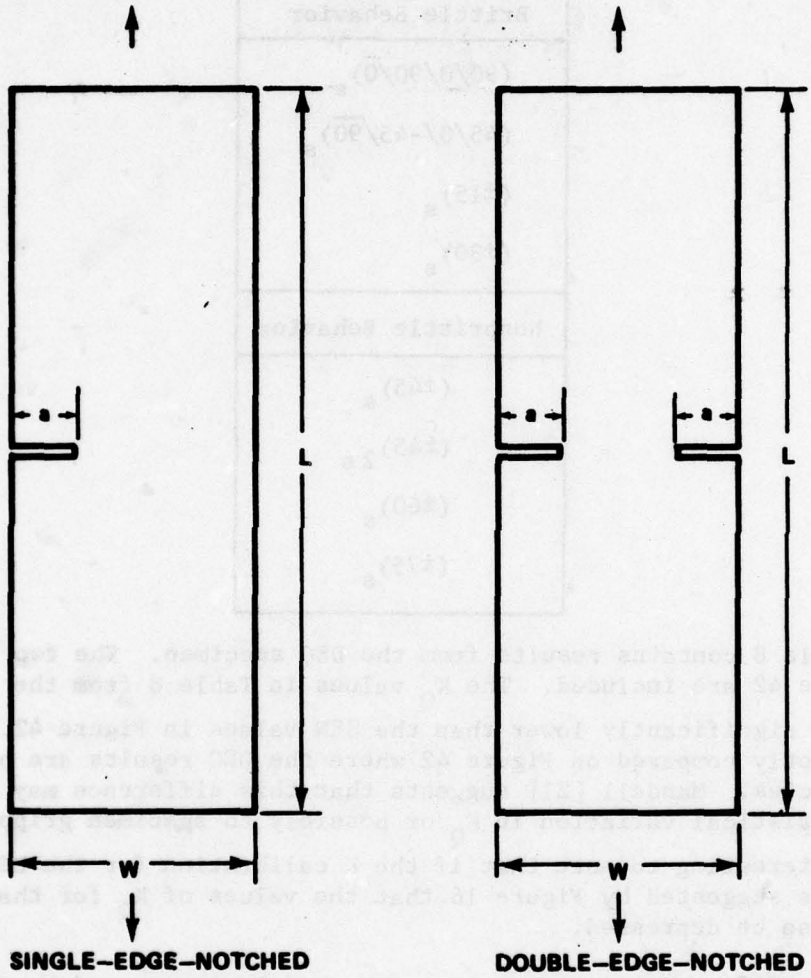

Figure 41. SEN and DEC tensile fracture specimens.

TABLE 7. BRITTLE AND NONBRITTLE GRAPHITE/EPOXY PLY CONFIGURATIONS [21]

Brittle Behavior
$(90/0/90/\overline{0})_s$
$(45/0/-45/\overline{90})_s$
$(\pm 15)_s$
$(\pm 30)_s$
Nonbrittle Behavior
$(\pm 45)_s$
$(\pm 45)_{2s}$
$(\pm 60)_s$
$(\pm 75)_s$

Table 8 contains results from the DEC specimen. The two laminates of Figure 42 are included. The K_Q values in Table 8 from the DEC specimens are significantly lower than the SEN values in Figure 42. These are directly compared on Figure 42 where the DEC results are plotted as open circles. Mandell [21] suggests that this difference may be related to a statistical variation in K_Q or possibly to specimen gripping problems. It is interesting to note that if the K calibration for the DEC specimen is low as suggested by Figure 16 that the values of K_Q for that specimen would also be depressed.

The SEN tension specimen was also used by Olster and Woodbury [22] to find the fracture toughness of several glass, boron, and graphite epoxies. The plate width was 0.750 in. and the edge crack length was 0.230 in., a bit short for valid data (Section 4.2). Results are shown in Table 9. Several replica tests were run for each configuration. Even though the crack length was below the desired minimum, the data in Table 9 serve as good indicators of the effect of lay-up configuration on fracture toughness. Two values of critical k_I are given: one corresponds to the onset of fracture and, while it was not specifically stated, the other probably corresponds to the maximum load. It is felt that the onset value should be used in residual strength calculations. This procedure is at the least conservative. Also, the increase in k_I

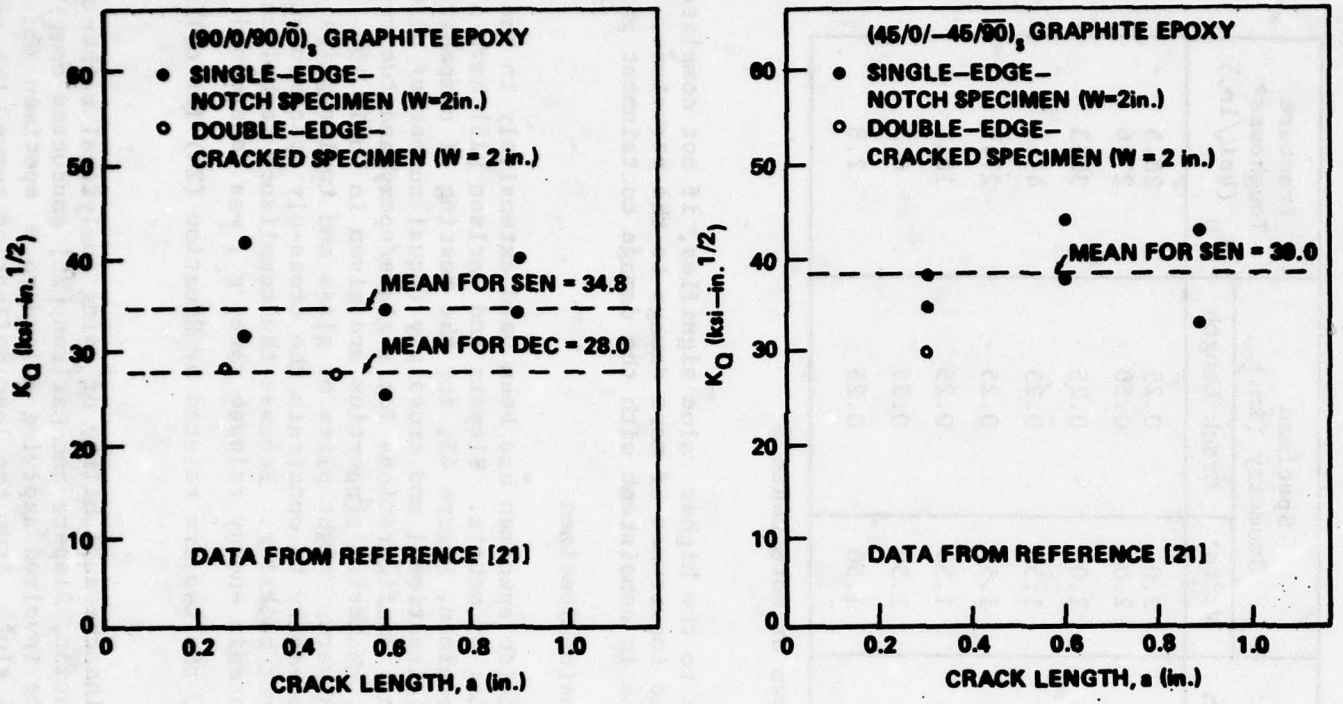

Figure 42. Comparison of toughness values from the SEN and DEC specimens for two laminates.

TABLE 8. CALCULATED VALUES OF FRACTURE TOUGHNESS ASSUMING BRITTLE BEHAVIOR, DOUBLE-EDGE-NOTCHED SPECIMENS (GRAPHITE EPOXY) [21]

Ply Configuration	Specimen Geometry (in.)		Fracture Toughness* K_Q (ksi$\sqrt{in.}$)
	Width	Crack Length	
$(90/0/90/\overline{0})_s$	2.0	0.25	28.5
	2.0	0.50	27.6
$(45/0/-45/\overline{90})_s$	2.0	0.25	30.3
$(\pm 15)_s$	1.50	0.25	47.1
$(\pm 30)_s$	1.50	0.25	27.9
$(\pm 45)_s$	1.50	0.25	15.1
$(\pm 60)_s$	1.50	0.25	6.7
$(\pm 75)_s$	1.50	0.25	2.8

*Average of two or more tests.

from the onset value to the higher value signifies, if not complete failure, at least the incurrence of more damage to the structure. Thus, using the lower value is consistent with the damage containment philosophy.

4.4 The Compact Tension Specimen

The compact tension specimen has been used extensively in the fracture toughness testing of metals. Slepetz and Carlson [25] have also investigated this specimen, Figure 43, for the testing of composites. They tested both unidirectional and cross ply (equal number of plies in orthogonal directions) configurations for a glass/epoxy and two types of graphite/epoxies. Material properties are given in Table 10. The laminate thicknesses were: eight plies of glass and twelve plies of graphite. It was necessary to constrain the cross-ply specimen with side plates to prevent buckling. Because the compliance technique was used, the critical strain energy release rate, g_c, was determined rather than K_Q. Of course, the two are related by Equation (24) for colinear crack growth.

To determine the suitability of using analytical rather than experimental calibration, Slepetz and Carlson [25] conducted compliance tests. The technique involved applying a load to a specimen which contained an initial slot. From the load deflection curve, the compliance

TABLE 9. FRACTURE TOUGHNESS VALUES FOR SEVERAL BORON, GRAPHITE, AND GLASS EPOXIES [22]

Material	k_Q[1] At Onset of Fracture (ksi-in.$^{1/2}$)	k_Q[1] Fracture Toughness (ksi-in.$^{1/2}$)
Boron/Epoxy		
$(0/\pm45/0)_s$	15.2	21.1
$(0_2/\pm45/0/90)_s$	25.8	32.6
$(0/\pm60_2/0)_s$	14.8	18.2
Graphite/Epoxy		
$(0/\pm45/0)_s$	21.6	27.5[2]
$(0_2/\pm45/90)_s$	13.5	20.8[2]
$(0_2/\pm60_3/0_2)_T$	17.4	26.3[2]
Glass/Epoxy		
$(0/\pm45_2/0)_s$	39	59.2[3]

Notes:

1. Recall $K_Q = \sqrt{\pi}\, k_Q$.
2. Values are computed but are not considered the true notch toughness because mode of failure was by interply separation with lack of uniform crack path.
3. Values are computed but are not considered the true notch toughness because specimens exhibited longitudinal cracking and finally failed as a tension specimen having a reduced cross section.

(reciprocal stiffness) was determined for the given crack length. The load was increased until crack extension occurred. Then the crack typically arrested due to load drop-off assoicated with fixed grip conditions. The new crack length was measured and the specimen was unloaded and reloaded to obtain a new compliance for the new crack length. This process was continued until the crack had propagated approximately 80% of the distance across the specimen.

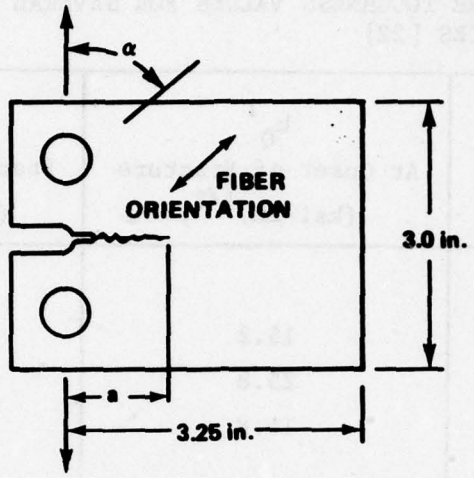

Figure 43. Compact tension specimen configuration [25].

TABLE 10. PROPERTIES OF LAMINATES TESTED [25]

Material	E_1	E_2	G_{12} (lb/in.^{2} × 10^6)	ν_{12}	Fiber Volume (%)
1002 S-glass/epoxy					
Unidirectional	6.9	2.3	1.0	0.28	55
Cross Ply	4.7	4.7	1.1	0.14	
MOD I-5208 graphite/epoxy					
Unidirectional	19.9	1.11	0.93	0.32	40
Cross Ply	12.0	12.0	0.93	0.021	
MOD II-5208 graphite/epoxy					
Unidirectional	19.5	0.96	1.02	0.32	60
Cross Ply	12.1	12.1	0.95	0.035	

The strain energy release rate can be determined in terms of the compliance, C, [25]:

$$g = \frac{F^2}{2B} \frac{dC}{da}$$

where F is the load, B is the thickness and a is the crack length. The critical value, g_c, is the value at which the crack grows unstable before being arrested. This occurs at a load value, F_c, which was taken to be the maximum load in the cycle of crack growth.

The compliance results were interesting. In Figure 44 for the unidirectional S-glass/epoxy, the experimental compliance (open circles) is compared with results from a finite element program (dashed lines). The experimental compliance is considerably lower (specimen stiffer) than the analytical results indicate. The apparent reason for this is that the unidirectional specimens exhibited fiber bridging behind the advancing crack tip, holding the fracture surfaces together somewhat and increasing the stiffness. To study this effect, Sleptz and Carlson [25] machined away these fibers after each cycle of crack growth in tests on several S-glass specimens. The compliance values for the machined cracks are shown in Figure 44 as solid circles. The values for the machined cracks are higher than the finite element results.

The compliance for the graphite cross-ply specimens is shown in Figure 45. In contrast to the unidirectional specimens, the finite element compliance values were considerably below those observed experimentally. Slepetz and Carlson [25] suggest that some splitting and delamination of the cross plies may have increased the compliance in Figure 45. In view of the wide variance of the finite element solution with the experimental compliance, the decision was made to use the experimental compliance in finding g_c.

The fracture toughness values for the unidirectional S-glass/epoxy are shown in Figure 46 for the case of $\alpha = 90°$ (fibers parallel to the crack). The values obtained from the specimens with natural cracks depend upon the crack length up to approximately 30% of the specimen width. After that, g_c levels off at a mean value of approximately 7.6 lb/in. The variation with length is believed to have been due to the fiber bridging action already discussed. Though considerable scatter is present, the values obtained with the machined cracks indicate no dependency upon crack length. The average for the machined crack was 3.18 lb/in. The results for the natural crack are considerably higher than for the machined crack indicating that the fiber bridging contributed significantly to the toughness.

The unidirectional results for both types of graphite/epoxy are shown in Figure 47, for $\alpha = 0$ and $\alpha = 90°$. The values for $\alpha = 0°$ could be obtained only by cutting a deep side groove in a cross-ply specimen such that only two plies remain. These two plies were normal to the plane of the crack. The mean value for $\alpha = 0$ was approximately 355 lb/in. This is more than two orders of magnitude larger than for $\alpha = 90°$. The value is also considerably higher (factor of two) than the value of 117 lb/in. in Table 6, obtained by Konish et al. [7]. The $\alpha = 90°$ specimens exhibit a great deal of scatter but no significant variation with crack length. The averages of values for the Mod I and II materials, respectively, were 2.30 lb/in. and 1.88 lb/in., again roughly twice the value of 0.943 lb/in. found by Konish et al. [7]. Though the materials used by Konish, et al. [7]

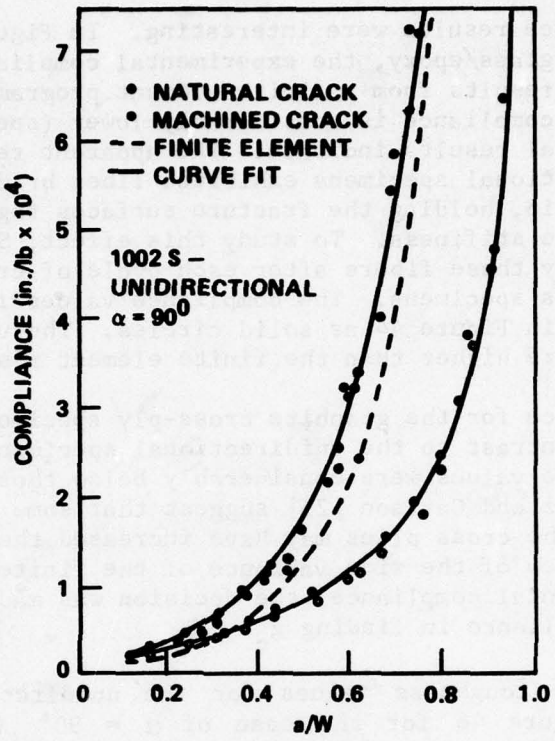

Figure 44. Compliance versus crack length curves for S-glass/epoxy specimens with machined and natural cracks [25].

and Slepetz and Carlson [25] were both graphite epoxies, they may exhibit different fracture toughness values because of fiber volume ratios, etc.

The cross-ply results (plies at 0° and 90°) for graphite are shown in Figure 47. The mean values of g_c were 124 lb/in. and 117 lb/in. for Mod I and Mod II, respectively. For the cross plies oriented at 45°, g_c values were not found because the crack propagated along 45° lines in a zig-zag fashion making the compliance technique questionable.

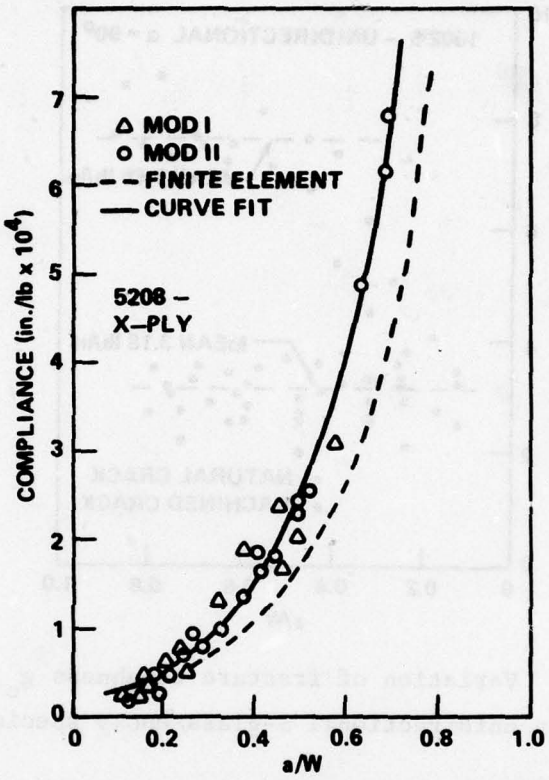

Figure 45. Compliance versus crack length curves for Mod I and Mod II cross-ply specimens (α = 0 and 90°) [25].

The S-glass cross plies proved to be so tough that no crack could be made to propagate. Instead, a system of superficial cracks developed over a broad area of the notch tip and the load displacement curve became highly nonlinear in a way characteristic of gross plastic deformation of a metal.

The tests on the unidirectional materials for α = 30°, 45°, 60°, and 90° could not be analyzed by the compliance technique because the crack propagated along the fibers under a combined mode condition.

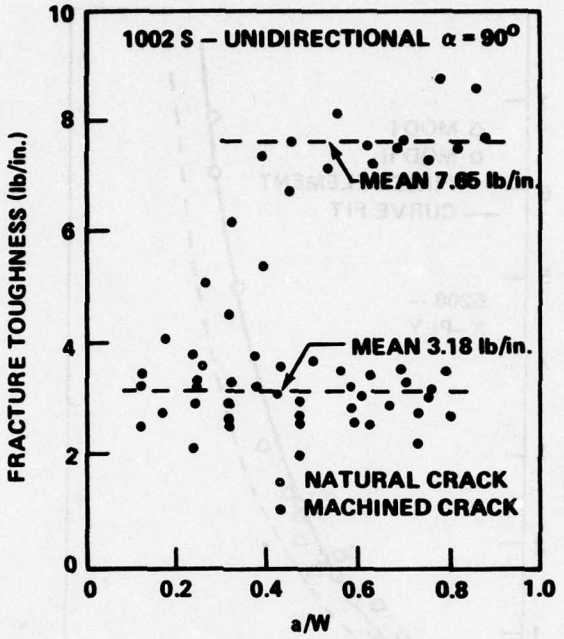

Figure 46. Variation of fracture toughness g_c, with crack length in unidirectional S-glass/epoxy specimens [25].

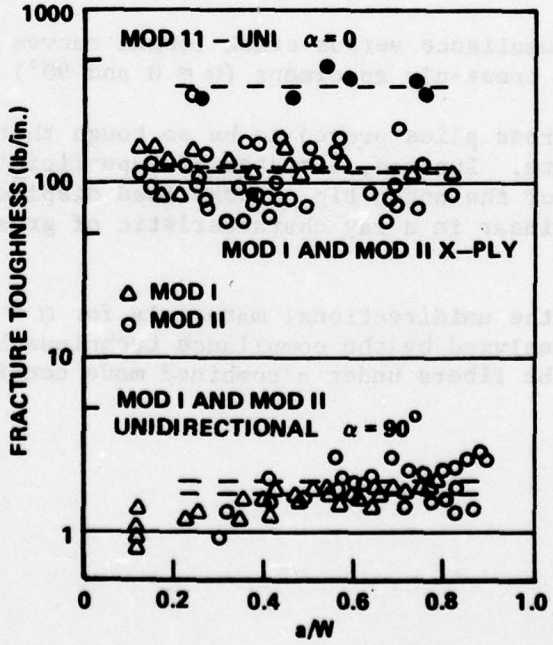

Figure 47. Variation of fracture toughness, g_c, with crack length in unidirectional and cross-ply graphite/epoxy specimens [25].

4.5 Toughness of Aluminum Matrix Composites

Thus far, the discussion of epoxy matrix composites has indicated that the critical value of K is a material constant. Perhaps it has been implied that this might be true for aluminum matrix materials as well as for epoxy ones. One very strong difference in the behavior of the two materials is the ductility exhibited by the aluminum. Thus, it becomes necessary to inquire to what extent, in general, the toughness will depend upon such things as the matrix yield strength, fiber diameter, and fiber volume ratio. Some aluminum matrix materials are included in the survey by Chang [38]. Recently, Wright et al. [39, 40] investigated the R-curve and J-integral approaches to fracture toughness for boron-aluminum. The bulk of the discussion here will rest on work carried out by Hoover [41]. He addressed the preceding questions by conducting a test program on two series of unidirectional boron-aluminum (B-Al) composites. To investigate the effects of fiber volume fraction and fiber diameter, three composites with an 1100 Aluminum (Al) matrix were used. The parameters of the three were 20 v/o 5.6 mil B-1100 Al, 48 v/o 5.6 mil B-1100 Al and 49 v/o 8.0 mil B-1100 Al. The properties are given in Table 11.

TABLE 11. FOUR-POINT BEND TEST* RESULTS FOR B-1100 AL COMPOSITES [41]

	20 v/o 5.6 mil B-1100 Al	48 v/o 5.6 mil B-1100 Al	49 v/o 8.0 mil B-1100
Composite Yield Strength (ksi)	13.6	23.2	21.9
Standard Deviation (ksi)	1.23	0.53	1.86
Composite Ultimate Strength (ksi)	88.4	221.3	199.7
Standard Deviation (ksi)	7.9	18.8	11.8
Elastic Modulus (psi)	16.15×10^6	30.4×10^6	28.7×10^6
Strain-to-Fracture (%)	0.875	0.90	0.84
Standard Deviation (%)	0.05	0.04	0.01

*All tests were conducted on specimens 0.400 in. wide and 0.203 in. thick with a minor span of 3.0 in. and a major span of 7.5 in. The strain was measured with a strain gage on the tensile surface. A minimum of three samples of each material were tested.

A second series of tests was run on specimens taken from a plate of 48 v/o B-6061 Al and subjected to three different heat treatments. The resulting specimen had three different matrix and composite yield strengths. Properties are given in Table 12. These were used then

TABLE 12. FOUR-POINT BEND TEST* RESULTS FOR B-6061 AL COMPOSITES [41]

	48 v/o B-6061-O[1]	48 v/o B-6061-F[2]	48 v/o B-6061-T6[3]
Composite Yield Strength (ksi)	17.1	37.2	99.0
Standard Deviation (ksi)	0.52	4.5	2.9
Composite Ultimate Strength (ksi)	228	235	244.3
Standard Deviation (ksi)	10.4	4.6	10.0
Strain-to-Fracture (%)	0.94	0.98	0.97
Standard Deviation (%)	0.04	0.01	0.01

*All tests were conducted on specimens 0.400 in. wide and 0.208 in. thick with a minor span of 3.0 in. and a major span of 7.5 in. The strain was measured with a strain gage on the tensile surface. A minimum of three samples of each condition were tested.

1. Annealed for 2 hours at 420° C and furnace cooled.
2. As fabricated condition.
3. Solution treated for 30 min. at 490°C, ice-water quenched and aged for 18 hours at 155°C.

to investigate the effect of matrix yeild strength on toughness. Hoover [41] used the rule of mixtures to calculate the effective yield strengths for the three materials. Matrix yield strengths were: 5.7 ksi for the 0 condition, 12.4 ksi for the F condition, and 33.0 ksi for the T6 condition.

The specimens were loaded in four-point bending. The specimens were 0.400 in. deep, 0.200 in. thick with a span of 1.57 in. The starter notch varied from 0.120 to 0.330 in. The notch root radius varied from 0.0005 to 0.005 in. The fibers were normal to the notch.

Figure 48 shows a load-deflection curve for the 5.6 mil B-1100 Al. The curves exhibited substantial nonlinearity and a pop-in load value, P_c, characterized by a small dip in the curve. The pop-in load P_c was used to calculate K_Q, using the formula for isotropic materials. It should be noted that the pop-in load is considerably higher than the critical load which would be found from the graphical method of ASTM. Using the pop-in value for all tests, however, should lead to a nt consistent comparison for evaluating the effects of matrix ductility,[3] etc. Table 13 shows the K_Q values found by Hoover for various crack lengths in the B-1100 Al composites. It can be seen that

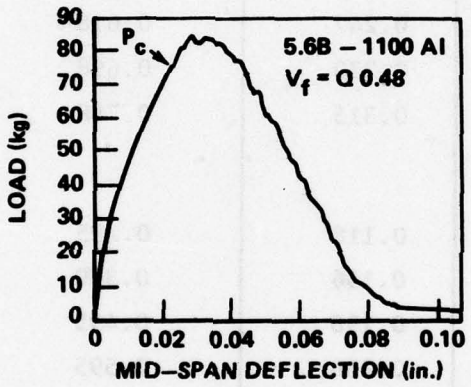

Figure 48. Typical load-deflection behavior of a 5.6 mil B-1100 Al composite [41].

K_Q has a constant value for all crack lengths except for $a \approx 0.32$ in. For that case, the width of the uncracked portion of the beam was only 0.08 in., i.e., a free boundary was very close to the crack tip. The values of K_Q found for the smallest crack length, $a \approx 0.12$ in., were in agreement with the others. That such small crack lengths would yield a constant value of K_Q is surprising. For metals, ASTM requires that the crack length and specimen thickness both exceed $2.5\,(K_{IC}/\sigma_{ys})^2$ where K_{IC} is the critical stress intensity factor and σ_{ys} is the yield strength. In the present case, if this criterion is evaluated using the composite yield strength from Table 11 then a crack length and specimen thickness of several inches results. This criterion appears unrealistic for B-Al composites, since Hoover found constant K_Q values for all crack lengths except the longest. Recent tests by Adsit and Waszczak [42] indicate also that K_Q for B-Al is a constant. Their results, based primarily on two specimens (a tensile specimen with a center hole and a DEC specimen), indicate a minimum required flaw size considerably higher than Hoover's.

TABLE 13. TOUGHNESS DATA FOR B-1100 AL COMPOSITES [41]

Sample	Crack Length a, (in.)	Crack Length to Width Ratio, a/w	Fracture Toughness K_Q (ksi$\sqrt{in.}$)
20 v/o 5.6 mil B-1100 Al			
1	0.115	0.288	16.1
2	0.123	0.308	16.5
3	0.199	0.498	17.8
4	0.247	0.618	17.3
5	0.279	0.698	18.4
6	0.315	0.788	11.1
48 v/o 5.6 mil B-1100 Al			
1	0.118	0.295	28.8
2	0.156	0.390	25.9
3	0.198	0.495	29.0
4	0.238	0.595	28.0
5	0.281	0.703	29.5
6	0.318	0.795	22.4
49 v/o 8.0 mil B-1100 Al			
1	0.115	0.288	27.6
2	0.158	0.395	27.2
3	0.195	0.488	28.6
4	0.242	0.605	30.3
5	0.276	0.690	28.1
6	0.324	0.810	24.2

Their curve shown in Figure 49 monotonically approaches a constant value of K_Q at a flaw size of approximately 0.3 in. as contrasted with Hoover's minimum crack size of approximately 0.12 in. Their curve contains the combined influence of two specimens—one with a hole and one with DEC. From the viewpoint of fracture toughness testing, a hole does not simulate a crack. Thus, the hole specimen may have unduly influenced the variation of K_Q with flaw size. The main point is that K_Q for

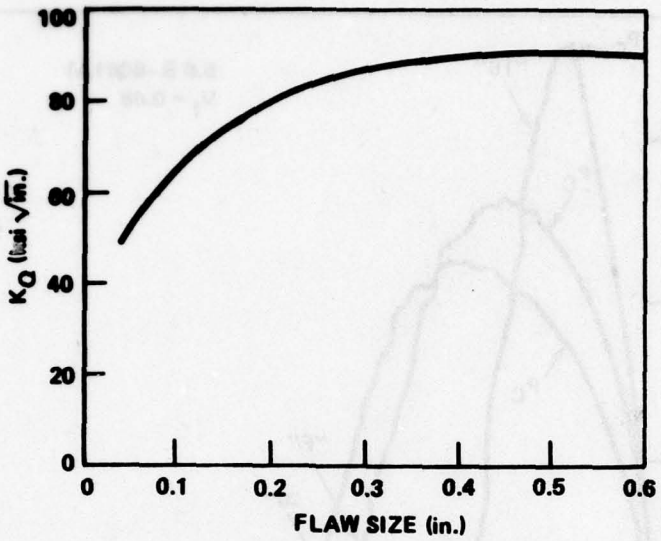

Figure 49. K_Q of unidirectional boron/aluminum as a function of flaw size [42].

unidirectional B-Al does appear to be a material constant independent of crack size and specimen dimensions.

Table 13 shows the influence of the fiber volume fraction. The toughness for the 48 v/o (approximately 28 ksi/in.$^{1/2}$) is approximately 60% greater than the 20 v/o (approximately 17 ksi-in.$^{1/2}$). The effect of fiber diameter is also shown in Table 13. There is no apparent difference in the toughness of the 5.6- and 8.0-mil materials.

The effect of crack tip plasticity as influenced by heat treatment of the B 6061 Al is shown in the load-deflection curves of Figure 50. Both the annealed (0 condition) material and the as-fabricated (F condition) material exhibit considerable nonlinearity prior to the pop-in load, as is usually characteristic of metals with substantial crack tip plasticity. The T6 material has a higher pop-in load and a more nearly linear load-displacement curve. The T6 heat treatment increases the yield strength, thus decreasing the extent of crack tip plasticity so that more nearly linear behavior results. The heat treatment did not appear to change the value of deflection at which pop-in occurred. The resulting fracture toughness values for the three heat treatments is shown in Table 14.

Hoover points out that when the load is applied to the composite, work is required at the crack tip to stretch the fibers elastically and to deform the Al matrix elastically and plastically. The crack-tip work is thus partitioned between the fibers and matrix. The yield strength of the matrix influences the partitioning between the fibers and matrix.

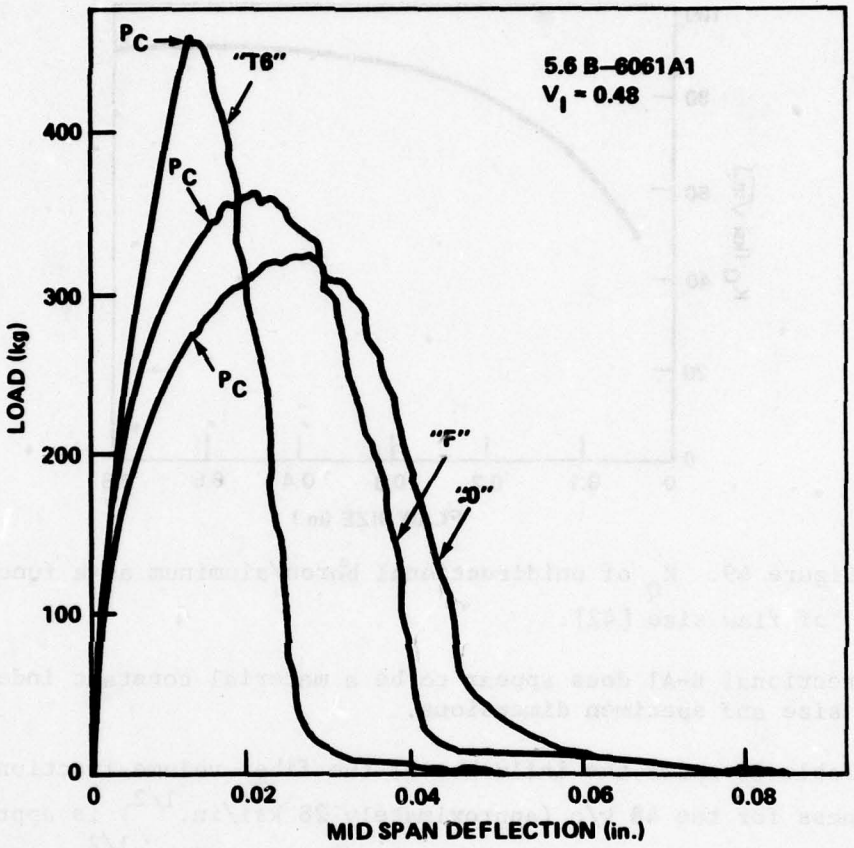

Figure 50. The effect of heat treatment on the load-deflection response of B-6061 Al composite [41].

Because the matrix yield strength did not affect the deflection at which crack initiation occurred, the difference in toughness is due to the difference in energy partitioning at the crack tip. The material with the highest yield strength (T6 treatment) absorbs more energy to the matrix, resulting in a higher toughness.

Hancock and Swanson [43] have reported a fracture toughness value of 33.7 ksi-in.$^{1/2}$ for 30 v/o, 4 mil, B-6061-T6, Al. As already noted for a higher volume fraction, the toughness should be greater. The value in Table 15 for a volume fraction of 48 is, in fact, larger by approximately 30%. Adsit and Waszczak [42] reported a toughness value for 5.6 mil, B-6061, Al in F condition; the fiber volume fraction was not reported. The toughness reported by them of 106.7 ksi-in.$^{1/2}$ seems too high in comparison with the value of approximately 34 ksi-in.$^{1/2}$ in Table 14 for the F condition material.

TABLE 14. TOUGHNESS DATA FOR 48 V/O 5.6 MIL B-6061 AL COMPOSITES [41]

Sample		Crack Length a, (in.)	Crack Length to Width Ratio, a/w	Fracture Toughness K_c (ksi$\sqrt{in.}$)
B-6061-	0-1	0.109	0.273	25.6
	0-2	0.141	0.353	27.5
	0-3	0.191	0.478	27.6
	0-4	0.237	0.593	28.5
	0-5	0.271	0.678	26.0
	0-6	0.313	0.783	18.9
B-6061-	F-1	0.120	0.300	33.5
	F-2	0.158	0.395	33.9
	F-3	0.197	0.493	36.7
	F-4	0.242	0.605	34.3
	F-5	0.265	0.663	30.3
	F-6	0.325	0.813	21.1
B-6061-	T6-1	0.116	0.290	45.0
	T6-2	0.150	0.375	45.1
	T6-3	0.192	0.480	43.6
	T6-4	0.226	0.565	44.2
	T6-5	0.293	0.733	44.2
	T6-6	0.311	0.778	25.9

Chapter 5. FRACTURE OF COMPOSITES CONTAINING STRESS CONCENTRATIONS

The application of fracture mechanics to a structural component of a given material requires a knowledge of that material's fracture toughness, whether obtained from the literature or from a fracture toughness testing program as discussed in Chapter 4. This chapter also discusses fracture toughness, but in light of three very specific applications relating to composites containing various stress concentrations.

Certain fiber composites with notches display peculiar fatigue behavior: surviving specimens of a fatigue test may show a residual strength equal to or greater than a specimen which has not been fatigue loaded. Moreover, the tensile static strength of laminated composites containing circular holes depends upon the hole size. This is not predicted by the classical stress concentration factor. These two features will be considered in this chapter.

5.1 Inherent Flaw Model

The behavior of fiber composites with stress raisers presents a marked contrast with that of metals. Typically, fatigue loading of notched specimens fails to produce fatigue cracks. The residual strength of the notched survivors of a fatigue test is almost the same as for unnotched specimens. Moreover, the fracture of such specimens, in the absence of a distinct fatigue crack, is nonetheless brittle. Furthermore, static tests of specimens with circular holes have shown that the laminate strength varies with hole size, even though the stress concentration factor does not. Waddoups et al. [44] presented the data in Table 15, which show the residual strength of notched, graphite/epoxy laminates after fatigue loading. The residual strength of the notched laminates is nearly the same as the unnotched laminate. The residual strength of the notched, fatigued laminates exceeded the static strength of those not fatigued.

Tables 16 and 17 present data by Waddoups et al. [44] based on tests performed at General Dynamics. These tables show the effect of hole size on laminate strength. As hole size increases, the static strength decreases.

Waddoups [44] introduced a model to explain the preceding behavior. The model consists of a hole from which two intense energy regions radiate (Figure 51). The intense energy regions are modeled as cracks which have a small but finite length a. The length a is taken to be the characteristic length of an inherent flaw. If it is now assumed that the isotropic stress intensity factor applies to the geometry of Figure 51, then the Bowie solution [1] or [3] for cracks emanating from a hole can be used. The Bowie solution is written as

$$K_I = \sigma\sqrt{\pi a}\, f\left(\frac{a}{R}\right) \tag{63}$$

AD-A051 866 ARMY MISSILE RESEARCH AND DEVELOPMENT COMMAND REDSTO--ETC F/G 20/11
FRACTURE MECHANICS DESIGN HANDBOOK FOR COMPOSITE MATERIALS.(U)
SEP 77 D G SMITH, B R MULLINIX

UNCLASSIFIED DRDMI-T-78-6 NL

2 OF 2
AD
A051866

END
DATE
FILMED
4-78
DDC

TABLE 15. $[0/90]_s$ GRAPHITE/EPOXY FATIGUE* [44]

Specimen** Diameter (in.)	Average Static Strength (psi)	Average Residual Strength After 5×10^6 cycles (psi)
No stress concentration	83,500	77,200
0.063 Hole	68,900	77,700
0.063 Hole + 0.018 × 0.004 Notch	72,200	74,300
0.063 Hole + 0.078 × 0.004 Notch	58,300	79,400

*This study was conducted under an in-house experimental program at General Dynamics Convair Aerospace Division Fort Worth Operation by E. L. McKague and R. J. Stout.
**Coupon specimens 1.0 in. wide and 9.0 in. long.

TABLE 16. SMALL HOLE DATA SUMMARY [44]

Specimen** Hole Diameter (in.)	Static Strength (psi)
Control	67,240
0.062	45,000
0.031	51,500
0.015	60,900

*This work was sponsored by the Air Force Materials Laboratory under Contract F33615-69-C-1494.
**Coupon specimens were 1.0 in. wide and 9.0 in. long.

where f (a/R) is a correction factor accounting for the hole boundary. Let critical conditions apply, $k_I \rightarrow k_Q$, and $\sigma \rightarrow \sigma_c$, where k_Q is the critical stress intensity factor and σ_c is the critical stress:

$$k_Q = \sigma_c \sqrt{\pi a}\, f\left(\frac{a}{R}\right) \quad . \tag{64}$$

TABLE 17. LARGE HOLE DATA SUMMARY* [44]

Specimen** Hole Diameter (in.)	Static Strength (psi)	
	Actual	Corrected for Finite Width
Control	76,000	76,000
1.0	26,600	27,900
2.5	15,900	22,800
3.0	13,250	23,000

*This work was sponsored by the Air Force Materials Laboratory under Contract F33615-69-C-1494.
**Coupon specimens were 5.0 in. wide and 38.0 in. long.

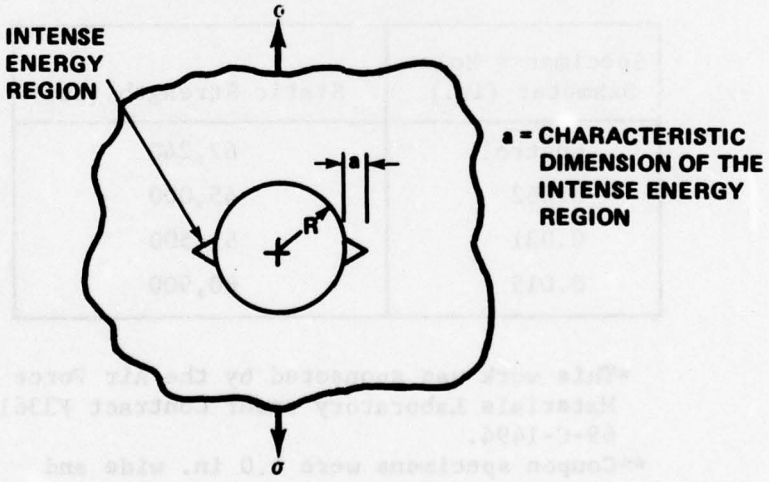

Figure 51. Fracture model of Waddoups et al. [44].

The stress intensity factor for a specimen with no hole, but only an inherent flaw of length a, is

$$k_I = \sigma\sqrt{\pi a} \quad . \tag{65}$$

Because a is assumed to be small, the free edge correction factor is unity. Assuming that K_Q is a material constant, the control specimen failed at a critical stress of σ_o so that

$$k_Q = \sigma_o\sqrt{\pi a} \quad . \tag{66}$$

From Equations (64) and (66)

$$\frac{\sigma_o}{\sigma_c} = f\left(\frac{a}{R}\right) \quad ; \tag{67}$$

thus, the ratio of the failure stress σ_o of a control specimen and the failure stress σ_c of a notched specimen is given by the Bowie correction factor if a, the inherent flaw length, is known. Figure 52 shows the ratio σ_o/σ_c in terms of the hole radius R for four assumed values of a.

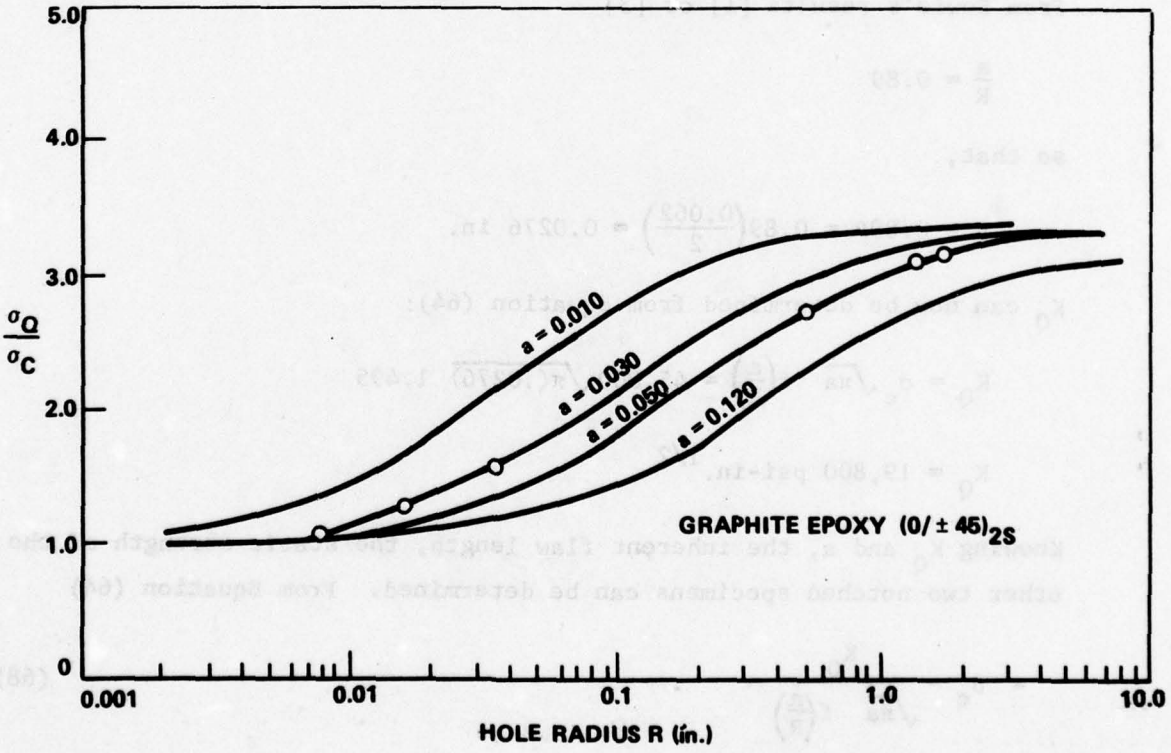

Figure 52. Parametric study of critical stress and flaw length [44].

The failure stresses from Tables 16 and 17 are also plotted there. It can be seen that a value of a $\approx$ 0.04 in. fits both sets of data points with reasonable accuracy.

Based on the strength of a control specimen and a notched specimen with the Waddoups model it is possible to predict the strength of other notched laminates of similar geometry. The method is a two-parameter one; the two parameters are K_Q and a. Equation (67) is used to find the function f(a/R). With f(a/R) known, the Bowie solution is used to find the ratio a/R. For the notched test specimen, R is known and with a/R known, the inherent flaw length a can be calculated. With a known, then either Equation (64) or Equation (66) can be used to find K_Q, the critical stress intensity factor. With K_Q and a known, Equation (64) can be used to predict the critical stress σ_c of other notched laminates. A numerical example will clarify the procedure. If the data for hole radii less than 0.5 in. in Table 16 are considered and the strengths of the first two specimens are substituted specimens into Equation (67), the result is

$$f\left(\frac{a}{R}\right) = \frac{\sigma_o}{\sigma_c} = \frac{67,240}{45,000} = 1.495 \quad .$$

From Bowie's results [1] or [3]

$$\frac{a}{R} = 0.89$$

so that,

$$a = 0.89R = 0.89\left(\frac{0.062}{2}\right) = 0.0276 \text{ in.}$$

K_Q can now be determined from Equation (64):

$$K_Q = \sigma_c \sqrt{\pi a} \quad f\left(\frac{a}{R}\right) = 45,000 \sqrt{\pi(.0276)} \; 1.495$$

$$K_Q = 19,800 \text{ psi-in.}^{1/2}$$

Knowing K_Q and a, the inherent flaw length, the static strength of the other two notched specimens can be determined. From Equation (64)

$$\sigma_c = \frac{K_Q}{\sqrt{\pi a} \quad f\left(\frac{a}{R}\right)} \quad . \tag{68}$$

The specimen with the 0.031 in. diameter hole is considered:

$$R = \frac{0.031}{2} = 0.0155$$

$$\frac{a}{R} = \frac{0.0276}{0.0155} = 1.78$$

and from the Bowie solution,

$$f\left(\frac{a}{R}\right) = 1.24 \quad .$$

(Note: Some of the numbers here differ slightly from those in Reference 44.) From Equation (68):

$$\sigma_c = 54{,}200 \text{ psi} \quad .$$

This agrees reasonably well with the measured value of 51,500 psi. For the specimen with a hole of 0.015 in., σ_c is found to be 60,200 psi as compared to the measured value of 60,900 psi.

The data in Table 17 are now considered for hole diameters of 1.0 to 3.0 in. Using σ_o for the control specimen and σ_c for the 1-in. hole,

$$f\left(\frac{a}{R}\right) = \frac{\sigma_o}{\sigma_c} = \frac{76{,}000}{27{,}900} = 2.72$$

from the Bowie solution

$$\frac{a}{R} = 0.100$$

so that

$$a = 0.100 \left(\frac{1.0}{2}\right) = 0.0500 \text{ in.}$$

and from Equation (64)

$$K_Q = 30{,}100 \text{ psi-in.}^{1/2}$$

For the specimen with the 2.50-in. hole,

$$\frac{a}{R} = \frac{0.050}{1.25} = 0.040$$

and

$$f\left(\frac{a}{R}\right) = 3.13 \quad ,$$

then $\sigma_c = 24{,}300$ psi .

which compares well with the measured value of 22,800 psi. Similarly, for the laminate with a 3.0-in. hole, σ_c is found to be 23,900 psi as compared to a measured value of 23,000 psi.

The values found for the inherent flaw lengths of 0.0276 and 0.0500 in. bracket the nominal value of 0.0400 in. noted before from Figure 52.

The physical basis for an inherent flaw, a, has been enforced somewhat by Cruse [27]. Cruse modeled circular notches with equivalent ideal cracks. The equivalent crack length was obtained by calculating stress intensity factors for the notches based on the similarity, over a given region of the transverse stresses ahead of a notch and a crack. The equivalent half-crack length was greater than the hole radius by an amount which was close to the inherent flaw length. The inherent flaw length calculated from Equation (63), was nearly the same for the two laminates $(0_4/\pm 45)$ and $(0/\pm 45)$. This implied the possibility that the inherent flaw size is real and relatable to the microstructure.

The Waddoups model has been discussed by Brinson and Yeow [45] who compared the model stresses with measured failure stresses on several graphite epoxy laminates containing holes. The comparison was not direct; it was necessary to adjust the data for the finite-width plates before comparison with the theory which is for infinitely wide plates. The correlation between theory and experiment was better for unidirectional laminates than for angle ply laminates.

It has been pointed out by Kanninen et al. [46] from a philosophical viewpoint that the Waddoups model is essentially empirical, a two parameter empirical correlation of limited test data. Nevertheless, the model may afford a useful method of predicting the strength of notched structural components. It needs further verification for a number of laminate materials and configurations.

5.2 Stress Fracture Criteria for Notched Laminates

The fracture of laminates containing holes has been investigated by Whitney and Nuismer [47, 48] using two stress criteria. While it is not a fracture mechanics approach, their method assumes the existence of an inherent flaw. By applying their criteria to the case of a crack, they derive a basic relationship for the effect of crack length on fracture toughness.

A hole of radius R in an orthotropic laminate subjected to a remote stress of σ parallel to the y-axis is considered. The normal stress σ_{yy} along the x-axis in front of the hole is

$$\sigma_{yy}(x, o) = \frac{\sigma}{2}\left\{2 + \left(\frac{R}{x}\right)^2 + 3\left(\frac{R}{x}\right)^4 - \left(K_T^{\infty} - 3\right)\left[5\left(\frac{R}{x}\right)^6 - 7\left(\frac{R}{x}\right)^8\right]\right\}$$

$$x > R \qquad (69)$$

where K_T^{∞} is the orthotropic stress concentration factor for an infinite plate and is determined from

$$K_T^{\infty} = 1 + \sqrt{\frac{2}{C_{22}}\left(\sqrt{C_{11}C_{22}} - C_{12} + \frac{C_{11}C_{22} - C_{12}^2}{2\,C_{22}}\right)} \quad . \qquad (70)$$

The constants C_{ij} are the in-plane laminate stiffness coefficients of Equation (12). In terms of the effective elastic moduli for the laminate which are the same form as Equations (3), but indicated by an overline here, Equation (70) becomes,

$$K_T^{\infty} = 1 + \sqrt{2\left(\sqrt{\frac{\overline{E}_{11}}{\overline{E}_{22}}} - \overline{\nu}_{12}\right) + \frac{\overline{E}_{11}}{\overline{G}_{12}}} \qquad (71)$$

For the isotropic case $K_T^{\infty} = 3$, Equation (69) reduces to the first three terms which are the exact isotropic distribution.

$$\frac{\sigma_{yy}}{\sigma} = 1 + \frac{1}{2}\left(\frac{R}{x}\right)^2 + \frac{3}{2}\left(\frac{R}{x}\right)^4 \qquad (72)$$

For the sake of simplicity, the remaining discussion will be based on this equation for an isotropic or quasi-isotropic laminate rather than the more complex expression in Equation (69). If Equation (72) is plotted in the usual manner as a function of the nondimensional variable, x/R, then the results obviously are independent of the hole size. In terms of physical distance from the edge of the hole (x-R), however, the distribution will be different for different hole sizes. For example, Figure 53 shows the distribution for two cases: R = 1.0 and R = 0.1. It seems reasonable that the strength of the laminate with the larger hole would be lower. For the larger hole, a greater volume of material is subjected to high stress, increasing the probability that an inherent flaw will exist in a region of high stress, thus lowering the strength of the plate. From Figure 53 it also appears that the smaller hole has a better opportunity to redistribute the stress resulting in a higher strength for the plate with the small hole. These two observations suggested to Whitney and Nuismer that a criterion based on the stress magnitude at a point — in this instance, the edge of the hole — was not reasonable and that the stress distribution over some characteristic length must be considered.

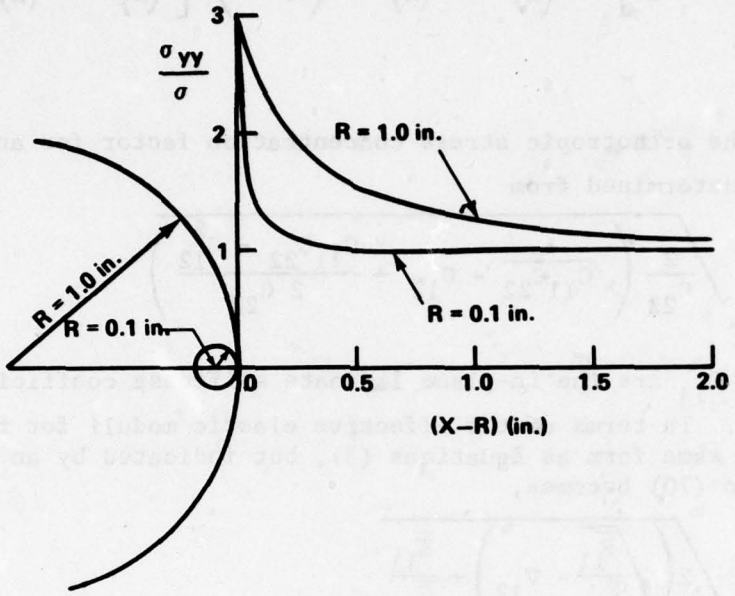

Figure 53. Stress distribution for a hole in an infinite isotropic plate [47].

They chose two models, each involving a characteristic length denoted by d_o and a_o. The first model assumes that failure occurs when the normal stress at a fixed distance, d_o, from the edge of the hole reaches a value of σ_o, the unnotched tensile strength of the laminate. The distance d_o is assumed to be a material constant; it represents the distance over which the material must be highly stressed to find a flaw sufficiently large to initiate fracture. The criterion in equation form is

$$\sigma_{yy}\ (o, x)\ \Big|_{x = R + d_o} = \sigma_o \quad . \tag{73}$$

Using Equation (72) results in the ratio of the notched to unnotch strength

$$\frac{\sigma_N}{\sigma_o} = \frac{2}{\left(2 + \xi_1^2 + 3\xi_1^4\right)} \tag{74}$$

where σ_N is the notched strength and $\xi_1 = R/(R + d_o)$. For small holes, $\xi_1 \to 0$ and $\sigma_N/\sigma_o \to 1$ and Equation (74) predicts no strength reduction; whereas for large holes, $\xi_1 \to 1$ and $\sigma_N/\sigma_o \to 1/3$, so that the strength reduction is governed by the classical stress concentration factor. Thus

Equation (74) gives the correct limits. The appropriate value of d_o must be determined from test data. Whitney and Nuismer [47] compared Equation (74) using varying values of d_o to test data on a quasi-isotropic glass/epoxy of different hole radii. Their results are shown in Figure 54. The values of d_o are the same as those found by Waddoups [44] for boron/epoxy using the Bowie crack model: 0.03 in. fits the small hole data, 0.05 in. fits the large hole data, and 0.04 in. is a good compromise value to represent all data with reasonable accuracy.

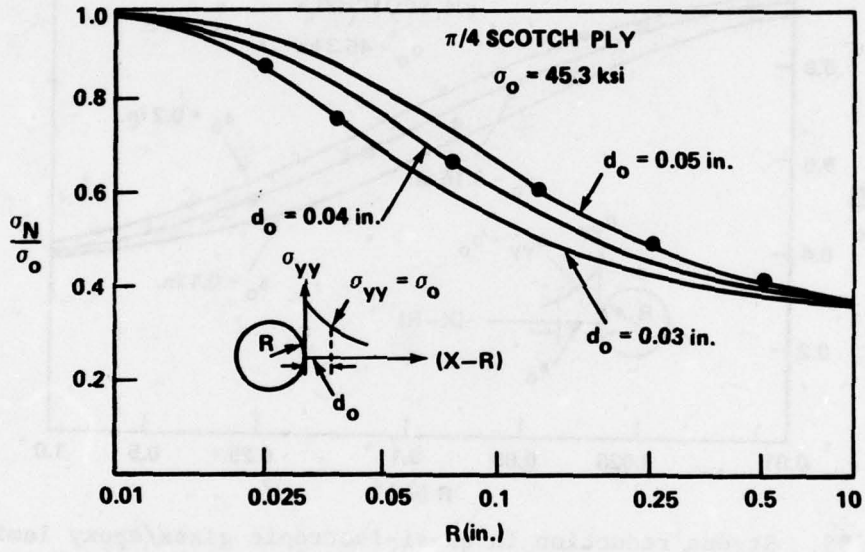

Figure 54. Stress reduction in quasi-isotropic glass/epoxy laminates due to the presence of a circular hole, point stress criterion [47].

A second approach developed by Whitney and Nuismer [47] requires calculating the average stress over some distance a_o, also taken to be a material constant independent of laminate construction and stress distribution. Physically, this distance is assumed to represent a length over which failure has occurred with subsequent stress redistribution. Failure is assumed to occur when the average stress reaches the unnotched tensile strength, σ_o. In equation form,

$$\frac{1}{a_o} \int_R^{R+a_o} \sigma_{yy}(x, o)dx = \sigma_o \quad . \tag{75}$$

Substituting Equation (72) into Equation (75) and doing the integration results in

$$\frac{\sigma_N}{\sigma_o} = \frac{2(1 - \xi_2)}{\left(2 - \xi_2^2 - \xi_2^4\right)} \tag{76}$$

where $\xi_2 = R/(R+a_o)$. Equation (76) is compared with glass/epoxy data in Figure 55. The values of a_o shown are 0.1, 0.15, and 0.2 in., with the value of 0.15 in. giving the best comparison with data.

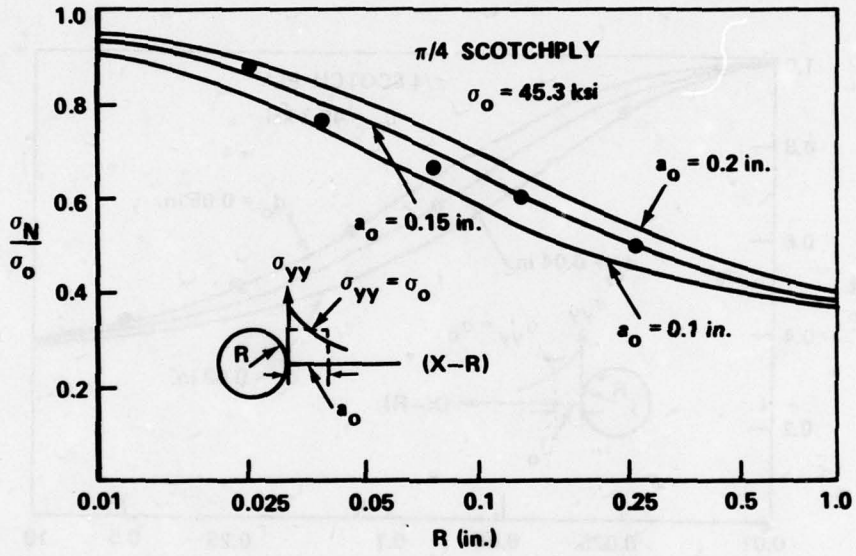

Figure 55. Stress reduction in quasi-isotropic glass/epoxy laminates due to the presence of holes, average stress criteria [47].

The data in Figures 54 and 55 are too limited to conclude whether the point stress or the average stress criteria is most accurate. Nuismer and Whitney [47] have compared the two models for a number of laminate configurations of both glass/epoxies and graphite/epoxies. The comparison, based on the general anisotropic results in Equation (69), was inconclusive due to data scatter. Brinson and Yeow [45] compared the two models with test data on several graphite epoxy laminates. After adjusting the finite-plate data to the infinite plate case, the comparison was rather inconclusive. As a design tool, either of the two models seems reasonably accurate.

The two models of Whitney and Nuismer [47] also provide insight into the question of K_Q dependency on crack length. A straight crack of length 2a, in an infinite anisotropic plate loaded remotely by a stress normal to the crack surface is considered. If the origin of the x-y coordinate system is located at the crack center, the normal stress σ_{yy} ahead of the crack tip is approximated by

$$\sigma_{yy} = \frac{K_I}{\sqrt{2\pi(x - a)}} \quad . \tag{77}$$

This is the usual fracture mechanics stress. For this case, $K_I = \sigma\sqrt{\pi a}$. Equation (77) is accurate at points within, say, a/10 of the crack tip. Obviously for short cracks, small a, the region of applicability is very narrow. Therefore, Whitney and Nuismer proposed using the exact expression

$$\sigma_{yy} = \frac{K_I x}{\sqrt{\pi a(x^2 - a^2)}} = \frac{\sigma x}{\sqrt{x^2 - a^2}} \quad . \tag{78}$$

Equations (77) and (78) are compared in Figure 56 for a = 0.1 and 1.0 in. The stress in Equation (77) as a function of (x - a), is independent of the crack length and gives the same curve for both crack lengths; this is shown

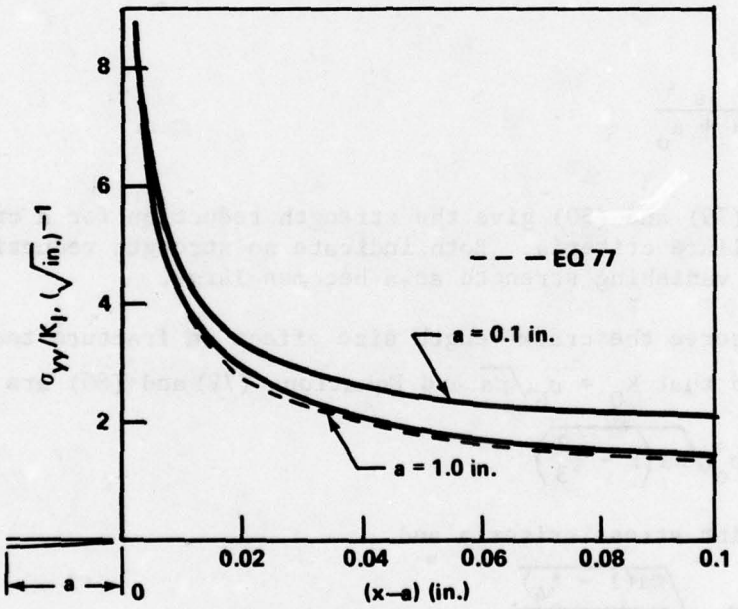

Figure 56. Stress distribution for a crack in an infinite anisotropic plate.

as a dashed line. Equation (78) shows a considerable difference in the stress for the two crack lengths. For the long crack, the approximate and exact expressions, Equations (77) and (78), show good agreement. It is apparent that if failure is assoicated with a fixed characteristic length such as d_o or a_o, constant for all crack lengths; then for short cracks, Equation (78) should be used.

Now the exact stress Equation (78) is used in both failure criteria (changing R to a) in Equations (73) and (75). For the point stress and average stress criteria, respectively, results are

$$\frac{\sigma_N}{\sigma_o} = \sqrt{1 - \xi_3^2} \tag{79}$$

where

$$\xi_3 = \frac{a}{a + d_o}$$

and

$$\frac{\sigma_N}{\sigma_o} = \sqrt{\frac{1 - \xi_4}{1 + \xi_4}} \tag{80}$$

where

$$\xi_4 = \frac{a}{a + a_o}$$

Equations (79) and (80) give the strength reduction for a crack according to each failure criteria. Both indicate no strength reduction for short cracks and vanishing strength as a becomes large.

To observe the crack length size effect on fracture toughness, K_Q, it is noted that $K_Q = \sigma_N\sqrt{\pi a}$ and Equations (79) and (80) are rewritten as

$$K_Q = \sigma_o\sqrt{\pi a\left(1 - \xi_3^2\right)} \tag{81}$$

for the point stress criteria and

$$K_Q = \sigma_o\sqrt{\frac{\pi a(1 - \xi_4)}{(1 + \xi_4)}} \tag{82}$$

for the average stress criteria. For long crack lengths, Equations (81) and (82) asymptotically approach the respective constant values of

$$K_Q = \sigma_o\sqrt{2\pi d_o} \tag{83}$$

and

$$K_Q = \sigma_o \sqrt{\frac{\pi a_o}{2}} \tag{84}$$

which result from the approximate stress given by Equation (77). Figures 57 and 58 show the crack length effect for both criteria compared with graphite/epoxy data. The figures show that no constant value of K_Q should be expected below a crack length, a, of approximately 0.4 in. This compares well with the recommended minimum crack size noted in Chapter 4 based on Figure 40.

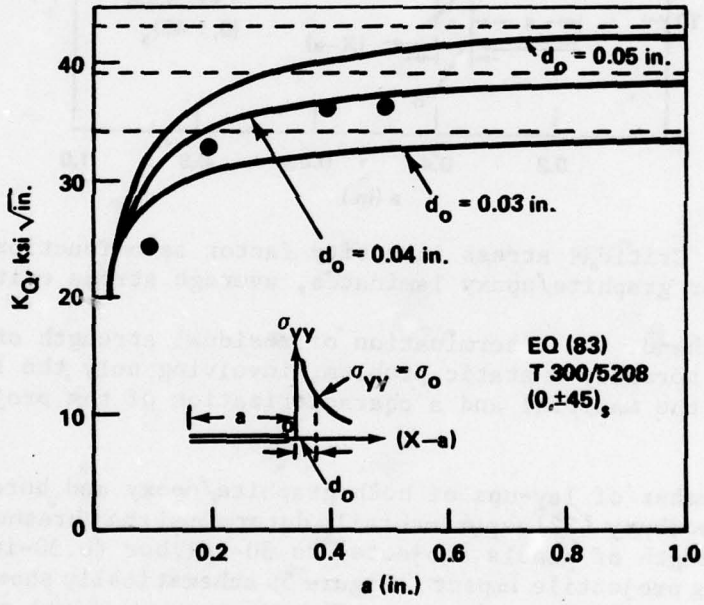

Figure 57. Critical stress intensity factor as a function of crack length for graphite/epoxy laminates, point stress criterion [47].

5.3 Fracture Due to Ballistic Impact

The hazard of ballistic impact is one which must be considered in the design of military aircraft. Two quantities are of immediate interest: the threshold strength and the residual strength. The threshold strength is the applied load at which the structure will immediately fail upon impact by a given type of projectile impact. The residual strength refers to the maximum load the structure will still sustain subsequent to projectile damage. Analytically, the determination of threshold strength is a dynamic problem influenced by time dependent material response and the nature of the target-projectile interaction.

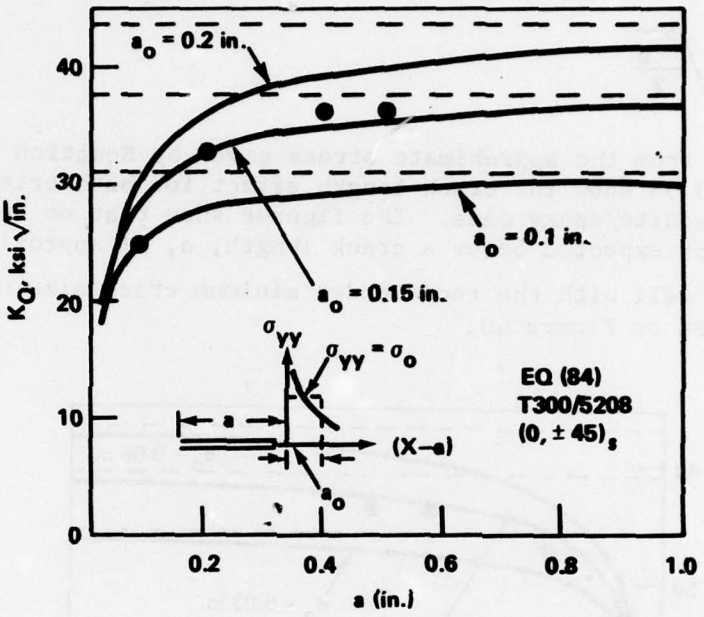

Figure 58. Critical stress intensity factor as a function of crack length for graphite/epoxy laminates, average stress criterion [47].

On the other hand, the determination of residual strength of a damaged component is normally a static problem, involving only the fracture toughness of the material and a characterization of the projectile damage.

For a number of lay-ups of both graphite/epoxy and boron/epoxy, Olster and Woodbury [22] experimentally determined the threshold strength and residual strength of panels subjected to 30-caliber (0.30-in. diameter) armor piercing projectile impact. Figure 59 schematically shows the loaded specimens in the experimental setup. The measured residual strengths of graphite/epoxy panels for various lay-ups varied from approximately 61% to 73% of the true ultimate tensile strength. The threshold strengths were slightly lower, varying from approximately 51% to 65% of the tensile strength. For boron/epoxy, the residual strength varied from approximately 52% to 65% of the tensile strength. Again, the threshold strength was only slightly less, approximately 92% of the residual strength. The measured residual strengths for the various lay-ups are shown in Table 18.

Because the threshold strength appears to be only slightly less than the residual strength, predictions of the residual strength also provide a rough approximation to the threshold strength. The advantage of this observation is that residual strength predictions are much easier to make than are threshold predictions. To make residual strength calculations, the character of the expected damage and the fracture toughness of the material must be known.

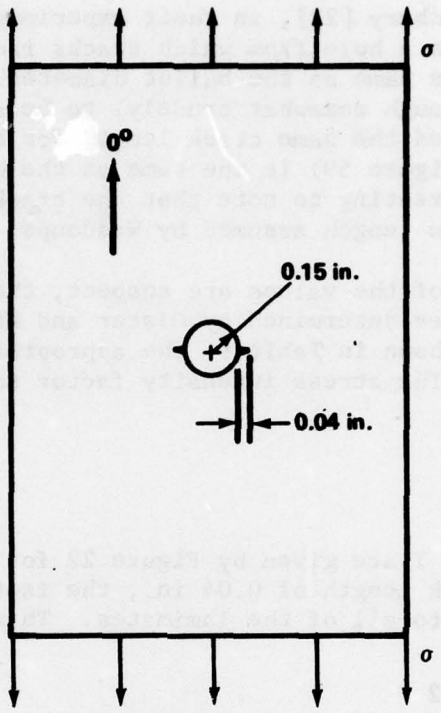

Figure 59. Fracture mechanics model of a laminate panel damaged by ballistic impact of a 30-caliber armor piercing projectile.

TABLE 18. COMPARISON OF THE PREDICTED AND MEASURED RESIDUAL STRENGTH OF A BALLISTICALLY DAMAGED PANEL

Laminate Configuration	Fracture Toughness kc (ksi $\sqrt{in.}$)	Residual Strength		
		Predicted	Measured	
		$\sigma_c = \frac{kc}{Y(a)^{1/2}}$	Measured (ksi)	Percent of True Ultimate Strength
Boron Epoxy				
$(0/\pm45/0)_s$	21.1	46.8	44.8	52.6
$(0_2/\pm45/0/90)_s$	32.6	72.6	74.9	65.6
$(0/\pm60_2/0)_s$	18.2	40.5	41.2	60.6
Graphite Epoxy				
$(0/\pm45/0)_s$	21.6*	48.0	51.9	73.0
$(0_2/\pm45/90)_s$	13.5*	30.0	36.0	63.1
$(0_2/\pm60_3/0_2)_T$	17.4*	38.6	32.9	61.4

*At onset of failure.

Olster and Woodbury [22], in their experiments, characterized the projectile damage as a hole from which cracks radiate. The hole diameter is approximately the same as the bullet diameter. The hole-edge cracks were measured (although somewhat crudely) to be approximately 0.04 in. in length. They used the same crack length for both boron and graphite. Now this problem (Figure 59) is the same as the Waddoups [44] model. In fact, it is interesting to note that the crack length is the same as the inherent flaw length assumed by Waddoups.

Although some of the values are suspect, the fracture toughness for the subject laminates determined by Olster and Woodbury [22] were already discussed and are shown in Table 9; the appropriate values are repeated here in Table 18. The stress intensity factor solution needed for the problem is

$$k_I = Y\sigma a^{1/2} \tag{85}$$

where the values of Y are given by Figure 22 for the various laminates. However, for a crack length of 0.04 in., the isotropic solution gives a good approximation to all of the laminates. Therefore, $Y \approx 2.24$ is used so that

$$k_I = 2.24\ \sigma a^{1/2} \tag{86}$$

It should be noted that the definition of k_I being used here is $k_I = K_I/\sqrt{\pi}$. In Equation (86) let k_I assume its critical value for each respective laminate and $a = 0.04$ in.; then σ, the residual strength, is easily calculated.

These calculated values of residual strength are compared with the measured residual strength in Table 18. There is good agreement for boron/epoxy. The agreement for graphite/epoxy is fair. It must be explained that different definitions of fracture toughness were used for the two materials. Two sets of values were given in Table 9, one [22] corresponds to the fracture toughness; the other corresponds to the value of k at the onset of fracture. These two definitions were used for boron and graphite, respectively. This is an unfortunate ambiguity caused by the lack of a working definition of exactly what constitutes fracture (i.e., a definition in terms of load displacement behavior such as that for metals) during a toughness test. To contrast the behavior of the two materials under discussion here, it was noted [22] that during the toughness tests the boron materials fractured in a manner characteristic of a valid test with very little delamination whereas the graphite materials suffered considerable crack-tip delamination before final fracture. Although the vigor of this example is compromised by the ambiguous use of the fracture toughness values, it

nevertheless serves to illustrate methods of strength calculations and the potential usefulness of making residual strength predictions.

LIST OF SYMBOLS

a	Crack length, half crack length
a_o	Distance over which average stress is computed
a_{11}, a_{12}, a_{16}, etc.	Compliance coefficients for an anisotropic laminate, Equation (15)
A	Area
A_{11}, A_{12}, A_{16}, etc.	Stiffness coefficients for an anisotropic laminate, Equation (9)
b	Half plate width; semiminor axis of an ellipse
B	Laminate thickness
C	Compliance of fracture specimen
C'	Constant
C_{11}, C_{12}, C_{16}, etc.	Stiffness coefficients for an anisotropic laminate, Equation (12)
d_o	Distance from edge of hole at which a characteristic stress occurs
E	Young's modulus for isotropic material
E_{11}, E_{22}	Young's moduli in material's principal directions for orthotropic plate
$\bar{E}_{11}$, $\bar{E}_{22}$	Effective Young's moduli in material's principal direction's for orthotropic laminate
E_x, E_y	Young's moduli in x and y directions for orthotropic plate, Figures 15, 17, and 18
f (a/R)	Isotropic correction factor for the stress intensity for cracks emanating from the edge of a hole
F	Force
g	Strain energy release rate
g_c	Critical value of the strain energy release rate

g_Q	Candidate critical value of g
g_I, g_{II}	Strain energy release rate for Mode I and Mode II loading
G	Shear modulus for an isotropic material
G_{12}	Shear modulus for orthotropic plate
$\bar{G}_{12}$	Effective shear modulus for an orthotropic laminate
G_{xy}	Shear modulus for orthotropic plate, Figures 15, 17, and 18
h	Half average clear spacing between fibers
h_1, h_2 h_3, etc.	Ply thickness
H	Anisotropic correction factor to isotropic solution, Equation (30)
k, K	Stress intensity factors, $K = \sqrt{\pi}\, k$
k_c, K_c	Critical stress intensity factors, $K_c = \sqrt{\pi}\, k_c$
k_Q, K_Q	Candidate values of fracture toughness, $K_Q = \sqrt{\pi}\, k_Q$
k_I, K_I	Mode I stress intensity factors, $K_I = \sqrt{\pi}\, k_I$
k_{II}, K_{II}	Mode II stress intensity factors, $K_{II} = \sqrt{\pi}\, k_{II}$
k_{IC}, K_{IC}	Mode I fracture toughness, $K_{IC} = \sqrt{\pi}\, k_{IC}$
k_{IIC}, K_{IIC}	Mode II fracture toughness, $K_{IIC} = k_{IIC}$
K_T^{∞}	Orthotropic stress concentration factor for a hole
ℓ	Length of end tabs
ℓ_f	Distance between crack tip and a free edge
L	Plate length
m	Slope of straight line
N_x, N_y, N_{xy}	In-plane stress resultants
p_j, q_j	Combination of certain elastic properties, Equation (20)

P	Load
P_c	Critical value of load in fracture test
q_j, P_j	Combination of certain elastic properties, Equation (20)
Q_{11}, Q_{12}, Q_{16}, etc.	Stiffness coefficients for anisotropic plate Equation (1)
$\bar{Q}_{11}$, $\bar{Q}_{12}$, $\bar{Q}_{16}$, etc.	Stiffness coefficients for orthotropic plate referred to arbitrary in-plane coordinate axes, Equation (6)
r, θ	Crack-tip polar coordinates
r_o	Radius of core region, Figure 31; radius of damage zone, Equation (62)
R	Hole radius; fiber radius
S	Strain energy density factor
S_c	Critical value of S with $\theta = \theta_c$.
S_{11}, S_{12}, S_{16}, etc.	Compliance coefficients for orthotropic plate, Equation (4)
$\bar{S}_{11}$, $\bar{S}_{12}$, $\bar{S}_{16}$, etc.	Compliance coefficients for orthotropic plate referred to arbitrary in-plane coordinate axes, Equation (8)
u, v	Displacement components in the x and y directions, respectively
v_f	Fiber volume fraction, V_R/V_T
V_R	Volume of fibers
V_T	Total volume of matrix and fiber
W	Plate width; strain energy
x, y	Rectangular coordinates
Y	Anisotropic free edge correction factor
Y^*	Isotropic free edge correction factor
α	Fiber angle

α_{11}, α_{12}, α_{22}	Coefficients in the expression for S, Equation (51)
β	Angle of crack with load, Figure 32
β_1, β_2	Combinations of elastic constants, Equation (32)
ϵ_1, ϵ_2, γ_{12}	Strain components referred to orthotropic plate's principal axes
ϵ_{xx}, ϵ_{yy}, γ_{xy}	Strain components
θ	Transformation angle between principal axes and arbitrary axes
θ_o	Direction of maximum value of S
θ, r	Crack-tip polar coordinates
μ_1, μ_2, μ_3, μ_4	Roots of characteristic equation, Equation (17)
ν	Poisson's ratio for an isotropic material
ν_{12}, ν_{21}	Poisson's ratios for an orthotropic material
$\bar{\nu}_{12}$	Effective Poisson's ratio for an orthotropic laminate
ν_{xy}, ν_{yx}	Poisson's ratio for orthotropic plate Figures 15, 17, and 18
ξ_1	Equal to $R/(R + d_o)$
ξ_2	Equal to $R/(R + a_o)$
ξ_3	Equal to $a/(a + d_o)$
ξ_4	Equal to $a/(a + a_o)$
σ	Normal stress, usually remote load
σ_c	Critical value of stress at fracture
σ_o	Failure stress of an unnotched control specimen
σ_N	Failure stress of a notched specimen

σ_{ys}	Yield stress
σ_{1U}	Ultimate stress in fiber direction
σ_1, σ_2, τ_{12}	Stress components referred to orthotropic plate's principal axes
σ_{xx}, σ_{yy}, τ_{xy}	Stress components
$\bar{\sigma}_{xx}$, $\bar{\sigma}_{yy}$, $\bar{\tau}_{xy}$	Laminate average stress components, Equation (11)
τ	Shearing stress, usually remote load
$\phi(1)$, $\psi(1)$	Solutions to Fredholm integral equations

LIST OF TABLES

LIST OF FIGURES

REFERENCES

1. Smith, D. G. and Mullinix, B. R., Fracture Mechanics Design Handbook, US Army Missile Command, Redstone Arsenal, Alabama, December 1976, Technical Report RL-77-5.

2. Sih, G. C., Paris, P. C., and Irwin, G. R., "On Cracks in Rectilinearly Anisotropic Bodies," International Journal of Fracture Mechanics, Vol. 1, No. 3, September 1965, pp. 189-203.

3. Paris, P. C. and Sih, G. C., "Stress Analysis of Cracks," Fracture Toughness Testing and Its Applications, American Society for Testing and Materials, 1965, pp. 30-83, ASTM STP 381.

4. Griffith, A. A., "The Phenomena of Rupture and Flow in Solids," Philosophical Transactions, Royal Society of London, Series A, Vol. 221, March 1921, pp. 163-198.

5. Wu, E. M., "Application of Fracture Mechanics to Anisotropic Plates," Journal of Applied Mechanics, Vol. 34, 1967, pp. 967-975.

6. Wu, E. M. and Reuter, R. C., Jr., Crack Extension in Fiberglass Reinforced Plastics, University of Illinois, Urbana, Illinois, February 1965, T and AM Report No. 275.

7. Konish, H. J., Jr., Swedlow, J. L., and Cruse, T. A., "Experimental Investigation of Fracture in an Advanced Fiber Composite" Journal of Composite Materials, Vol. 6, 1972, pp. 114-124.

8. Konish, H. J., Jr. and Cruse, T. A., A Study of Fracture Phenomena in Fiber Composites Laminates, Vol. III, Air Force Materials Laboratory, Air Force Systems Command, Wright Patterson Air Force Base, Ohio, September 1973, Technical Report AFML-TR-73-145.

9. Konish, H. J., Jr., Swedlow, J. L., and Cruse, T. A., "Fracture Phenomena in Advanced Fiber Composite Materials" AIAA Journal, Vol. 11, No. 1, 1973, pp. 40-43.

10. Astronautic Structures Manual, Vol. III, Structures and Propulsion Laboratory, NASA, George C. Marshall Space Flight Center, Marshall Space Flight Center, Alabama, August 1975, NASA TM X-73307.

11. Ashton, J. E., Halpin, J. C., and Petit, P. H., Primer on Composite Materials: Analysis, Stamford, Connecticut: Technomic Publishing Co., Inc., 1969.

12. Corten, H. T., "Fracture Mechanics of Composites," Fracture-An Advanced Treatise, Vol. 7, Fracture of Nonmetals and Composites, H. L. Liebowitz-Ed., New York: Academic Press, 1972.

13. Lekhnitiskii, S. C., Theory of Elasticity of an Anisotropic Body, New York: Holden-Day Inc., 1963.

14. Tada, H., The Stress Analysis of Cracks Handbook, Hellertown, Pennsylvania, Del Research Corporation, 1973.

15. Cruse, T. A. and Osias, J. R., Exploratory Development on Fracture Mechanics of Composite Materials, Air Force Materials Laboratory, Air Force Systems Command, Wright Patterson Air Force Base, Ohio, April 1974, Technical Report AFML-TR-74-111.

16. Snyder, M. D. and Cruse, T. A., Crack Tip Stress Intensity Factors in Finite Anisotropic Plates, Air Force Materials Laboratory, Air Force Systems Command, Wright Patterson Air Force Base, Ohio, August 1973, Technical Report AFML-TR-73-209.

17. Cruse, T. A. and Swedlow, J. L., Interactive Program for Analysis and Design Problems in Advanced Composites Technology, Air Force Materials Laboratory, Air Force Systems Command, Wright Patterson Air Force Base, Ohio, December 1971, Technical Report AFML-TR-71-268.

18. Atluri, S. N., Kobayashi, A. S., and Nakagaki, M., "A Finite Element Program for Fracture Mechanics Analysis of Composite Material," Fracture Mechanics of Composites, American Society for Testing and Materials, 1975, pp. 86-98, ASTM STP 593.

19. Bowie, O. L. and Freese, C. E., "Central Crack in Plane Orthotropic Rectangular Sheet," International Journal of Fracture Mechanics, Vol. 8, No. 1, March 1972, pp. 49-58.

20. Konish, H. J., Jr., "Mode I Stress Intensity Factors for Symmetrically-Cracked Orthotropic Strips," Fracture Mechanics of Composites, American Society for Testing and Materials, 1975, pp. 99-116, ASTM STP 593.

21. Mandell, J. F., Wang, S. S., and McGarry, F. J., Fracture of Graphite Fiber Reinforced Composites, Massachusetts Institute of Technology, prepared for Air Force Materials Laboratory, July 1973, AD-775 729.

22. Olster, E. F. and Woodbury, H. A., Evaluation of Ballistic Damage Resistance and Failure Mechanism of Composite Materials, Air Force Materials Laboratory, Air Force Systems Command, Wright Patterson Air Force Base, Ohio, April 1972, AFML-TR-72-79.

23. Irwin, G. R., Analytical Aspects of Crack Stress Field Problems, University of Illinois, 1962, T and AM Report 213.

24. Lauraitis, K., Tensile Strength of Off-Axis Unidirectional Composites, University of Illinois, August 1971, T and AM Report No. 344.

25. Slepetz, J. M. and Carlson, L., "Fracture of Composite Compact Tension Specimens," Fracture Mechanics of Composites, American Society for Testing and Materials, 1975, pp. 143-162, ASTM STP 593.

26. "Plane-Strain Fracture Toughness of Metallic Materials," American Society for Testing and Materials Standards, Vol. 31, 1973, E 399.

27. Cruse, T. A., "Tensile Strength of Notched Composites," Journal of Composite Materials, Vol. 7, April 1973, pp. 218-229.

28. Cruse, T. A. and Stout, M. G., "Fractographic Examination of Graphite/Epoxy Fracture Specimens," Journal of Composite Materials, Vol. 7, 1973, pp. 272.

29. Sih, G. C., "A Special Theory of Crack Propagation," Mechanics of Fracture, Vol. 1, Methods of Analysis and Solutions of Crack Problems, G. C. Sih—Ed., Noordhoff, International Publishing, Leyden, 1972.

30. Sih, G. C. and Chen, E. P., "Fracture Analysis of Unidirectional Composites," Journal of Composite Materials, Vol. 7, April 1973, pp. 230-244.

31. Sih, G. C. and Chen, E. P., Fracture Analysis of Unidirectional and Angle-Ply Composites, Lehigh University, Bethlehem, Pennsylvania, 1973, Technical Report NADC-TR-73-1.

32. Sih, G. C. and Chen E. P., Material Characterization on the Fracture of Filament-Reinforced Composites, Lehigh University, Bethelem, Pennsylvania, 1974, Report No. IFSM-74-66.

33. Broutman, L. J. and Gaggar, S. K., Fracture Toughness of Fiber Composite Materials, Illinois Institute of Technology, Chicago Illinois, February 1975, AD-A015 454.

34. Zimmer, J. E., "Fracture Mechanics of a Fiber Composite," Journal of Composite Materials, Vol. 6, April 1972, pp. 312-315.

35. Beaumont, P. W. R. and Phillips, D. C., "Tensile Strengths of Notched Composites," Journal of Composite Materials, Vol. 6, 1972, pp. 32-46.

36. Phillips, D. C., "The Fracture Mechanics of Carbon Fiber Laminates," Journal of Composite Materials, Vol. 8, April 1974, pp. 130-141.

37. Guess, T. R. and Hoover, W. R., "Fracture Toughness of Carbon-Carbon Composites," Journal of Composite Materials, Vol. 7, January 1973, pp. 2-20.

38. Chang, G. C., A Study on Fracture Toughness of Advanced Structural Composites, US Naval Academy, July 1973, EW-4-73.

39. Wright, M. A., Welch, D. and Kulkarni, H., Compare the Fracture Toughness of Metal-Matrix Composites as Determined by Four Different Techniques, Part I, University of Tennessee Space Institute, Tullahoma, Tennessee, December 1976.

40. Wright, M. A., Kulkarni, H. and Welch, D., Compare the Fracture Toughness of Metal Matrix Composites as Determined by Four Different Techniques, Part II, University of Tennessee Space Institute, Tullahoma, Tennessee, December 1976.

41. Hoover, W. R., "Crack Initiation in B-Al Composites," Journal of Composite Materials, Vol. 10, April 1976, pp. 106-117.

42. Adsit, N. R., and Waszczak, J. P., "Fracture Mechanics Correlation of Boron/Aluminum Coupons Containing Stress Risers," Fracture Mechanics of Composites, American Society for Testing and Materials, 1975, pp. 163-176, ASTM STP 593.

43. Hancock, J. R. and Swanson, G. D., "Toughness of Filamentary Boron-Aluminum Composites," Second ASTM Conference on Composite Materials, April 20-22, 1971, Anaheim, California.

44. Waddoups, M. E., Eisenmann, J. R., and Kaminski, B. E., "Macroscopic Fracture Mechanics of Advanced Composite Materials," Journal of Composite Materials, Vol. 5, October 1971, pp. 446-454.

45. Brinson, H. F. and Yeow, Y. T., "An Investigation of the Failure and Fracture Behavior of Graphite/Epoxy Laminates," Virginia Polytecnnic Institute and State University, Blacksburgs, Virginia, September 1975, VPI-E-75-23.

46. Kanninen, M. F., Rybicki, E. F., and Brinson, H. F., "A Critical Look at Current Applications of Fracture Mechanics to the Failure of Fibre-reinforced Composites," Composites, January 1977, pp. 17-22.

47. Whitney, J. M. and Nuismer, R. J., "Stress Fracture Criteria for Laminated Composites Containing Stress Concentrations," Journal of Composite Materials, Vol. 8, July 1974, pp. 253-265.

48. Nuismer, R. J. and Whitney, J. M., "Uniaxial Failure of Composite Laminates Containing Stress Concentrations," Fracture Mechanics of Composites, American Society for Testing and Materials, 1975, pp. 117-142, ASTM STP 593.

DISTRIBUTION

	No. of Copies
Headquarters SAC/NRI (Stinfo Library) Offutt Air Force Base, Nebraska 68113	1
Commander Rock Island Arsenal Attn: SARRI-RLPL-Technical Library Rock Island, Illinois 61201	1
Commander (Code 233) Naval Weapons Center Attn: Library Division China Lake, California 93555	1
Department of the Army US Army Research Office Attn: Information Processing Office P. O. Box 12211 Research Triangle Park, North Carolina 27709	1
ADTC (DLDSL) Eglin Air Force Base, Florida 32542	1
University of California Los Alamos Scientific Laboratory Attn: Reports Library P. O. Box 1663 Los Alamos, New Mexico 87545	1
Library US Army War College Carlisle Barracks, Pennsylvania 17013	1
Tennessee Technological University Department of Engineering Science Attn: Dallas G. Smith Cookeville, Tennessee 38501	20
Defense Documentation Center Cameron Station Alexandria, Virginia 22314	12

	No. of Copies
Superior Technical Services, Inc. Attn: T. Ward 4308 Governors Drive Huntsville, Alabama 35805	1
DRSMI-LP, Mr. Voigt	1
DRDMI-T, Dr. Kobler	1
-TL, Mr. Lewis	1
-TLA, Mr. Pettey	1
Dr. Mullinix	195
-TBD	3
-TI (Record Set)	1
(Reference Copy)	1